Science

AAAS

Supplementary Materials for

The macroevolutionary singularity of snakes

Pascal O. Title *et al*.

Corresponding author: Daniel L. Rabosky, drabosky@umich.edu

The PDF file includes:

Materials and Methods
Figs. S1 to S44
Tables S1 to S5
References

Other Supplementary Material for this manuscript includes the following:

MDAR Reproducibility Checklist
Data S1 to S3

Materials and Methods

1 Inferring the squamate phylogeny

1.1 Overview

Our phylogenetic approach was a multi-stage process. First, we collected 5462 loci from 891 in-group individuals across the squamate tree and augmented this dataset with previously published phylogenomic data from 319 in-group individuals. After filtering, we generated a phylogenomic constraint backbone consisting of 1018 species. Second, we downloaded all squamate genetic sequences from NCBI GenBank; in total, this resulted in a 72,152 bp alignment (56 loci) across 6,885 species. We created a supermatrix alignment from these data. With this supermatrix alignment, we inferred a phylogeny using our phylogenomic backbone as a topological constraint. To do so, we used maximum likelihood to estimate family-specific trees and grafted the resulting trees onto the phylogenomic backbone. Third, we time-calibrated our phylogenomic tree. We first identified the minimum set of species that would allow us to place our 31 fossil calibrations; we then dated a subsampled phylogenomic tree containing just these 134 tips. We used the dates from the phylogenomic phylogeny as secondary calibrations to date the phylogeny of all 6,885 species. We refer to this phylogeny as the primary tree, and it served as the basis for the results shown in the main text. We then performed two additional steps to account for uncertainty at several levels. For diversification analyses, we generated a distribution of pseudo-complete (sometimes labeled "fully sampled") phylogenies by using imputation to place the 3,872 species that lacked genetic data (out of 10,757 currently accepted squamate species). We also created a distribution of phylogenies to account for uncertainty in phylogenetic inference, divergence dating, and imputation. Across this distribution, we repeated our core comparative analyses: we estimated diversification rates, inferred rates of trait evolution, and identified nodes on which patterns of trait evolution shifted.

1.2 Inferring a phylogenomic backbone

1.2.1 Sampling

We sampled broadly across the squamate phylogeny, targeting species that reflect the full phylogenetic breadth of the clade. Where possible, we targeted samples from specimens that have been accessioned into museums, as it is increasingly clear that whole-body preserved voucher specimens are essential to maximize the long-term utility of genetic data (*44–46*). Ninety-one percent of our phylogenomic samples are represented by an associated whole-body voucher specimen accessioned into global natural history collection network (*47*). Table S1 details the provenance and voucher numbers for these phylogenomic samples. Samples not represented by voucher specimens in natural history museums are associated with either (a) tissues lacking whole-body voucher specimens (e.g., tail tips), or (b) field-collected specimens with pending accessions in the global natural history collection network. All specimens included in the project under the latter category were collected with appropriate scientific research permits and animal ethics approvals from the relevant institutional and governmental authorities; see MDAR reporting form for additional details.

In total, our sampling spanned 891 species-level taxa. In a few cases, two or more individuals were sampled from the same nominal species because the species exhibited cryptic diversity that had yet to be formally recognized. Some of these data (*n* = 136 samples) were previously-published in regionally-focused projects from our research groups (*48–51*); however, we reanalyzed all data under a common framework for this study.

We augmented our data collection with previously-published phylogenomic studies on squamates. On September 8, 2017, we searched "phylogenom* AND (squam* OR lizard* OR snake*)" on Web of Science and Google Scholar. In total, we identified 15 papers from which we could extract data. After excluding all species already represented in our new dataset, these previously published studies added an additional 319 species (Data S1). Where possible, we downloaded the original raw high-throughput sequencing reads so that we could reanalyze these data across a common pipeline.

After removing individuals with poor data quality (see below; fig. S30) and outgroups, we sampled phylogenomic data from 1,083 species, and 55 of the 68 currently-recognized families in squamates.

1.2.2 Data Collection

We employed a target-capture approach to collect 5,462 loci from each individual (*51*). This Squamate Conserved Loci (SqCL) set spans three types of loci: 372 anchored hybrid enrichment loci (AHE; (*52*)), 5,052 ultraconserved elements (UCE; (*53*)), and 38 single-copy loci commonly used in traditional phylogenetics (*54*).

For each individual, we extracted DNA from either liver or tail tissues using high-salt extractions or phenol-chloroform DNA extraction (*55*) and then quantified DNA quality and quantity using a QuBit v2 and Nanodrop 2000. We then contracted with Rapid Genomics (Gainesville, Florida, USA) to prepare dual-indexed sequencing libraries per sample. Approximately one ng of DNA was fragmented to a modal 400 base pairs (bp) using sonication and then standard Illumina protocols were followed to generate sequencing libraries. We created sample pools, combining equimolar amounts of each library across 16 samples. Samples were pooled by taxonomic identity to reduce competition for target binding (*56*). We then contracted with Arbor Biosciences (Ann Arbor, Michigan, USA) to conduct target-capture experiments. Target loci were captured following the MyBaits v3 protocol with the SqCL v2 probe set. This protocol was slightly modified to use the NimbleGen xGen Blockers, which have been shown to increase capture efficiency in non-human taxa (*57*). Following target capture, we combined across 6 pools in equimolar amounts to result in a final pool of 96-samples. Each of 96-set of samples was sequenced across one 125-bp paired end lane of Illumina HiSeq 4000 sequencing at the Advanced Genomics Core at the University of Michigan (Ann Arbor, Michigan, USA).

To generate outgroup sequences, we downloaded from the NCBI database full genomes for a set of non-squamate vertebrates: chicken (galGal5), human (hg38), zebra finch (taeGut2), western painted turtle (chrPic1), and American alligator (allMis1). From these genomes, we mapped our target loci sequences from the SqCL set to each genome using blat v36x1 (*58*) and extracted the sequence using samtools v1.3 (*59*). For ultraconserved markers, because our target locus only

spans the conserved region of ~150-200 base pairs, we extracted an additional 1000 base pairs around this central region.

1.2.3 Data Processing

We processed newly collected and previously published raw sequencing data using a previously published pipeline (*51*). Briefly, we demultiplexed reads and then removed adaptors using Trimmomatic v0.39 (*60*), trimmed low-quality regions using Trimmomatic, and merged overlapping-paired reads using PEAR v0.9.11 (*61*). We assembled cleaned reads using Trinity v2.1 (*62*) and annotated assemblies by identifying reciprocal best-hit matches to our target loci with blat. We mapped trimmed reads to annotated loci with bwa v0.7.15 (*63*) and called variants using samtools v1.5 (*59*). Most individuals were captured for most loci, and captured loci averaged ~800 bp in length and had high coverage (>60x; fig. S2).

1.2.4 Phylogenomic inference

We aligned data by locus using mafft v7.310 (*64*). Visual inspection of alignments found that alignments for some loci (particularly the tail-ends of ultraconserved elements) contained excessive gaps. To improve the quality of these alignments, we implemented four stages of filtering. First, we removed any individuals whose sequences were <300 bp in length. Second, we removed any sites that consisted of >70% gaps. These filters were chosen based on a visual inspection of ~10 alignments. Particularly for UCEs, alignments can be ragged at the ends. We found this filter removed many of these sites which appear poorly aligned. These filters are similar to those used in other vertebrate phylogenomic papers and which have been shown to perform satisfactorily (*65*). Third, we applied a filter in which stretches of sequence with excessive private or near-private alleles were removed (*65*). This approach measures the frequency of sites that contain private alleles across sliding windows of variable length and then trims any sequences with >25% of private alleles. Finally, we removed any individuals that were sampled at <5% of the targeted loci and any loci that consisted of <30% of sampled individuals.

Using these trimmed alignments, we implemented two phylogenetic approaches: a coalescent-based approach based on gene trees and a concatenated maximum likelihood approach. For the coalescent based approach, we first inferred gene trees for each trimmed alignment under the GTRGAMMA model implemented in RAxML v8.2.11 (*66*). We calculated nodal support across all nodes using the Shimodaira-Hasegawa-like approach (*67*). We then collapsed all nodes with branch lengths less than 5e-5 and <10 support and used the resulting gene trees as input to ASTRAL-III (*68*). The resulting ASTRAL tree included several unexpected relationships inconsistent with common understandings of squamate evolution. To determine possible causes for these discrepancies, we conducted a series of analyses, which included:
- filtering loci more aggressively for missing data
- being more and less lenient in which nodes we collapsed based on support levels
- identifying putative outlier loci by calculating Robinson-Foulds distances among loci and ordinating distance matrices

- removing loci that showed strong evidence for rate and substitution heterogeneity as measured by root-tip variance

Even following aggressive filtering, the coalescent-based approach continued to result in questionable tree topologies (fig. S31). For example, Rhineurinae is neither sister to Lacertinae nor nested within Amphisbaena. Others have reported similar pathologies with coalescent-based approaches (*65*), including a recent study that inferred a phylogenomic tree spanning all squamates (*69*). Thus, we focused all subsequent inference and analysis on a concatenated approach. However, we note that concatenated approaches can also return spurious results with respect to tree topology. Spurious results are most likely during rapid radiations with short internode lengths that fall within the "anomaly zone" (*70*). Previous phylogenetic analyses have shown that several branches within Squamata fall in the anomaly zone, particularly in the Iguania group (*50, 71*).

For the concatenated maximum-likelihood approach, we concatenated all loci and then inferred an initial topology using ExaML v3 under a GAMMA model (*72*). Based on this initial topology, we identified both rogue loci and rogue taxa. Previous phylogenomic studies have shown that a few discordant loci can have a disproportionate effect on phylogenetic inference (*73*). Accordingly, for each locus, we compared its log-likelihood under the gene tree topology versus the log-likelihood of the same locus constrained to the concatenated topology. Log-likelihoods in both cases were calculated using RAxML under a GTRGAMMA model. If the difference in log-likelihood was large, this indicates the concatenated topology is a bad fit to the locus and might suggest it is potentially a rogue locus. 232 loci had large log-likelihood differences, and thus, we removed these loci in subsequent analyses. We additionally used RogueNaRok to identify potential rogue taxa (*74*). To do so, we created 100 bootstrap alignments that randomly sampled 1% of the loci. For each of these subsampled alignments, we inferred the topology using ExaML. We then used this set of 100 bootstrapped trees and our initial tree based on a full alignment as inputs to RogueNaRok. This approach identified 49 potential rogue taxa. After removing these "rogue" loci and taxa, we re-inferred the concatenated topology using ExaML. Finally, using the ExaML topology as the starting tree and the filtered concatenated alignment, we re-inferred the tree and generated 1,000 ultrafast bootstraps using IQTree v2.0-rc1 (*75*) (fig. S32).

Other studies have shown that phylogenetic trees inferred with large datasets can lead to high bootstrap values even when there is underlying phylogenetic uncertainty (*76*). Accordingly, as an alternate measure of phylogenetic uncertainty, we mapped levels of gene tree discordance across nodes using phyparts v0.0.1 (*77*). This approach identified numerous cases of phylogenetic uncertainty (fig. S33), some of which were explored in greater depth in (*50*).

1.3 Maximizing species coverage: supermatrix approach

1.3.1 Mining previously published GenBank data

To generate a supermatrix alignment of all previously-published genetic data published for Squamata, we used the program PyPHLAWD to mine the NCBI GenBank database (*78*). PyPHLAWD can be run using either a baiting approach in which target loci are used to retrieve homologous loci from a defined taxonomic span or a clustering approach in which all loci from a

defined taxonomic span are downloaded and clustered by sequence identity. We used the clustering approach because initial explorations found that the clustering approach resulted in a greater number of high-quality sequences than the bait approach. We ran PyPHLAWD in clustering mode with Squamata as the taxonomic clade of interest.

Most clusters mapped to single-copy genes that are traditionally used in genetic-based phylogenetic studies of squamates (e.g., those included in (*54*)). A handful of clusters were more complicated and required manual annotation. First, many of the clusters stemming from mitochondrial data spanned several mitochondrial genes. For these clusters, we split up sequences across loci by annotating locus boundaries using mitochondrial reference proteins and exonerate v2.4.0 (*79*). We then created locus-specific sequence sets. Second, one cluster consisted of two different paralogs (*SLC8A3* and *SLC8A1*). For this cluster, we split up the sequences by paralog identity by re-clustering the data at a higher percent-identity cutoff with vsearch v1.3 (*80*). Finally, one cluster consisted of *RAG1*, which is a long gene. Most studies either sequence the first half or the second half of the gene. However, both halves of the gene formed one cluster. To improve alignment quality, we split the two halves of *RAG1* into two separate locus datasets.

1.3.2 Mining Sanger loci from newly collected data

Many of the loci identified from the PyPHLAWD clustering analysis were also collected for our phylogenomic samples. We extracted these loci from our phylogenomic datasets and added them to the GenBank data. See Table S4 for a mapping of SqCL loci to genes downloaded from GenBank.

Our phylogenomic data collection did not capture any mitochondrial data. However, the majority of the data in our PyPHLAWD clustering analysis derived from the mitochondrial genome. When collecting target capture data, anywhere from 40-80% of reads are on-target, and the remainder derive from other genomic regions. The majority of this so-called by-catch map to the mitochondria, and thus the by-catch can be used to reconstruct mitochondrial genomes. We used MITObim v1.9.1 (*81*) to assemble mitochondrial genomes. For each individual, we downloaded from GenBank the full mitochondrial genome from the closest possible phylogenetic relative as initial bait. We then extracted the mitochondrial genes from the reconstructed mitochondrial genomes after annotating the genome using the protein2genome function of exonerate and mitochondrial protein sequences. The mitochondrial protein sequences were obtained from the PyPHLAWD clustering analysis. We identified the non-coding 12S and 16S ribosomal RNA genes using the dna2dna function of exonerate and reference sequences from the PyPHLAWD clustering analysis. We added all these data to our existing GenBank loci sets.

1.3.3 Taxonomic reconciliation

Each sample or sequence in both our phylogenomic dataset and our NCBI GenBank-based supermatrix is attached to a species name. However, species names do not always reflect the most up-to-date understanding of current taxonomies. Some species names have undergone numerous revisions through the years – e.g., as subspecies are elevated to species, cryptic species

are formally recognized. In such cases, a species name might ambiguously map to multiple species names in the current taxonomy. In order to address these issues and provide a standardized taxonomy, we cross-referenced all species names to a single, relatively current taxonomy: the species list included in ReptileDatabase published on 19 December 2019 (*82*).

For the phylogenomic samples, 930 of the 1083 samples were assigned to a species that mapped unambiguously to a species in the ReptileDatabase. We manually identified the species name for the remaining 153 phylogenomic samples.

For the NCBI GenBank-based sequence accessions, 83% of accessions' species identities mapped one-to-one to a species in the ReptileDatabase. For the remaining 17% of accessions, we used the following iterative approach to update their taxonomy. First, we checked if these accessions were included in two other recent supermatrices of squamates: (*83*) and (*84*). In cases of overlap, we used the taxonomy determined by the squamate experts involved in these studies. Next, we evaluated accessions manually to determine the most likely species name, referencing locality of sample and original published literature as necessary. Finally, for any remaining accessions, we kept the original taxon names as according to the NCBI taxonomy.

In some cases, updating the taxonomy led to some species being represented by multiple sequences at the same locus. In these cases, we first chose to keep the sequence generated internally, then accessions shared with (*83*) and (*84*), then accessions that mapped to a species with less ambiguity, and then finally the longest locus. Our taxonomic reconciliation and resolution of synonymies can be found in Data S2 as well as accessions for each locus.

1.3.4 Aligning loci

In order to ensure high-quality alignments across this phylogenetic scale, we focused on the coding sequence portion of loci only and guided alignment of these loci based on their amino acid sequences. To do so, we first used exonerate to ensure that all sequences were in the 5'-3' direction by comparing locus data to the amino acid sequence for that locus. Again using exonerate's alignment of the protein sequence to DNA sequence, we extracted the coding sequence from the locus and used the SuperCrunch coding translate test to ensure the coding sequence was in the right frame (*83*). We then ran MACSE v2 on the coding sequences to identify any frameshifts in the locus sequences (*86*). We aligned the resulting translated amino acid sequences using Mafft (with the L-large-INS-1 strategy; (*87*)) and then used the amino acid alignment to derive the nucleotide alignment using the pxaa2cdn function in phyx (*88*). Next, we trimmed the nucleotide alignments with the trimAlignment module of MACSE to remove any positions at the end of the alignments that had <10% occupancy. Then, to identify potential rogue taxa for each given locus alignment, we used quartet sampling (*89*). Each internal branch in a phylogeny subtends four clades. In quartet sampling, single tips from each clade are randomly sampled to generate a four-taxon set for which a phylogenetic topology is then inferred. One metric calculated in quartet sampling is Quartet Fidelity. For a given tip, Quartet Fidelity takes all four-taxon trees including the tip and calculates the percentage of those four-taxon trees that are concordant with the consensus phylogeny. Tips with low Quartet Fidelity scores are potentially rogue taxa and were thus removed. We then concatenated these filtered

alignments to create our supermatrix, which resulted in a 72,152 bp alignment (56 loci) across 6,885 species (fig. S34).

1.3.5 Phylogenetic inference

To take advantage of the data-rich inference afforded by our phylogenomic dataset, we used the phylogenomic tree as a backbone to infer a phylogeny with the supermatrix alignment. We first took the phylogenomic tree and conservatively collapsed any nodes that varied across replicate runs of IQTree. This resulted in the collapse of <2% of total nodes. Then, per taxonomic family, we both extracted the corresponding clade from the phylogenomic tree and created a clade-specific subset of the supermatrix alignment. Using IQtree, we inferred a family-level phylogeny using the phylogenomic family tree as a topological constraint. Several families (20 out of 52) had two or fewer phylogenomic tips; for these families, we inferred an unconstrained phylogeny. In all cases, we inferred the phylogenies with 8 partitions: one for each codon position, for mitochondrial and nuclear genes separately, and separate partitions for the ribosomal genes 12S and 16S). Each IQtree analysis started with 50 runs and was followed by a final optimization step using the nearest neighbor interchange algorithm. After inferring family level trees, we knitted all the resulting phylogenies together in R, guided by the family relationships inferred in the phylogenomic analysis. A modest number of taxa (n = 50; 0.7% of all taxa) belonged to a family too small to include in its own analysis. To place these taxa, we used IQTree to run a final analysis of the full Squamata supermatrix with the concatenated family-level trees as a constraint, along with the phylogenomic backbone. In this final run, we included *Sphenodon punctatus* as an outgroup sequence.

We repeated this analysis using a fully unconstrained approach to determine how topological constraint affected phylogenetic inference (fig. S35).

1.4 Estimating divergence times

1.4.1 Fossils

Using a combination of fossils from previously published studies (*71*, *83*, *85*, *90*) and previously described fossils not previously used for large-scale squamate phylogenetics, we identified 31 fossils across the Squamata tree of life to use as calibrations (see Table S1). These fossils span both deep nodes (314 Ma) and more-shallow (recent) nodes (6.3 Ma) and the full diversity of Squamata. A few well-known fossil calibrations could not be included because our tree did not include the taxa spanning the constraint.

Primaderma nessovi is used here to constrain the minimum divergence date of *Heloderma+Anguis+Anniella+Xenosaurus* (Neoanguimorpha of (*71*)). Its anatomy suggests that it is more closely related to *Heloderma* than any other extant taxon (*91–93*). Multiple 40Ar/39Ar measurements from volcanic ash associated with the fauna provide a mean age of 98.39±0.07 Ma (*92*). Therefore, 98.32 Ma is used here as a minimum age.

Afairiguana avius is used here to constrain the minimum age of *Anolis+Gambelia* to 49.1 Ma. Phylogenetic analysis of 50 taxa with 202 morphological characters suggests that the affinity of *Afairiguana avius* lies well within Iguanidae and possibly within Polychrotidae (*95*). It therefore provides a minimum date for the major radiation within Iguanidae. The specimen comes from the Green River Formation exposed at Warfield Springs locality, Wyoming, USA (*95*), which is dated to a minimum age of 49.1 Ma (*96*).

Odaxosaurus roosevelti is used here to constrain Anguidae to a minimum age of 74.5 Ma. Material of *Odaxosaurus roosevelti* comes from the Kaiparowits Formation exposed at locality OMNH V5, Garfield County, Utah, USA (*97*). The geological context of the Kaiparowits Formation has undergone extensive study. Stratigraphic and isotope analyses indicate an age range of 74.5–76.6 Ma (*98*). Therefore, we use 74.5 Ma as a minimum age constraint.

Some studies have inferred fossils from the Jurassic to represent snakes (e.g. (*99, 100*)). However, the affinity of these fossils is controversial, and they are again in the process of being redescribed with new more complete material (*101, 102*).

Tepexisaurus tepexii from the Cretaceous of Mexico (*103*) has been placed by several phylogenetic analyses as more closely related to Xantusiidae than its extant sister taxon Cordylidae (*104–106*). These results suggest that Xantusiidae and Cordylidae must have diverged before the age of this fossil (~100 Ma). However, the fossil taxon has also been placed within Lacertoidea (*108*) suggesting that further fossils and analyses are required to be certain of the affinities of this taxon.

1.4.2 Divergence dating with MCMCtree and TreePL

For divergence time estimation, we used a two-step approach. First, we dated a phylogenomic tree that spanned a subset of the tips and included a subset of the loci using MCMCTree. Second, we used the resulting node ages as secondary calibrations to date the full tree with TreePL.

To date the phylogenomic topology, we used the program MCMCTree from the PAML software v4.10 (*109*). Given the computational demands of divergence dating with molecular data, we subsampled our phylogenomic dataset by both individual and locus. First, we identified the species that needed to be included in order to place fossils onto the phylogeny. Where multiple species were possible, we included the species with the most complete locus sampling. In total, we pruned our phylogenomic tree to include 134 species, which spanned major deep nodes as well as nodes that would be fossil-calibrated. We additionally included three outgroups (*Gallus gallus, Alligator mississippiensis, Homo sapiens*). Then, we created a subsampled locus alignment of 10 loci. To identify the 10 loci for inclusion, we used SortaDate (commit version 8d3aef3) to identify the loci that were in the 90th percentile for individual-wide sampling, in the 90th percentile for support values as measured by SH-values, and in the bottom 10th percentile for tip-root variance (*110*). This approach maximizes matrix completeness and ensures the loci being chosen are more clock-like and informative than average.

We fixed the tree topology to the phylogenomic tree, pruned to just the 134 ingroup and three outgroup taxa required to place all fossils. Each of our 10 loci was set to its own partition. Given the size of our dataset, we used the approximate likelihood method. Of the 31 fossils, we could specify both a minimum and maximum age constraint for seven of them. For these, we specified a uniform prior distribution with soft bounds (soft lower bound of 0.01 and soft upper bound of 0.05). For those 24 fossils with exclusively minimum age constraints, we specified skew-Normal prior distributions (soft lower bound of 0.001, soft upper bound of 0.05, scale parameter 0.05, shape parameter of 7), with an upper bound arbitrarily set to the lower bound + 20 mya. We ran the CorrTest approach (*111*) to determine which type of clock model to employ, and found that our dataset was most consistent with a relaxed clock model with autocorrelated rates. We ran MCMCTree for 10.5 x 10^6 generations, sampling every 500 generations, and discarding a burnin of 500,000 generations, resulting in 20,000 posterior samples. We employed a data-driven birth-death tree prior (*112*). We ran three independent iterations to verify convergence.

We used a non-parametric rate-smoothing approach, implemented in the software TreePL (*113*), in order to time-calibrate our full tree of 6,885 taxa sampled for both phylogenomic and supermatrix data. We treated the 133 divergence dates estimated with MCMCTree (medians from the posterior distributions of dates) as secondary calibrations to be applied to the full squamate phylogeny. To account for possible molecular clock heterogeneity across the tree, we split the squamate phylogeny into 6 clades and time calibrated these independently. For each clade, to find the best smoothing parameter for TreePL, we evaluated 125 different combinations of TreePL parameters (the opt, optad and optcvad parameters) for cross-validation and identified the smoothing parameter with the lowest chi squared score. Each cross-validation run was repeated 5 times to account for potential local optima. The smoothing value for each clade was identified as the value most commonly identified across cross-validation runs. We repeated this procedure for a "scaffold" tree designed to facilitate the merging of these six clades back together. We then ran final TreePL runs on each clade with the optimized smoothing parameters, and with 50 replicates to increase the chances that the program had found the global optimum. In all cases, the 10 replicates with the best likelihood scores had highly correlated divergence times ($r > 0.995$). We finally merged all best scoring time-calibrated clades together to produce a fully time-calibrated squamate phylogeny, where all nodes that were present in the MCMCTree analysis reflect those divergence times. This time-calibrated phylogeny with all 6,885 tips is referred to as the primary tree.

1.5 Imputing phylogenetic position of unsampled taxa

Of the 10,757 recognized squamate species, 6,885 of them are included in our tree. For the remaining 3,872 species (spanning 651 genera), we used phylogenetically informed imputation to generate a distribution of fully sampled phylogenies. These imputed phylogenies were only used for inferring speciation rates, because previous work has shown that inferring trait evolution on imputed trees can lead to spurious results (*114*). However, analyses of lineage diversification have increased power and lower estimation bias on "complete" phylogenies that include imputed taxa (*115*), relative to analyses that use sampling probabilities to account for missing taxa (*116*). Although we consider speciation rates from the "complete" imputed phylogenies (10,757 tips) to be more reliable than those from the "sampling fraction" approach (e.g., no imputation; analytical correction for incomplete sampling), these approaches overall gave tip rates that were

highly correlated (fig. S36). Speciation rate estimates and the relationship between rates from imputed and non-imputed approaches is discussed below in Section 3.

It is clearly impossible to know the phylogenetic position of missing taxa (e.g., with no genetic data) with absolute confidence, but it is also true that higher-level taxonomy, biogeography, and other information can provide plausible constraints on the distribution of phylogenetic positions for such unsampled lineages. We used a combination of taxonomic information, existing phylogenies (including the trees generated for this study), biogeography, and published literature to make determinations as to the most plausible genus or higher-level clade to which each unsampled taxon belonged. Constraints were assumed identical for all unsampled members of the same genus. Once all taxa had been assigned appropriate constraints, we used a conservative simulation procedure to estimate the distribution of unknown speciation times, conditional on the observed set of speciation times from our (sequence-based) phylogenetic tree. Missing species were then attached sequentially and randomly within the constraining subclade, subject to any exclusion constraints (details below), at the speciation times as simulated under the algorithm (*117*). This imputation procedure is conservative, because it minimizes among-lineage diversification rate heterogeneity within any constraining subclades.

For each genus with one or more species missing from the genetic dataset (n = 651), we first determined a maximally inclusive stem clade to which the missing taxon could provisionally be assigned. This is referred to as the *inclusion clade*. We then identified any major subclades within the *inclusion clade* where we had strong prior reasons to believe that the focal taxon should not be assigned; this latter category was used for only a small number of genera (n = 22) where we had strong prior evidence to exclude a particular clade. The scincine genus *Sphenomorphus* is an example of a clade with an exclusion constraint. Our phylogeny and prior results (*118*) indicate that *Sphenomorphus* is not monophyletic, and thus we conservatively assigned the 76 missing *Sphenomorphus* species to a much larger inclusion clade: the stem Sphenomorphinae. However, it is extremely unlikely that any of these unsampled *Sphenomorphus* species – none of which occur in Australia – are in fact nested within the phylogenetically, morphologically, and biogeographically coherent Australian subradiation of sphenomorphines (*118–121*). Hence, the Australian sphenomorphinae was an exclusion constraint for this genus, such that no unsampled *Sphenomorphus* species were placed within the Australian clade.

Each genus was classified into one of four constraint categories. Type 1 constraints were applied to genera that were both *present* and *monophyletic* in our phylogeny, and where there was no additional information implying non-monophyly. Type 2 constraints were applied to paraphyletic genera, with the constraint node fixed to the MRCA of all sampled species in the genus. Type 3 constraints were applied to species where either (A) the genus was either polyphyletic or incoherently paraphyletic (example: *Cnemaspis*), or (B) the genus was not present in sequence-based phylogeny but where a suitable higher-level constraint could be identified (example: the two species of *Mesobaena*, assigned to the family-level clade Amphisbaenidae). Type 4 constraints were similar to Type 2 or Type 3 but specified one or more exclusion clades. The majority of missing species (90%; n = 3,487) were assigned Type 1 or Type 2 constraints. Only 22 genera (145 species) were assigned constraints with exclusions (Type 4), and most of these (n

= 110 species) were from two genera: *Sphenomorphus* and *Geophis*. Data S3 provides information about all constraints used in these analyses.

To simulate the position of unsampled taxa, we determined the constant-rate birth-death speciation rate (λ) for the target clade for inclusion. For group 3, we used a global λ inferred for the whole tree. We then simulated a possible array of speciation times for missing taxa based on branching times of the target clade and our inferred λ, following (*117*). For group 4 constraints, we first clipped all clades marked for exclusion from our phylogeny and then simulated speciation times. Speciation times were simulated using the corsim function in R package TreeSim v2.4 (*120*), which generates distributions of "missing" speciation times conditional on the set of speciation times that have actually been observed. The missing species were then added iteratively to the subtree assuming a uniform prior over the distribution of possible topological placements. For our primary tree, we generated 100 imputations so that our estimates of speciation rate (see Section 3) could account for the inherent uncertainty of imputation. For our pseudo-posterior set of trees (see Section 1.6), we generated one imputation per tree.

1.6 Accounting for uncertainty

Uncertainty in our analysis comes from four major sources. First, there is uncertainty in our inference of the phylogenomic backbone, best captured as topological variance across bootstraps of our phylogenomic analysis. Second, there is uncertainty in our inference of an all-genetic phylogeny based on the phylogenomic backbone constraint. Third, there is uncertainty in divergence time estimates, best captured as the posterior distribution of node ages in the dated phylogeny. Fourth, there is uncertainty in imputation of taxa without genetic data. To account for these four sources of uncertainty, we first sampled 100 topologies from the set of 1,000 phylogenomic bootstraps. There is only modest topological variance across these 1,000 phylogenomic bootstraps. In total, there are only 29 unique topologies across this set, and eight topologies make up 61% of the distribution. Then, we used each of these topologies as a constraint for inferring the all-genetic phylogeny, resulting in 100 trees of 6,885 taxa each. We dated each of these trees. For each dated tree, we drew from the posterior distribution of the MCMCtree analysis and used the node ages as constraints in TreePL. Finally, for each dated phylogeny, we imputed all missing taxa as described above. This resulted in a pseudo-posterior set of trees that reflects all potential sources of uncertainty: a final distribution of 100 ultrametric trees, each consisting of 6,885 taxa placed on genetic data and 3,872 based on imputation (fig. S37).

To confirm that our primary findings (via the "primary tree") were robust to phylogenetic uncertainty, we repeated core analyses across this set of pseudo-posterior trees.

1. Using the primary tree, we found that net innovation and rate of trait evolution were higher in snakes than lizards. We calculated the snake:lizard ratio of innovation indices and trait rates across the pseudo-posterior trees and compared this distribution to the ratios from the primary tree (fig. S25A & B).
2. Using the primary tree, we found that the primary shift in trait state and rate occurred at the base of all snakes (or very near to it) across several traits. We repeated the canonical phylogenetic ordination (CPO) approach across the pseudo-posterior trees to determine whether we would infer similar shifts as those observed in the primary tree (fig. S25C).

3. Using the primary tree, we found that snakes had higher tip speciation rates than lizards. We calculated the difference in snake and lizard speciation rates in pseudo-posterior trees, based on CLaDS runs on these trees (fig. S25D).
4. Using the primary tree, we found that none of our sets of explanatory variables can explain the speciation rate variation seen across lizards and snakes. We repeated this phylogenetically corrected linear regression of predictor traits against speciation rates across the pseudo-posterior trees (fig. S25E).

For these analyses, we used diet composition as inferred by the phylogenetic-free Hierarchical Bayesian Clustering approach (see Section 2.2.6.3). All of our major findings are robust to the uncertainty captured by our pseudo-posterior set of trees; we find quantitatively and qualitatively similar patterns across these trees and our primary tree (fig. S25).

1.7 Comparison to previous squamate phylogenetic hypotheses

Relative to previously published squamate phylogenies (*20, 50, 54, 71, 83, 93, 108, 118, 123–127*), our phylogeny was based on more phylogenomic data and more single-copy genes and also included more species (fig. S38). While more data does not equate to better data, our phylogeny is thus the most comprehensive squamate phylogeny published to-date. The topology in our phylogeny is largely congruent with previous phylogenomic hypotheses published by (*20, 50, 54, 69, 71, 83, 93, 108, 118, 123–127*) (fig. S39). Most of the discordances occur in two known "anomaly zones" in squamates (Iguania and advanced snakes (*50*)), and a few family-level relationships (e.g., the monophyly of Amphisbaenia) remain variable across datasets (see fig. S23 versus fig. S33).

Similarly divergence times are largely congruent with previous phylogenomic hypotheses published by (*20, 50, 54, 71, 83, 93, 108, 118, 123–127*) (fig. S40, 41). The median estimate for the origin of crown group Squamata is in the Late Triassic (~213 Ma) with the shallow end 95% confidence interval extending to the boundary between the Triassic and Jurassic (fig. S4). An origin time for crown group Squamata near or just before the Jurassic-boundary is consistent with several previous molecular divergence analyses (*71, 90, 128, 129*), as summarized in figure 5 of (91) and Table 1 of (*130*). This date is also consistent with some evaluations of the fossil record (e.g. (*106, 108*)). A recent fossil from the Late Triassic of the UK is likely the first clear evidence of a crown group squamate within the Late Triassic (*131*). Aspects of the anatomy suggest it may even represent a relatively deeply nested member of Anguiformes (e.g., (*131*)). If correct, this affinity would imply an even deeper origin for crown group Squamata and a notably rapid appearance and divergence of the modern crown groups. Continued discovery and analyses of fossils, with due caution (e.g. (*132*)), will likely clarify both the origin time of crown squamates and their early diversification.

The divergence between Xantusiidae and Cordylidae is found to be deeper than the age of the Cretaceous putative stem xantusiids *Tepexisaurus tepexii* and *Retinosaurus hkamtiensis (103, 107)*. The estimated age of Lacertoidea is found to be deeper than the Cretaceous putative stem teiids *Purbicella ragei* and *Meyasaurus faurai (108, 133, 135)*.

There are several fossil constraints where the prior, effective prior, and posterior, have strongly overlapping distributions (e.g. *Odaxosaurus*, *Titanoboa*, *Egernia*, *Saniwa ensidens*,

Paleheterodon; fig. S5). However, there are also some where the posterior distribution is notably deeper in time compared to the prior and effective prior (e.g. *Cretaceogekko*, *Primaderma*, *Boipeba*, *Afairiguana*, Paramacellodidae, *Saichangurvel*). This discord may be due to the respective fossil being used to constrain a larger more inclusive clade than it actually represents, e.g. *Afairiguana* was used to constrain the divergence of *Anolis* and *Gambelia* but it may represent a more deeply nested clade (*95*). This possibility shouldn't be unexpected given that the emergence of notable synapomorphies may not occur immediately after a divergence (*135*). Even if older taxa closer to the divergence are known they may lack an adequate number of synapomorphies to identify them as such. There are a few fossil constraints which have a posterior distribution that is shallower than the prior and effective prior (e.g. *Pantherophis*, *Dorsetisaurus*). Assuming the posterior is correct it suggests these fossils may lie outside the clades they are being used to constrain.

2 Assembling the squamate trait dataset

2.1 Overview

To characterize phenotypic innovation across squamates and to determine how these patterns relate to speciation dynamics, we collated and synthesized a species-level dataset – e.g., morphological traits, trophic-related traits, parity mode, biogeographic information, and climate niche traits (Table S2). Traits were organized into four categories: primary, secondary traits (type 1), secondary traits (type 2), and biogeographic traits.

Primary traits are continuous, ordinal, or continuous-like traits where trait variability at the clade level is expected to correlate with species-level environmental or ecological diversity. More specifically, we define **primary traits** as those that have a well-defined distance metric associated with character state differences (e.g., excludes categorical data) and where trait values for individual species are not simply averaged or generalized state assignments applied to entire clades. Informally, we view this variational property of traits (c.f. (*136*)) as consistent with variation in fundamental "ways of life" across taxa, or variability in the capacity to evolve / adapt itself (evolvability, versatility, innovability). Traits in this category are: body mass, snout-vent length, elongation index, number of presacral vertebrae, multivariate skull shape, multivariate climate space, chemosensory index, multivariate diet composition, and diet breadth.

Secondary traits, type 1 are continuous, ordinal, or continuous-like traits where trait variability at the clade level has no relationship or ambiguous relationship with species-level environmental or ecological diversity. The only examples in our dataset are two traits associated with limb loss. Limb loss has many ecological consequences and, in non-snake lizards, is commonly but not exclusively associated with body elongation and burrowing. For non-burrowing examples: many pygopodids, *Chaemaesura* cordylids, and some anguids (e.g., *Ophisaurus*) are both limb-reduced and largely surface active; *Lialis* pygopodids are sometimes referred to as "slithering geckos". It is clear that being limb-reduced versus non-limb-reduced can be adaptively associated with different ways of life. But differences in degree of limb loss – for instance, lizards that have two hind digits versus three – are not known to have functional significance. In general, variation among species in degree of limb loss seems likely to represent points along an evolutionary trajectory leading to body elongation and complete limb loss. There is little evidence for

substantive ecological differences between species in clades that show extensive variability in numbers of limbs and digits, such as *Lerista* skinks; we therefore do not view clade-level variability in numbers of limbs and numbers of digits as indicative of ecological diversity. Traits in this category are: number of digits and number of limbs.

Secondary traits, type 2 are categorical data where metric distances between character states are undefined, or where available data are sufficiently coarsely coded as to aggregate across, or to eliminate, biologically significant true variability. For example, foraging mode and cranial kinesis are classic traits in squamate biology but available summaries typically assign entire clades (e.g, snakes) to a single state ("highly kinetic"), while masking extensive within-clade variation. Several traits in the dataset fall into this category, but were included for completeness due to their perceived importance for squamate biology. As most of these traits are categorical variables, innovation cannot meaningfully be computed, and we do not compute evolutionary rates for discrete characters that cannot be considered at least semi-continuous (e.g., vertebral counts are discrete, but trait distances are effectively metric and can be treated as such in Euclidean space). However, we do test whether these traits predict variation in speciation rate across squamates. Traits in this category are: skull kinesis type, prehension mechanism, parity, and foraging mode.

Biogeographic traits included midpoint latitude of species' geographic range (*latitude*) and mean elevation across the species range *(elevation)*. These traits were assessed as potential covariates of speciation rate.

Sample size varied substantially across different traits (n = 299 for skull phenotypic measurements to 9,591 for climatic niche). Below we summarize how we either measured or obtained these data.

2.2 Primary Traits

2.2.1 Body mass [primary]

Body mass was compiled from (*137*) and (*138*) for over 10,000 species and 97% of taxa in our phylogeny, as calculated from maximum body size based on clade-specific allometric equations. For species present in both publications, we retained the data from the more recent publication.

2.2.2 Snout-vent length (SVL) [primary]

We compiled SVL and total length data from (*137*, *138*), as was done for body mass. This dataset is not fully consistent however, with 100% of lizard taxa having SVL measurements, but snake taxa being a combination of SVL (7%) and total length (93%). We therefore took an imputation approach in order to convert total lengths to SVL for snake taxa.

We compiled body size ratios (SVL / total length) from a number of literature sources and museum databases, either as (1) measurements of total length and SVL from the same individual, (2) total length and tail length from the same individual, or as (3) relative body length or (4)

relative tail length. If any measurement records made mention of any damage to the tail, we ignored those records as the measurements could be unreliable.

If species were present in multiple data sources, we retained records in order of preference from: (1) (*139*), (2) (*140*) / (*141*) / (*142*), (3) UMMZ and (4) VERTNET. This ranking was made regarding perceived degree of data validation. If multiple records existed for a given species, we retained the one that was closest to the median body size ratio for that species.

We then divided our resulting dataset into a training dataset and a testing dataset. The training dataset (number of species = 1,112) was composed of all species records with body size ratio, and the testing dataset (number of species = 831) was the subset of the training dataset with SVL and total length measurements.

source	# species extracted	# species retained
Univ. of Michigan Museum of Zoology (UMMZ)	746	309
(*141*)	580	281
(*139*)	226	207
(*142*)	216	159
VERTNET	98	98
(*140*)	106	58

Using the snake clade from our phylogeny, we evaluated the degree of phylogenetic signal in body size ratio and found it to exhibit statistically significant signal (Pagel's lambda = 0.98, p-value << 0.0001). Using the R package Rphylopars (*143*), we then modeled body size ratio under a Brownian motion model of trait evolution and imputed values for missing species (982 of 2,094 snake species imputed).

To evaluate this approach, we conducted leave-one-out cross-validation, where we excluded each species one by one, fitting the Brownian motion model, and then comparing our imputed body size ratio to the known body size ratio. The imputed values were highly correlated with the known values (OLS regression R^2 = 0.78, p-value << 0.0001). Proportional error of imputed relative to known body size error had a mean of 1.00 and a standard deviation of 0.07 (fig. S42).

For all snake species for which we originally had total length but not SVL, we then estimated SVL based on total length and known or imputed body size ratios. Leave-one-out cross-validation of the ratios indicated that known SVL is very highly correlated with estimated SVL (OLS regression R^2 = 0.99, p-value << 0.0001).

2.2.3 Elongation index [primary]

We calculated the species elongation index by approximating squamates as an idealized cylinder with length as the species' SVL and volume as the species' mass (*49*).

If $mass\ (volume) = \pi * r^2 * SVL$

Then $elongation\ index = SVL\ /\ 2 * \sqrt{mass\ /\ (SVL * \pi)}$

This index spans the continuum of heavy-bodied, robust-limbed lizards, such as genera *Dipsosaurus*, *Sauromalus* and *Iguana* on the lower end of the spectrum, to long, slender-bodied snake genera such as *Pituophis* and *Pantherophis*, at the higher end of the spectrum.

2.2.4 Vertebral number [primary]

We compiled data on the number of presacral vertebrae for 2,324 species (*144–162*), in addition to using ventral and subcaudal counts of UMMZ snake specimens. Ventral and subcaudal counts are a reliable measure of vertebral number in snakes, correlating 1:1 in most species (*163*, *164*).

2.2.5 Skull morphology [primary]

Procrustes transformed coordinates for skull shape were acquired from (*9*). Most analyses of rate variation used all 40 coordinates. However, for a few visualizations, we first did a principal component analysis and then used the resulting PC1 and PC2 axes. These two axes explained 46.8% and 15.6% of the variation, respectively.

2.2.6 Trophic Mode [primary]

2.2.6.1 Diet data sources and recording formats

We compiled data from 751 populations of 345 lizard species from 33 lizard families. Most of the lizard diet data reflect primary data collected by the authors over more than five decades (70.4% of the dataset). We searched for additional diet records with a bibliographic search of online scientific databases from Google Scholar™ and Zoological Record™. Nearly all of the dietary records for individual lizards are associated with preserved voucher specimens in natural history collections. We used the keywords: lizard, diet, feeding habits, feeding ecology, and dietary aspects. Each observation recorded in the database describes the proportional utilization of a set of prey categories in the diet of a particular lizard species. Proportional utilization is calculated in four distinct ways based on (1) volume of prey in stomachs, (2) mass of prey in stomachs, (3) frequency of prey in stomachs, or (4) occurrence of prey in stomachs. Because of the heterogeneous nature of the data not all metrics are available for all species.

Data on snake diets were pulled from the open-source database SquamataBase described in (*163*). The data in SquamataBase were sourced primarily by keyword queries in academic search

engines and by systematic review of table of contents for herpetological journals that routinely publish data on squamate ecological interactions. The vast majority of observations in SquamataBase are from dissections of fluid-preserved museum specimens (64.9%) or from direct encounters of snakes in the field (35.1%). Each observation recorded in the database is a 2-tuple of counts describing a number of individual snakes of a particular species that ate a number of items of a particular food source: e.g., 12 *Thamnophis sirtalis* ate 34 toad tadpoles. Many of these observations have associated metadata (e.g., geographic location, age, sex, body size, etc.), but these additional data were not included in the analysis.

2.2.6.2 Diet data pre-processing

We conducted two pre-processing steps to map lizard and snake diet data onto a common recording format that could be used for subsequent analyses. First, all recorded prey items were mapped to a common set of 31 prey categories, including 15 vertebrate categories, 15 invertebrate categories, and one plant category (see fig. S18 & S19 for a full listing of these prey categories). These categories include many of the commonly used prey groups appearing in previous studies of squamate diet evolution (*7*, *24*, *25*), and the presence of dietary specialists for many of these prey groups indicates they are capturing relevant variation in squamate prey preferences.

After this first pre-processing step, the snake diet data consist of a standardized set of category counts describing the number of sampled snake stomachs that contained each prey category (or the number of sampled prey items in each category when the number of sampled stomachs was unavailable. This latter measure is generally very close to the number of sampled stomachs due to the tendency of snakes to consume a single prey item per meal). A second pre-processing step was necessary to bring the lizard data into the category count format. We did so by converting the lizard diet observations to "full stomach equivalents". This was achieved by multiplying the observed proportional utilization of a prey category by the number of lizard stomachs that contained prey and rounding to the nearest integer. With this step we are, in effect, imagining a hypothetical population of lizard stomachs – each full of a single prey – where each full stomach is sampled with probability equal to the observed proportional utilization of its given prey. Full stomach equivalents were calculated from observed prey utilization metrics in order of preference from: (1) volume, (2) mass, (3) frequency, or (4) occurrence.

2.2.6.3 Dietary niche estimation

Once lizard and snake diet data were brought into a common format, we used the category count model described in (*166*) to calculate a phylogenetically informed estimate of the dietary niche of each species while accounting for sample size variation. Briefly, this method postulates a number K of distinct dietary niche states and assumes their evolution is governed by a simple Jukes-Cantor-like model of change. Further, each dietary niche state corresponds to a latent multinomial distribution that describes the proportional utilization of different prey categories, and observed dietary count data are modeled as samples from these unobserved distributions. Fitting this model to data therefore results in an estimate of the posterior distribution of the dietary niche state (i.e., the latent multinomial parameters) for each species. The average of this posterior can be thought of as a phylogenetically smoothed version of the raw diet proportions.

For each $K = 20, 50, 100, 1000$ we ran a Gibbs sampler for 2^{15} iterations, recording a sample every 2^4 iterations for a total of 2^{11} posterior samples. Then for each $K = 20, 50, 100, 1000$ we assigned each species a continuous dietary niche state as the average over its posterior. Finally, we assigned each species an overall average continuous dietary niche state by taking the weighted average over $K = 20, 50, 100, 1000$ using the mean posterior probabilities of each run as weights.

We used these posterior averages or their log-ratio transformations for all subsequent analyses involving diet. Additionally, we used diet composition across all 31 prey categories in a principal component analysis. In a few visualizations, we show diet PC1 & 2 which explain 54% and 14% of the variation, respectively. Diet breadth was calculated using the inverse Simpson index of the estimated dietary proportions, and serves as a measure of the effective number of prey categories included in a particular diet.

As an additional check on our phylogenetic dietary niche state estimates, we performed a second set of estimates using Bayesian Hierarchical Clustering, a non-phylogenetic method that approximates a Dirichlet process mixture model (*167*). As before, each dietary niche state corresponds to a latent multinomial distribution and observed dietary count data are modeled as samples from these unobserved distributions. Species are assigned to niche states solely on the basis of their pattern of prey utilization without regard to phylogenetic relatedness. Analyses of changes in diet composition and rate of diet evolution were similar whether phylogenetic or non-phylogenetic methods were used (fig. S17).

2.2.7 Chemosensory Net Innovation Index (Ψ_{CHEM}) [primary]

Chemosensory innovation was measured on a semi-continuous scale from character codings at the family level (*5*), where a character had a value of zero (primitive condition), 1 or 2 (derived conditions). Only characters 1-7, 9 and 16 were considered as these were the most complete and allowed us to retain the greatest number of families in our analyses.

However, the number of traits is small; the extent to which parsimony changes can be treated as a metric character debatable; and the data extremely coarse – species were generally assigned a single combination of character states that was assumed to be fixed across the entire clade, e.g., all snakes receive a score of 12 following (*5*). Consequently, we consider this character insufficiently variable for evolutionary rate analysis but qualitatively reflective of innovation in chemosensory anatomy as Schwenk (*5*) coded these character states relative to inferred ancestral state.

2.2.8 Climate [primary]

19 Bioclimatic variables and net primary productivity were acquired from CHELSA-CLIM (*168, 169*). A climatic moisture index was also calculated based on CHELSA-CLIM input variables, using the envirem R package (*170*). Climatic variables were averaged across grid cells within each species geographic range polygon (*10*). We summarized across these variables using

a principal component analysis. A few analyses use climate PC1 & PC2 which explain 82% and 13% of the variation, respectively. When calculating climate niche rate, we retained the top six PC axes, which explain > 95% of the variance in the data.

2.3 Secondary Traits

2.3.1 Limbs and Digits [secondary, type 1]

We coded 6,890 species (all species in phylogeny except *Bachia talpa*) for number of limbs, number of digits on the forelimb, number of digits on the hindlimb, and number of digits overall. Number of digits were counted for one side only, such that counts ranged from 0-5 for individual sets of limbs and from 0-10 for overall digits. For lineages with variation in limb and digit states, we used the primary literature and an online database to code them (*82, 171–177*).

2.3.2 Cranial kinesis [secondary, type 2]

By any measure, most snakes have skulls that are vastly more kinetic than those of other lizards (*6*). However, we are unaware of any quantitative data on the relative degree of kinesis in snakes versus lizards. Quantitative data within squamates in general on the degree of kinesis is limited to a small number of species, so we chose to score species in a qualitative manner. All species in the phylogeny were coded for the presence or absence of mesokinesis, metakinesis, and hypokinesis based on clade-level assessments from (*6*), with a few exceptions where more detailed data were available. Note that our coding strategy allows individual species to exhibit multiple forms of kinesis. We created an ordinal ranking system where species were akinetic if they lacked all of these, low kinesis if one type of kinesis was present, mid kinesis if two types were present, and high kinesis if all three were present. Alethinophidian snakes – or, all non-blindsnakes which comprise 88% of snake diversity – have vastly more kinetic skulls than lizards due to their extensive streptostyly and other mobile skull elements (9, 165), as well as unilateral jaw mechanics attributable to the loss of the mandibular symphysis (*178*). We therefore added a fourth category, "hyperkinetic", to capture this general difference between alethinophidian snake and lizard skull mechanics. Scolecophidian snakes – also known as the blind snakes – exhibit a substantially less mobile skull than alethinophidian snakes, with multiple fused skull elements, and were excluded from the hyperkinetic category (*179*). Our coarse codings likely mask extensive variability within clades, but capture broad differences in kineticism between them (e.g. snakes have more kinetic skulls than geckos, which have more kinetic skulls than amphisbaenians).

2.3.3 Prehension mechanism [secondary, type 2]

Prehension refers to biomechanical aspects of the ingestion stage of feeding in lizards. A classic dichotomy in squamate biology involves taxa that manipulate prey items with their jaws (jaw prehension) versus those that manipulate prey with their tongue (lingual prehension) (*6*).

Cordylidae and Scincidae were coded as having both conditions. Thus, this trait is reflected by coarsely coded character state that has largely been applied to lizards exclusive of snakes and thus not directly comparable across groups. In addition, prehension as a concept does not map cleanly to snakes: it is one component of complex prey subjugation strategies that, in snakes, includes at least two major other innovations – venom and constriction.

2.3.4 Foraging Mode [secondary, type 2]

Foraging mode states (active or ambush) in snakes were coded at the familial level using state assignments from (*180*) with exceptions for individual species where known (e.g., *Acanthophis* is an ambush forager (*181*) in the active foraging Elapidae family). Foraging mode states for lizards were coded by family with information from (*182*), unless more specific information was available from a range of other references (*138*, *183–192*).

While this trait reflects classic splits in traditional snake lizard ecology, it is coarsely coded at the clade level and aggregates across extensive, biologically relevant variability within and among species. Further, it is a categorical, non-ordinal trait. Thus, we consider this as a secondary (type 2) trait.

2.3.5 Parity [secondary, type 2]

Parity mode was taken from (*193*), and updated with (*138*). This trait is coarsely coded as "viviparous" and "oviparous" and masks extensive biologically significant variation along a spectrum that includes lecithotrophy to complex placentation. Further, as coded, it is a categorical, non-ordinal trait. Thus, we consider this as a secondary (type 2) trait.

2.4 Biogeographic traits
Species-specific latitudinal centroid and range were extracted from the (*10*) range polygon dataset for squamates. Elevation was acquired from the GMTED2010 elevation dataset (https://www.usgs.gov/coastal-changes-and-impacts/gmted2010). Elevational variables were averaged across grid cells within each species' geographic range polygon (*10*).

3 Estimating speciation rates
Our analyses focused on "recent" speciation rates rather than net diversification rates, where "net diversification" is the difference between speciation (λ) and extinction (μ) rates. So-called "tip" speciation rates provide a lineage-specific estimate of the instantaneous rate of lineage splitting near the tips of a phylogenetic tree, conditional on a lineage's history up to that point in time. Typically, these estimators provide increased weight to a lineage's recent evolutionary history and downweight the contributions of deeper evolutionary events (*18*, *194*). In general, phylogenetic estimates of speciation rate are more reliable than those of extinction rate (*116*, *194*, *195*), and non-identifiability concerns regarding diversification rates are less acute for speciation rates near the present day (*196*).

Estimates of speciation rate can be biased by incomplete taxonomic sampling (*115*); we therefore generated fully imputed trees (all 10,757 taxa) to minimize the impact of sampling biases [discussed above; Section 1.5]. For our primary tree, we present average speciation rates across 100 imputed phylogenetic datasets. For our pseudo-posterior set of trees, we calculated speciation rate once for each tree. In all analyses of speciation rate and its correlates, we restrict inferences only to the set of 6,885 non-imputed taxa for which we have genetic data. However, the phylogenies on which those rates were computed included stochastic placements of the 3,872 unsampled taxa (see Section 1.5) and thus minimize the effects of incomplete sampling on the resulting rate estimates.

We used three different approaches to estimating speciation rate: the DR statistic (*18*), CLaDS (*197*, *198*), and BAMM (*199*). These methods give broadly congruent results, but make different assumptions about the nature of rate variation across phylogenies. BAMM assumes that rate shifts are infrequent and generally of large effect, but that lineages within rate regimes show little variation in rates. DR and CLaDS assume in effect that rates show near-continuous variation across the tree, but that changes are typically small. Comparative assessments of these methods have been provided by several recent studies (*194*, *197*, *200*) and have demonstrated that the relative performance of these methods depends on the unknown "true" nature of rate variation across the phylogeny, and for that reason we applied all three approaches.

The DR statistic (*18*, *201*) is a semi-parametric approach that estimates speciation rate as the weighted mean of the inverted branch lengths from a tip to its root. This measure thus more heavily weights recent splits compared to those deeper in the tree. We calculated the DR statistic using a custom script in R. CLaDS implements a model-based Bayesian approach in which speciation rates evolve across the phylogeny under a model where, after a speciation event, rates in each descendant lineage are drawn from lognormal distribution centered on the current rate and with a variance that is estimated from the data (*197*, *198*). We ran CLaDS on all 100 of the "fully sampled" phylogenies with all 10,757 tips as generated under the phylogenetic imputation scheme described above. For comparison, we also analyzed the 6,885 tip ML phylogeny (e.g., no phylogenetic imputation) with CLaDS while accounting for unsampled taxa using family-level sampling fractions. For both approaches (imputed trees; sampling fractions), we simulated the posterior distribution of CLaDS model parameters using Markov chain Monte Carlo (MCMC) until suitable convergence statistics were obtained, here measured by a Gelman statistic < 1.05 (*202*). CLaDS automatically ends the MCMC run when convergence is obtained. Thus, the number of simulated generations varied by run (range: 1,000 to 17,000 generations with a 25% burnin; the Gelman statistic ranged from 1.011 to 1.049). For one tree, we ran three independent CLaDS analyses, finding high concordance of rate estimates and thus suggesting that independent runs were indeed converging on similar posterior distributions.

We also analyzed speciation rates with BAMM (Bayesian Analysis of Macroevolutionary Mixtures; (*199*)), which assumes that lineages shift to new diversification rate regimes under a Poisson process. We used the primary tree with sampling fractions only for the BAMM analyses, due to the computational cost associated with running BAMM over multiple imputed phylogenies. Speciation and extinction rate priors were set to recommended values as estimated from the setBAMMpriors function in the BAMMtools R package (*203*); we specified a prior expected number of shifts of 10 and allowed speciation rate to vary through time within rate

regimes under a simple exponential decay model. To improve convergence for such a large phylogeny, we set MCMC tuning parameters *updateRateEventNumber* = 1 and *updateRateEventPosition* = 0.25, leaving all other parameters as default. We performed 10^8 generations of MCMC sampling for each of three replicate runs, sampling every 10,000 generations, and compared the resulting estimates of tip rates, log-likelihoods, and shift counts to assess convergence. After discarding a 10% burnin, the effective size of the log likelihood and of the number of rate regimes for the best performing of the three runs was 284.43 and 1,377.86, respectively.

We find high convergence across our three estimates of speciation rate (fig. S43) and across CLaDS run with imputed trees versus with sampling fractions (fig. S36).

4 Evaluating phenotypic diversification and speciation dynamics across the tree

4.1 Calculating innovation indices

For primary traits, we computed a simple phenotypic net innovation index (denoted by Ψ in the main text and elsewhere). The innovation index is defined on a per species basis as the distance between a species' measured phenotype and the maximum likelihood estimate (under Brownian motion) of the ancestral phenotype at the root of the squamate phylogeny. All distances are also standardized by their expected standard deviation under Brownian motion (i.e., the Mahalanobis metric). We calculated four innovation indices:

- Ψ_{skull}: distance to inferred skull composition of ancestor
- Ψ_{vert}: distance to inferred vertebral count of ancestor
- Ψ_{elong}: distance to inferred elongation index of ancestor
- Ψ_{diet}: distance to inferred diet composition of ancestor

We additionally include a chemosensory innovation index, Ψ_{chem}. Chemosensory innovation was measured as the sum of chemosensory character codings at the family level (*5*), where a character had a value of zero (primitive condition), 1 or 2 (derived conditions). Only characters 1-7, 9 and 16 were considered as these were the most complete and allowed us to retain the greatest number of families in our analyses.

As an alternative to our net innovation index, we also computed an index of net change along individual branches for the same traits, calculated as the absolute change in reconstructed states between parent and descendant nodes, to visualize where on the phylogeny net change in trait evolution is distributed (Fig. S7).

4.2 Estimating phenotypic rates

We use a DR-like statistic (*18*, *201*) to estimate recent rates of phenotypic evolution for individual species that we refer to as phenotypic tip rates (TR). The phenotypic tip rate TR_i for terminal node *i* is computed as

$$TR_i = \sum_{j=1}^{n_i} \frac{U_{i(j)} U_{i(j)}^T}{2^j}$$

where n_i is the number of ancestors on the path from tip i to the root, $\boldsymbol{U}_{i(j)}$ is a column vector of standardized contrasts for the j-th ancestor of tip i, and $U_{i(j)}{}^T$ denotes its transpose. Note that ancestors are numbered from 1 beginning with the most recent ancestor and ending with the most ancient ancestor on the tip-to-root path. Standardized contrasts are computed using the usual peeling algorithm (204). Note that for multivariate traits the tip rate calculation returns a matrix. In the main text, we reduce this matrix to a single value by taking the sum of the diagonal entries. The maximum likelihood estimate $\hat{\Sigma}$ of the evolutionary variance-covariance matrix can be recovered from the tip rates as

$$\hat{\Sigma} = \frac{1}{N-1}\sum_{i=1}^{N} TR_i$$

where N is the number of terminal nodes.

Because of the relationship between phenotypic tip rates and the evolutionary variance-covariance matrix, we expect that phylogenetic variation in the tempo of phenotypic evolution will be captured by these tip rates and visible as shifts in the value of the mean tip rate over different regions of phylogeny.

To validate this expectation, we simulated 10 multivariate trait datasets on the full squamate phylogeny for each of 0, 1, 2, …, and 10 rate-shifts for a total of 100 simulations. Each dataset had five trait dimensions. Rate-shift locations were chosen at random from among all internal nodes with at least five present-day descendants. The evolutionary variance-covariance matrix for each rate-shift was sampled independently from a Wishart distribution with 5 degrees of freedom and a diagonal scale matrix with scale parameter drawn uniformly from the interval $(0, \frac{1}{2\pi T\delta^2})$. Here, T is the maximum branch length in the rate-shift subtree and δ is a standard uniform random variable. This parameterization scales the height of the Gaussian transition kernel for each rate-shift to lie between 0 and 1 on all branches.

Simulation results are shown in Figure S44.

4.3 Phylogenetic regression
We ran a series of phylogenetic regressions to evaluate the relationship between phenotypic diversification and speciation rate dynamics (as described by CLaDS or BAMM estimated tip rates).

The general form of these regressions was

$$Y = XB + e$$

Where Y is a column vector of log-transformed speciation tip rates, X is a matrix of phenotypic predictors, B is a column vector of regression coefficients, and e is a column vector of phylogenetic residuals.

Prior to estimating regression coefficients, we pre-multiplied the left- and right-hand sides of the equation by a phylogenetic contrast matrix (205). This procedure leaves the regression

coefficients unchanged but removes phylogenetic correlation from the residuals, allowing us to estimate the coefficients using the technique of ordinary least squares. To compute the contrast matrix, we set all branch lengths to 1 and used the ordinary Felsenstein peeling algorithm as described by (*205*). This assumes the correlation structure in the logarithm of speciation tip rates is roughly Brownian. In particular, that the covariance between the logarithm of two tip rates is proportional to the number of shared branches between their most recent common ancestor and the root of the phylogeny. This branch length treatment aligns with the assumptions of the ClaDS model, which models lineage-specific speciation rates under the assumption that each speciation rate is a random draw from a constant variance log-normal distribution that is centered on the ancestral (log) speciation rate. As an additional check, we also performed a second set of regressions using the time-calibrated branch lengths.

We defined a total of 11 different regression models (Table S3) for different classes of phenotypic traits (including skull shape, diet, etc.). In general, we find very limited ability to explain speciation tip rates for the sets of phenotypic predictors examined, with the best model using CLaDS speciation rates achieving a phylogenetic R^2 of only 1% regardless of whether time-calibrated branch lengths are used or not.

4.4 Phylogenetic variance partitioning
One explanation for the limited ability of phylogenetic regression models to predict tip speciation rates is that only a small number of historical events are responsible for structuring variation in speciation rates and phenotypic traits. In such a scenario, phylogeny may still have substantial explanatory power because shifts in the mean structure of a trait are associated with particular clades (*19*). Canonical phylogenetic ordination (CPO) is a method designed to detect such a scenario. In its most basic implementation, CPO is an ordinary (least squares) regression that uses clade membership to predict variation in a dependent variable. Various selection techniques may be used to identify clades that should enter into the regression as important predictors. For example, in the original description of CPO a randomization technique was used to assess the statistical significance of individual predictors and to decide which clades to include in the final regression model (*19*).

To determine the extent to which deep history is responsible for structuring variation in the squamate trait dataset, we conducted a phylogenetic variance partitioning analysis (CPO) for speciation tip rates and for many of the different phenotypic predictors listed in Table S2. Formally, this analysis finds a set of K - 1 branches that partition the phylogeny into K subtrees such that the total sum of squared errors within each subtree is minimized. Equivalently, it identifies the K subtrees that best explain variation in the mean structure of a trait.

In contrast to the randomization technique used in the original CPO description, we used a greedy stepwise algorithm to find an optimal partition: using the optimal partition for $K = 2$, we find the optimal partition for $K = 3$, and so on up to some maximum number of subtrees. At each step, the optimal partition was defined to be the partition that explained the most variation (achieved the highest R^2) in the dependent variable.

25

Results of the variance partitioning are shown in Figure S14 & S15. In general, we find that a substantial fraction of variance in all examined traits is explained by typically just one or two subtrees from the larger squamate phylogeny, and that a node near the most recent common ancestor of snakes frequently explains the most variation. The only exception to this pattern was the climatic niche dataset.

4.5 Parametric models of phenotypic evolution

We used a stepwise procedure to fit multirate phenotypic models to primary traits in the dataset: multivariate skull morphology, multivariate climate, multivariate diet, mass, presacral vertebral count, and elongation index. For each trait, the general procedure entailed using a stepwise AIC procedure to find the configuration of rate shifts across the phylogeny that best explained the observed data. In each case, we assumed that trait distributions were generated by multiple rate regimes across the phylogeny, where each rate regime corresponded to a uniquely parameterized univariate or multivariate Brownian motion process. Thus, a "shift" on the phylogeny corresponded to a partial or full decoupling of the evolutionary rate matrices before and after the inferred shift event. We considered two distinct classes of shift models, which we refer to as *rate shift* and *rate-state shift* models, respectively. The rate shift and rate-state shift model differ in two important respects that are especially significant in the case of multivariate data. First, in the *rate shift* models, the multivariate rate matrices are still constrained to be scalar multiples of one another. Thus, the *relative* variances and covariances do not differ across the phylogeny, but regimes differ from one another by a scaling factor. In contrast, the *rate-state shift* models involve full decoupling of all parameters associated with different shift regimes: all covariances and variances for the evolutionary process are estimated separately for each regime. Moreover, under the *rate-state* shift models, the ancestral state for a focal clade is a parameter that is estimated from the data and which is fully decoupled from any state histories across earlier (ancestral) portions of the phylogeny.

The *rate-state shift* model thus accommodates "jumps" in phenotypic space; similar dynamics have been modeled by previous studies using Lévy process models (*12, 206*) and by allowing high rates to occur on single branches (*37, 207*). For the *rate-state* shift model, we implemented the "censored" multi-regime Brownian motion model as described by (*208*); this approach is nothing more than a standard multi-regime Brownian motion process (*119, 209*) but where the ancestral state for each rate regime is a free parameter to be estimated separately from the data. The censored framework affords a number of analytical and computational advantages, especially for large multivariate datasets. The primary advantage arises from the fact that the marginal likelihood of each shift can be computed from the matrix of independent contrasts for the corresponding subset of taxa assigned to that regime, independently from all other taxa (and associated rate regimes) across the phylogeny.

Note that the *rate-state* shift models require many more parameters than the *rate shift* models. For instance, a rate shift model for a multivariate trait with 10 substates (e.g. 10 diet categories) and with three shifts would have a total of 10 ancestral state parameters plus 90 variance and covariance parameters for the ancestral rate matrix, plus one scaling parameter for each of the three derived regimes (10 + 90 + 3 = 103 parameters). However, this same trait and shift configuration for the rate-state shift model would have 380 parameters: 10 ancestral states plus 90 variance and covariance terms, for each of the four regimes. Although this seems like an

extreme penalization for rate-state shift models, the parameter-rich rate-state shift models fit the observed phenotypic data better in all analyses that we performed (fig. S16).

For each trait dataset, we initially fit a single-process Brownian motion model to the entire phylogeny. We then fitted an increasingly complex set of rate shift and rate-state shift models to the tree, maximizing the log-likelihood for each model. For a model with $K = 1$ rate shifts, we simply identified the branch (= shift location) giving the highest log-likelihood. However, we added complexity in stepwise fashion such that, for a model with K shifts, we searched for the shift location that best explained the data while holding fixed the locations of the previously identified $K-1$ shifts. We recognize that stepwise approaches can only identify a constrained subset of possible models, because the stepwise procedure itself reduces the size of the set of candidate models that can be considered. However, it was not feasible to implement a non-stepwise procedure, because of the vast differences in the size of model spaces between stepwise and non-stepwise approaches. For a model with K shifts and M possible shift locations, the number of models to consider under the stepwise procedure is simply $M + (M-1) + (M-2) + \ldots (M-K+1) = KM + K(K-1)/2$. However, the non-stepwise approach has $M(M-1)(M-2)...(M-K+1)$ models, and thus involves a relative complexity increase on the order of $MK-1$. We also found that it was computationally infeasible to consider all possible branches across the phylogeny as shift locations (e.g., large M in the preceding calculations). We therefore reduced M by restricting the set of permissible shift locations to only those branches present in a reduced phylogeny that included crown representatives of each subfamily-level clade in the full squamate phylogeny. This reference phylogeny included 222 possible shift locations. For each dataset, we considered up to $K = 10$ shifts for both rate shift and rate-state shift models.

All analyses except skull morphology used log-transformed variables; skull traits were the vector of Procrustes coordinates for each taxon and were thus scaled, centered, and translated prior to analysis. For diet, the "traits" at the tips of the tree were the multinomial distributions (tip states) as inferred under a Dirichlet multinomial model. Because the diet states represent proportions under a simplex constraint, we chose one (of 31) diet categories as a reference and normalized the remaining 30 categories by dividing through by the reference value. Thus, each of the remaining states was an index of resource utilization relative to the reference category. These normalized values were then log-transformed.

One high-dimensional dataset (skull; 40 variables) faced additional challenges during model optimization. We were unable to numerically compute the log-likelihood of the data due to singular covariance matrix errors arising from high collinearity between some variables. We therefore repeated the full inference procedure on 50 random subsets of the complete dataset, in each case choosing 10 random variables (e.g., 10 columns of the data matrix). Importantly, despite some variation in numerical values of log-likelihoods and corresponding AICs (fig. S16), we found that the inferred shift locations were very similar across these random data subsets.
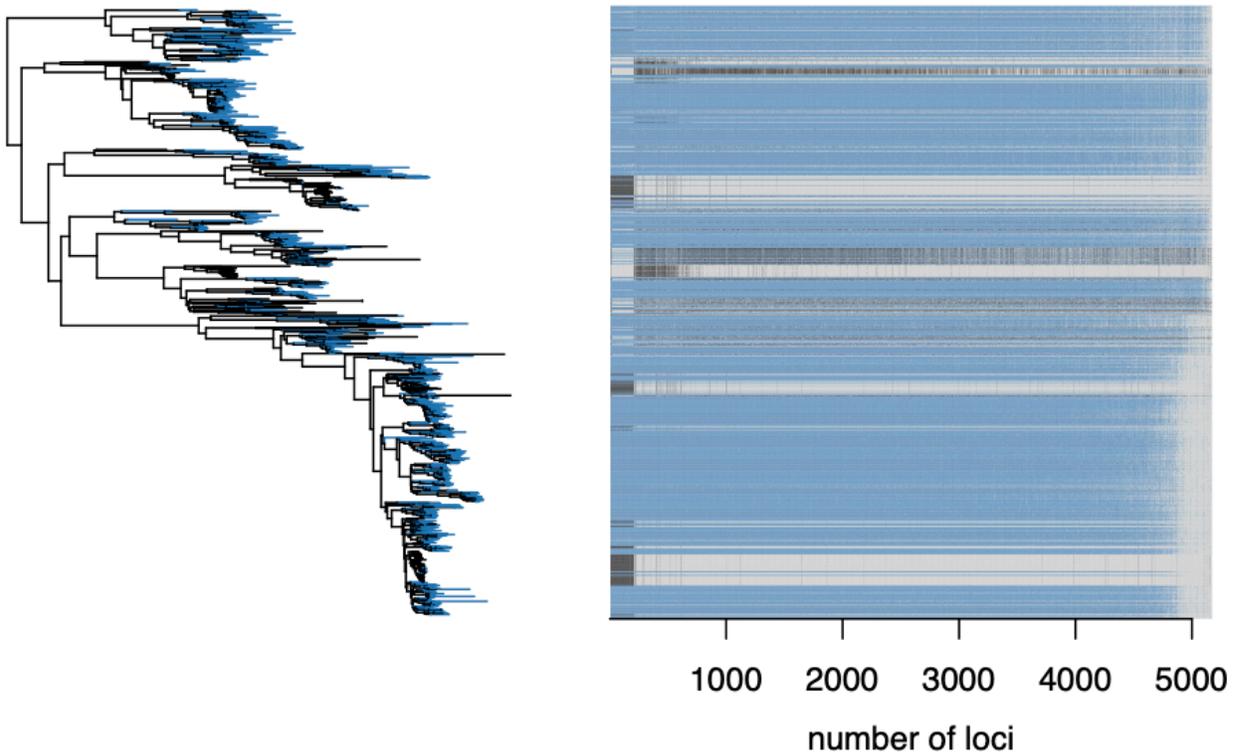
Figure S1: Completeness of phylogenomic data matrix. The tree shows the phylogenomic backbone with tips colored if they were newly collected (blue) or previously published (black). The locus matrix ranks loci (n = 5,180) by completeness across individuals; colors follow the tree. Our data matrix was fairly complete; on average, any given locus was sequenced for 75% of individuals. However, previously published data were less complete because they were only sequenced for one marker type (either anchored hybrid enrichment [AHE] or ultraconserved elements [UCE]).
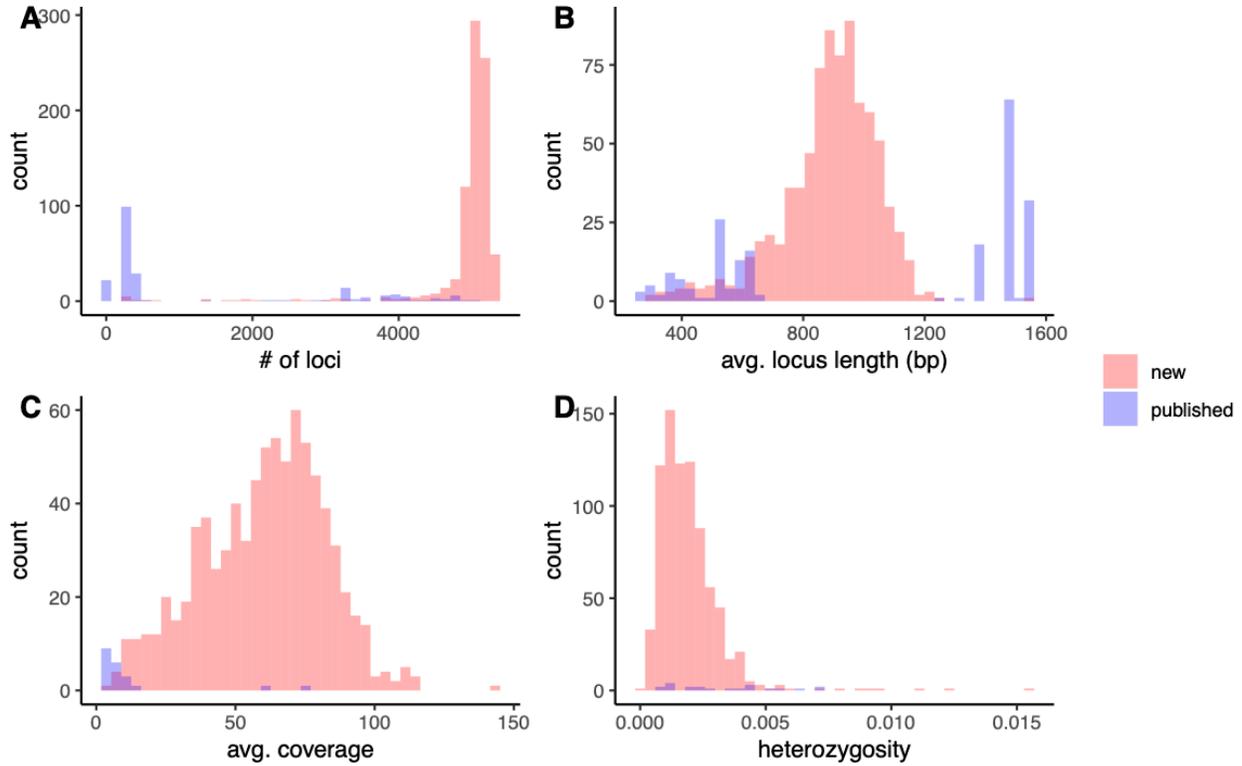
Figure S2: Quality of phylogenomic data per individual as measured by (**A**) average number of loci, (**B**) average length of locus, (**C**) average coverage, and (**D**) average heterozygosity. High heterozygosity can result from contamination, DNA damage, or high levels of collapsed paralogs. Shown are distributions for newly collected (n = 808) and previously published data (n = 210; Data S1) included in our phylogenomic constraint tree. Our newly collected data were of high quality. On average, we collected 4,945 loci per individual at 888 bp length, and read coverage was 59.9x across loci.
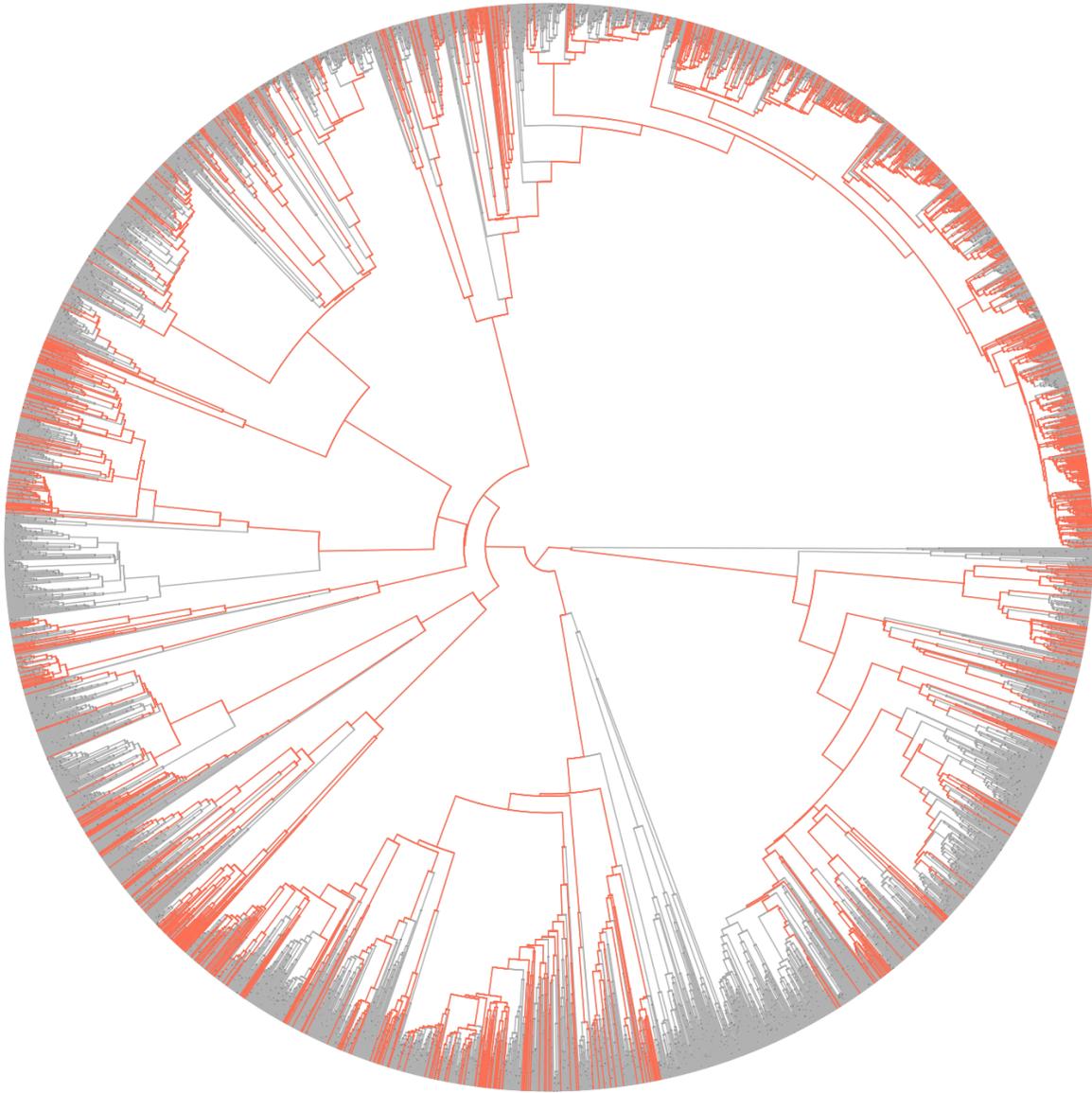
Figure S3: Our primary phylogeny (6,885 species); branches constrained by our phylogenomic constraint are colored orange. Our phylogenomic constraint consisted of 1,018 species inferred for nearly 5,000 loci. Our constraint tree spanned most higher-level relationships and many within-family and within-generic relationships, as well.
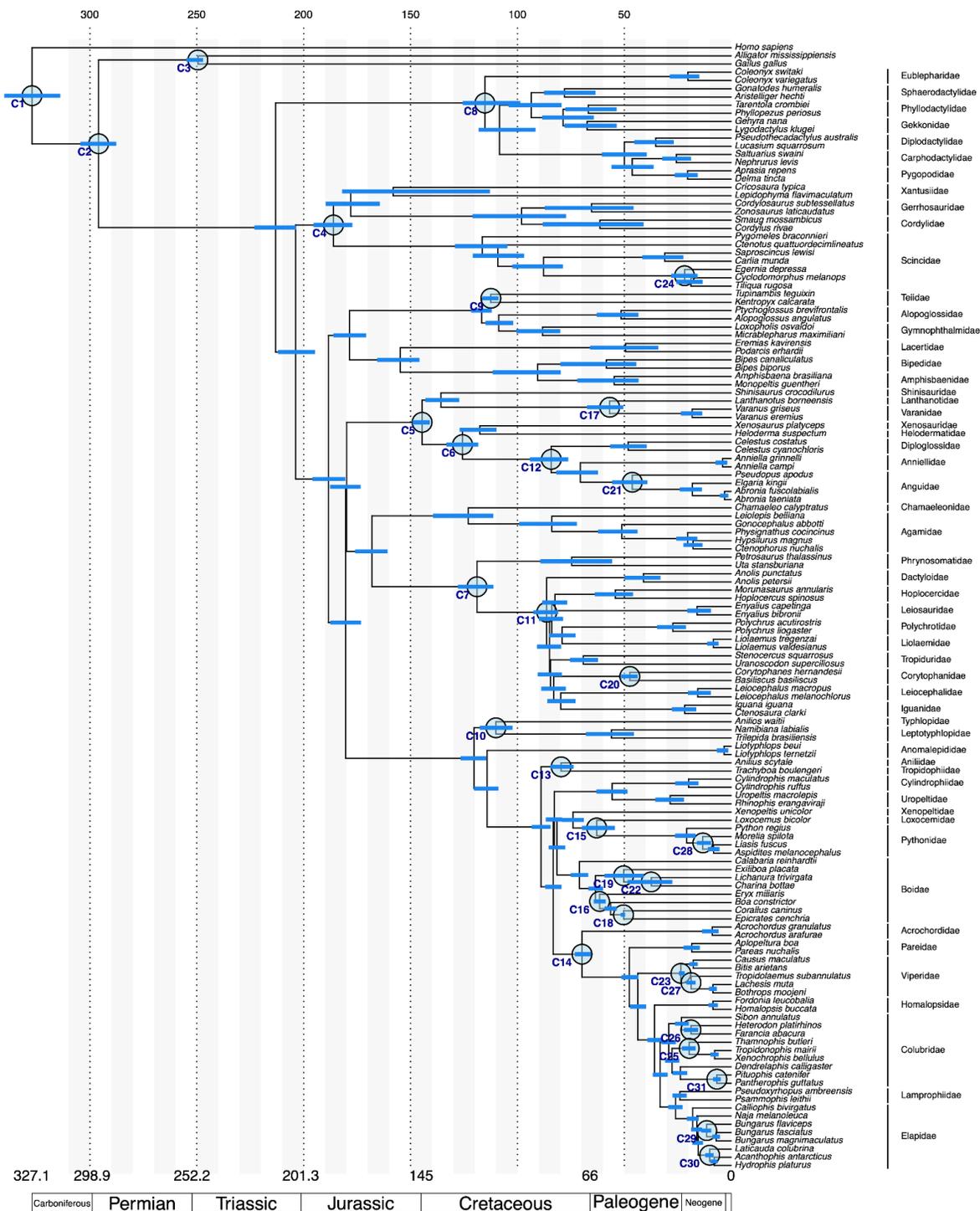
Figure S4: The genomic time-calibrated tree with 5-95% divergence time distributions (horizontal blue bars) and fossil-calibrated nodes (circles). Fossil-calibrated node labels correspond to Table S1, which contains additional information on the fossils used and their sources. We subsampled our full phylogenomic tree to 134 tips that spanned 31 fossils, and then we inferred an ultrametric tree using MCMCtree. Our fossil calibrations span both the taxonomic and temporal breadth of the squamate tree.

Hylonomus lyelli
Amniota

Protorosaurus speneri
Sauria

Xilousuchus sapingensis
Archosauria

crown squamata

Paramacellodidae
Scincoidae

Dorsetisaurus purbeckensis
crown Anguimorpha

Ptilotodon wilsoni
Teiidae

Primaderma nessovi
Heloderma+Anguis+Anniella+Xenosaurus

Cretaceogekko burmae
crown Gekkota

Odaxosaurus roosevelti
Anguidae

Australophis anilioides
Aniliidae+Tropidophiidae

Saichangurvel davidsoni
Pleurodonta

Boipeba tayasuensis
typhlopoid–leptotyphlopid divergence

Titanoboa cerrejonensis
stem Boinae

Procerophis sahnii
Colubroidea+(Acrochordus+Xenodermatidae)

Afairiguana avius
Anolis+Gambelia

32

Corallus priscus
Corallus+(Chilobothrus+Epicrates+Eunectes)

prior
effective prior
posterior

density

mya before present

Egernia gillespieae
Egernia

prior
effective prior
posterior

density

mya before present

Saniwa ensidens
Varanus+Lanthanotus

prior
effective prior
posterior

density

mya before present

Natrix aff.longivertebrata
crown Natricidae

prior
effective prior
posterior

density

mya before present

Geiseltaliellus maarius
Corytophanes+Basiliscus

prior
effective prior
posterior

density

mya before present

Crotalinae gen. & sp. indet. A
stem Crotalinae

prior
effective prior
posterior

density

mya before present

Messelopython freyi
stem Pythonidae

prior
effective prior
posterior

density

mya before present

Morelia riversleighensis
Morelia+Liasis

prior
effective prior
posterior

density

mya before present

Calamagras weigeli
Ungaliophiinae+Charininae

prior
effective prior
posterior

density

mya before present

Paleheterodon tiheni
Heterodon+Farancia

prior
effective prior
posterior

density

mya before present

Ophisaurus sp
Anguinae

prior
effective prior
posterior

density

mya before present

Pantherophis sp.
Pantherophis+Pituophis

prior
effective prior
posterior

density

mya before present

Vipera aspis complex
Crotalinae+Viperinae

prior
effective prior
posterior

density

mya before present

Bungarus sp.
genus Bungarus

prior
effective prior
posterior

density

mya before present

unnamed
Charina+Lichanura

prior
effective prior
posterior

density

mya before present

Incongruelaps iteratus
Laticauda+Oxyuraninae

prior
effective prior
posterior

density

mya before present

33

Figure S5: Specified prior, effective prior and posterior distributions for all fossil-calibrated nodes. Dotted vertical lines indicate minimum and maximum (if available) fossil ages. When both minimum and maximum ages were available, the specified prior was defined as a uniform distribution with soft bounds. When maximum age was not available, the specified prior was defined as a log-normal distribution with soft bounds. Four replicates of the MCMCTree analysis were run and were strongly correlated, and each replicate is shown as a separate posterior distribution.
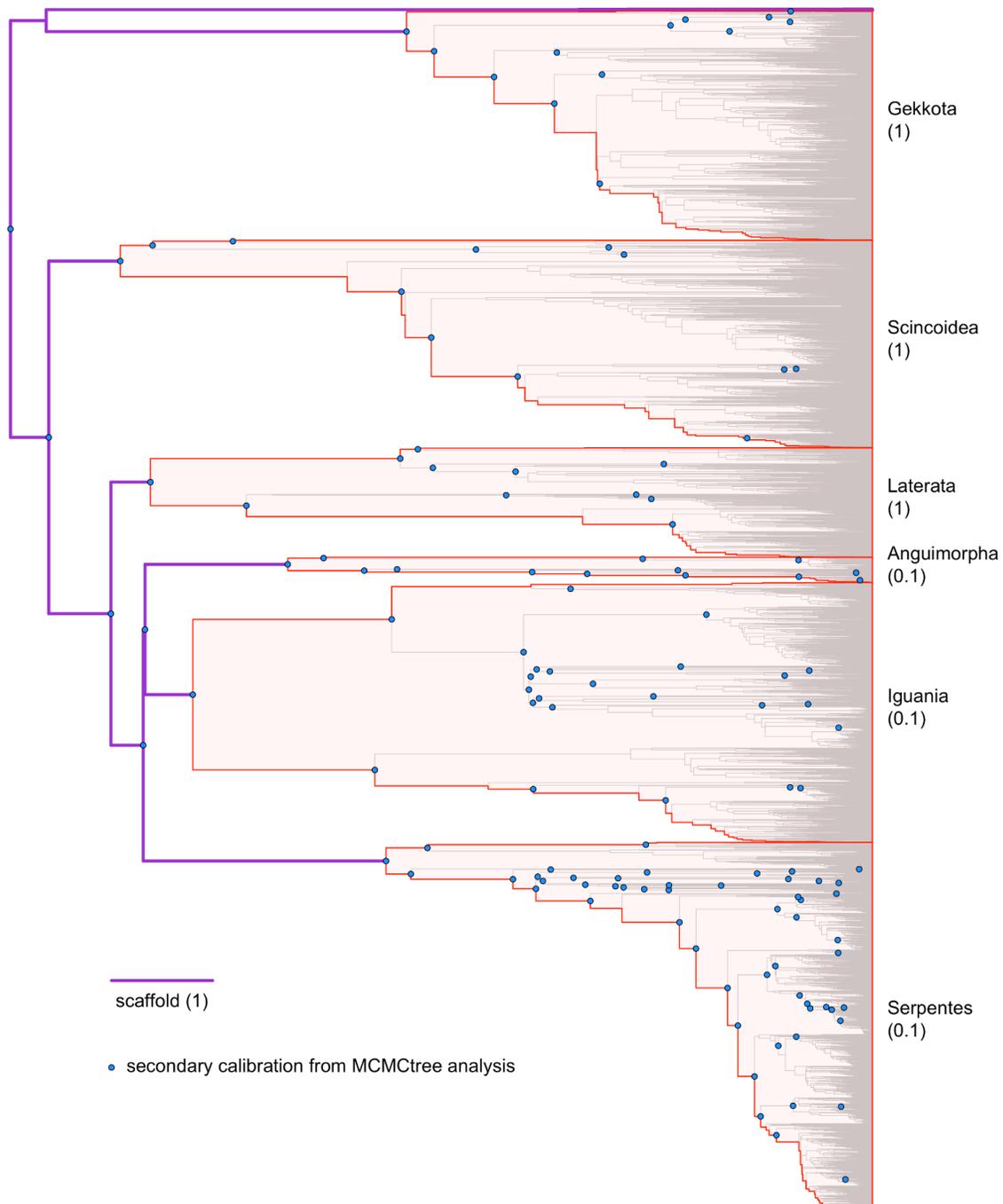
Figure S6: Calibration strategy for our genetic tree (6,885 species). To account for potential molecular clock heterogeneity, we time-calibrated seven clades of the full tree separately using TreePL and then merged those ultrametric trees together. Clades outlined in red were independently time-calibrated, and the best-fit treePL smoothing parameter is shown in parentheses. Dark purple branches show the phylogeny of major clades that was also time-calibrated separately for the purpose of merging the major clades. Nodes with secondary calibrations (as inferred with MCMCtree on a subsampled phylogenomic alignment) are indicated with blue circles at nodes.
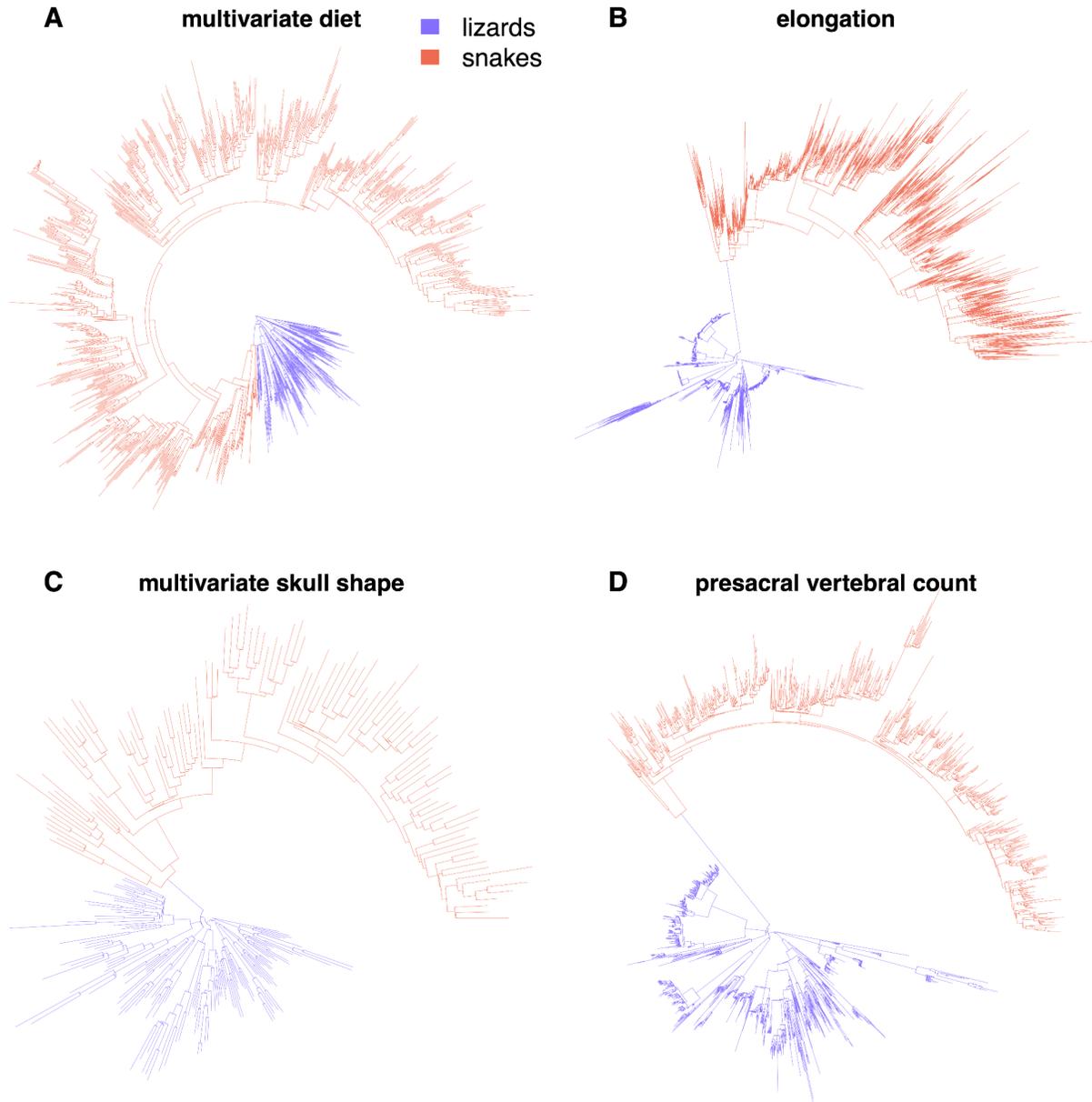
Figure S7. Evolutionary dynamics of four of the major traits, presented as absolute, branch-specific change along individual branches (e.g., absolute step change). Here, branches have been rescaled to the absolute amount of change that is inferred to have occurred between a node and its descendant nodes, under Brownian motion. We see that in all cases a great degree of change has occurred near the origin of snakes. Within snakes, there is also a large amount of change, as can be seen by the relatively long branches within the group, as compared to lizards.
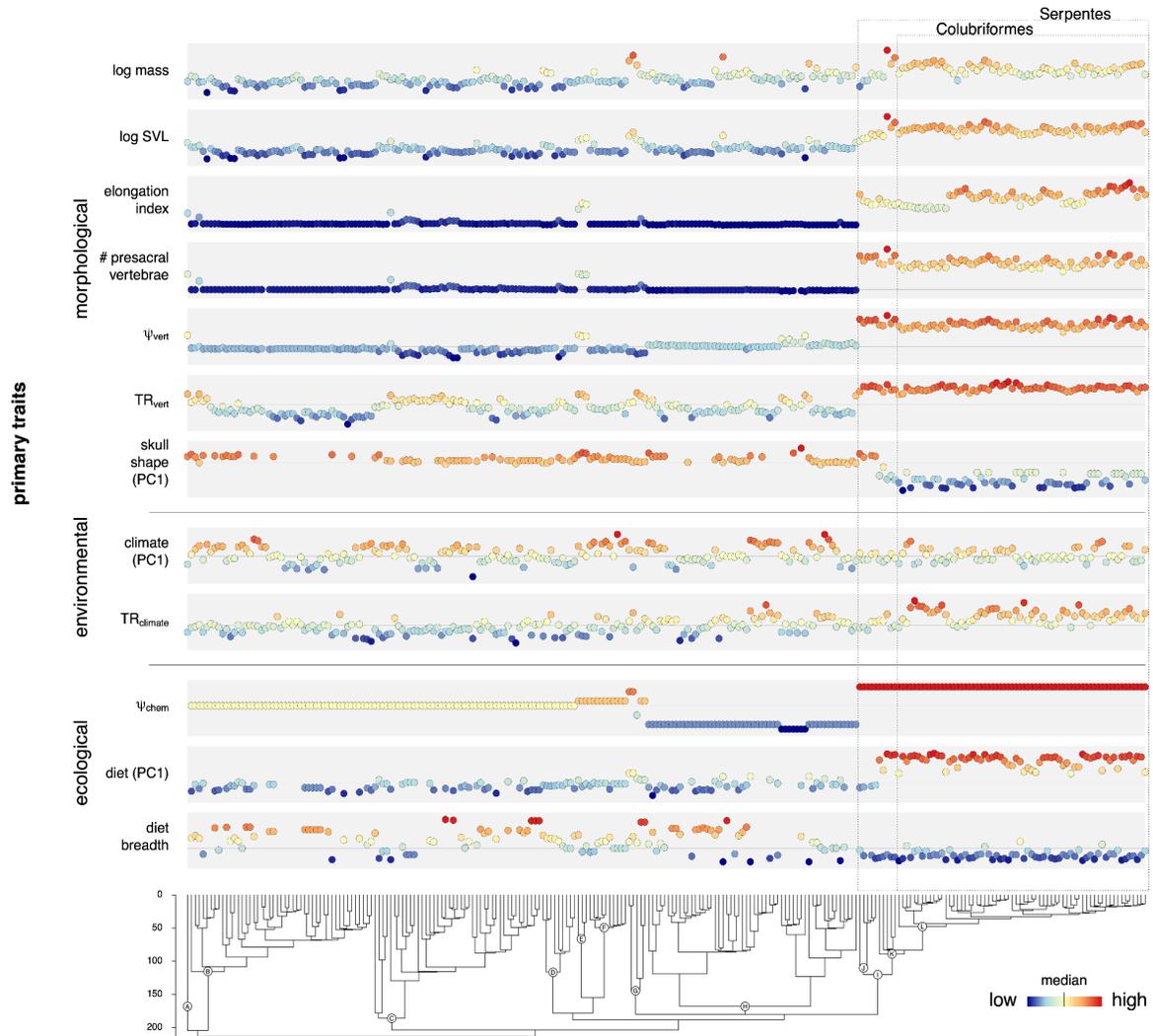
Figure S8: Phylogenetic structure of additional primary traits (see Table S2). Weighted averages of the traits are shown alongside a phylogeny reduced to 250 representative taxa, evenly sampled from the tree tips; a full phylogeny showing all taxa is shown in fig. S10. Squamates capture a wide range of trait diversity, and closely related clades often differ substantially for a given trait. Node labels are defined as in Figure 1 of the main text. Note that this figure presents trait values, rather than rates, and is thus distinct from the information shown in Fig. 1.
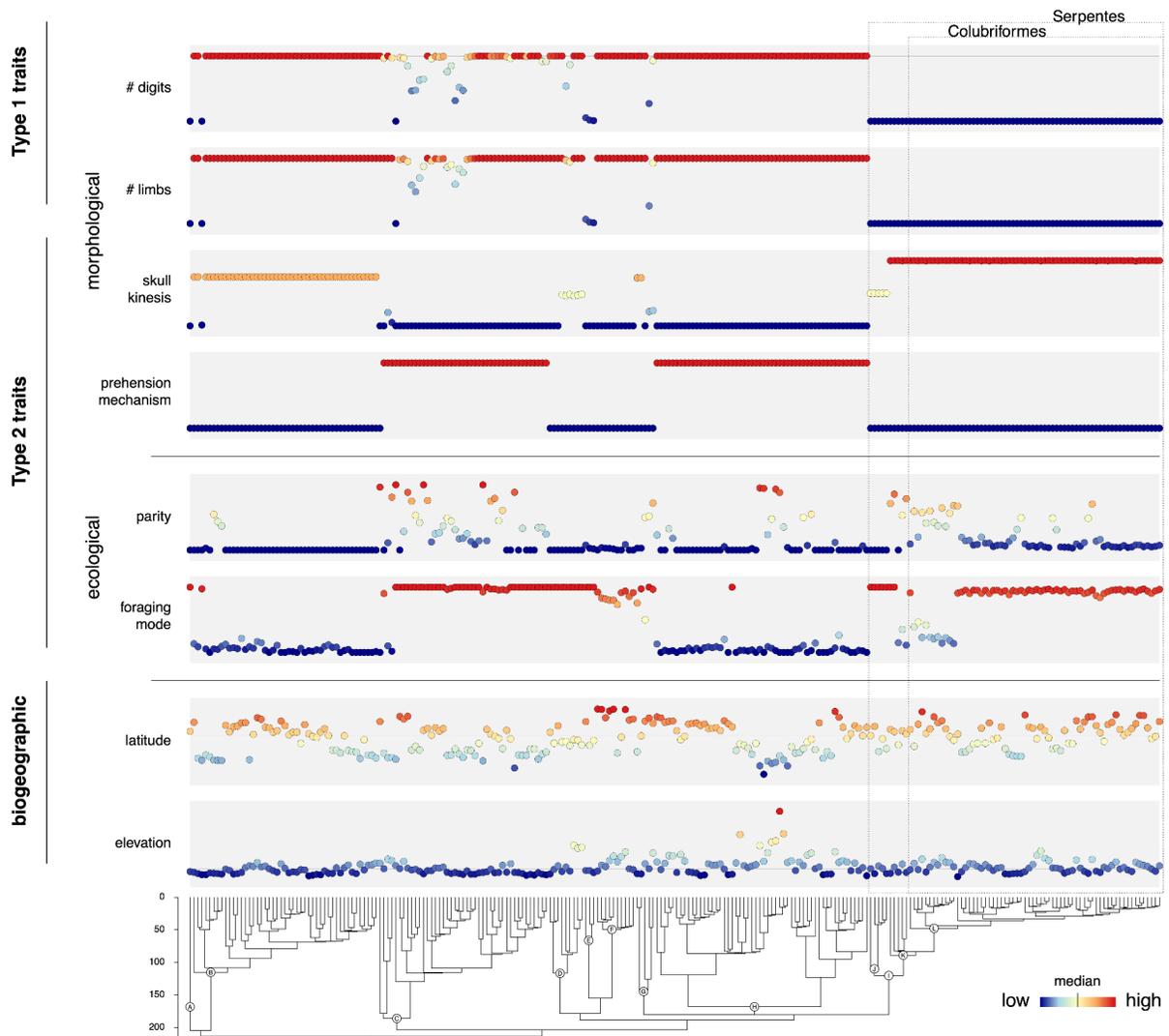
Figure S9: Phylogenetic structure of secondary and biogeographic traits (see Table S2). See Figure S8 caption above for figure details. Parity shows percentage of taxa that are viviparous. Prehension mechanism shows percentage of taxa that use lingual or both lingual and jaw prehension. Foraging mode shows percentage of taxa that exhibit active, herbivorous or mixed foraging (e.g., not ambush predators). Skull kinesis shows the average of the combined ordinal ranking. Node labels are defined as in Figure 1 of the main text.
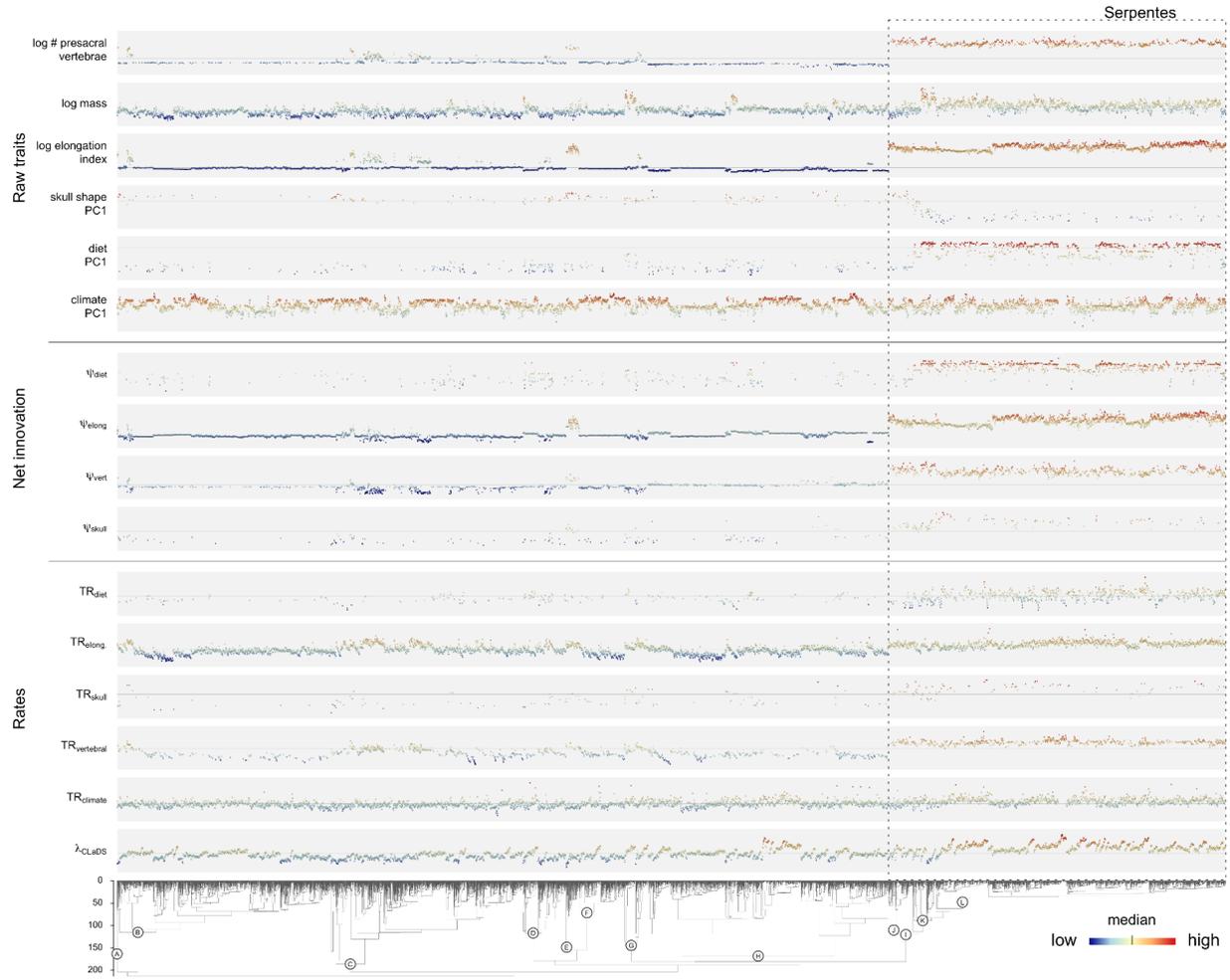
Figure S10: Species-level phylogenetic structure for ecomorphological traits. The tree and data are not subsampled or averaged. Squamate species capture a wide range of trait diversity, and closely related species often differ substantially for a given trait. Much of this diversity is captured in the Serpentes clade (snakes), which exhibits elevated rates of net innovation (Ψ), trait evolution (TR), and speciation (λ_{CLaDS}) relative to the rest of squamates. Node labels are defined as in Figure 1 of the main text.
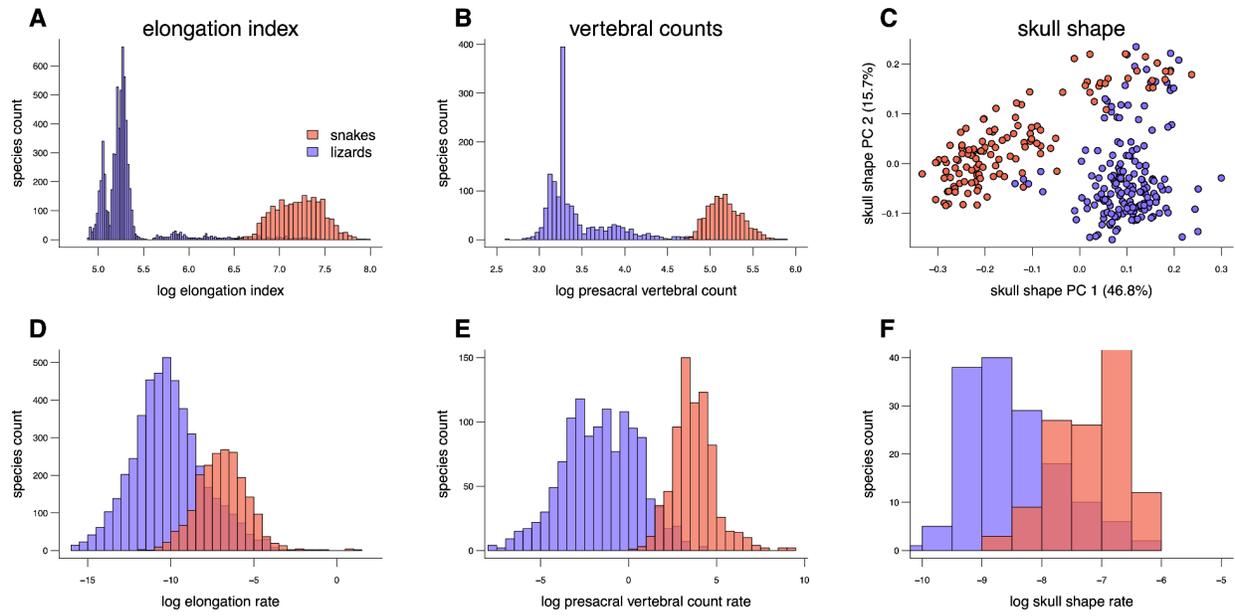
Figure S11. Distributions of snakes (red) and non-snake lizards (blue) for elongation index (**A, D**), presacral vertebrae count (**B, E**) and skull shape (**C, F**). Top row shows trait values; bottom row shows rates of trait evolution. Snakes and lizards show largely non-overlapping distributions for many trait values and rates, with snakes exhibiting higher rates of trait evolution than lizards.
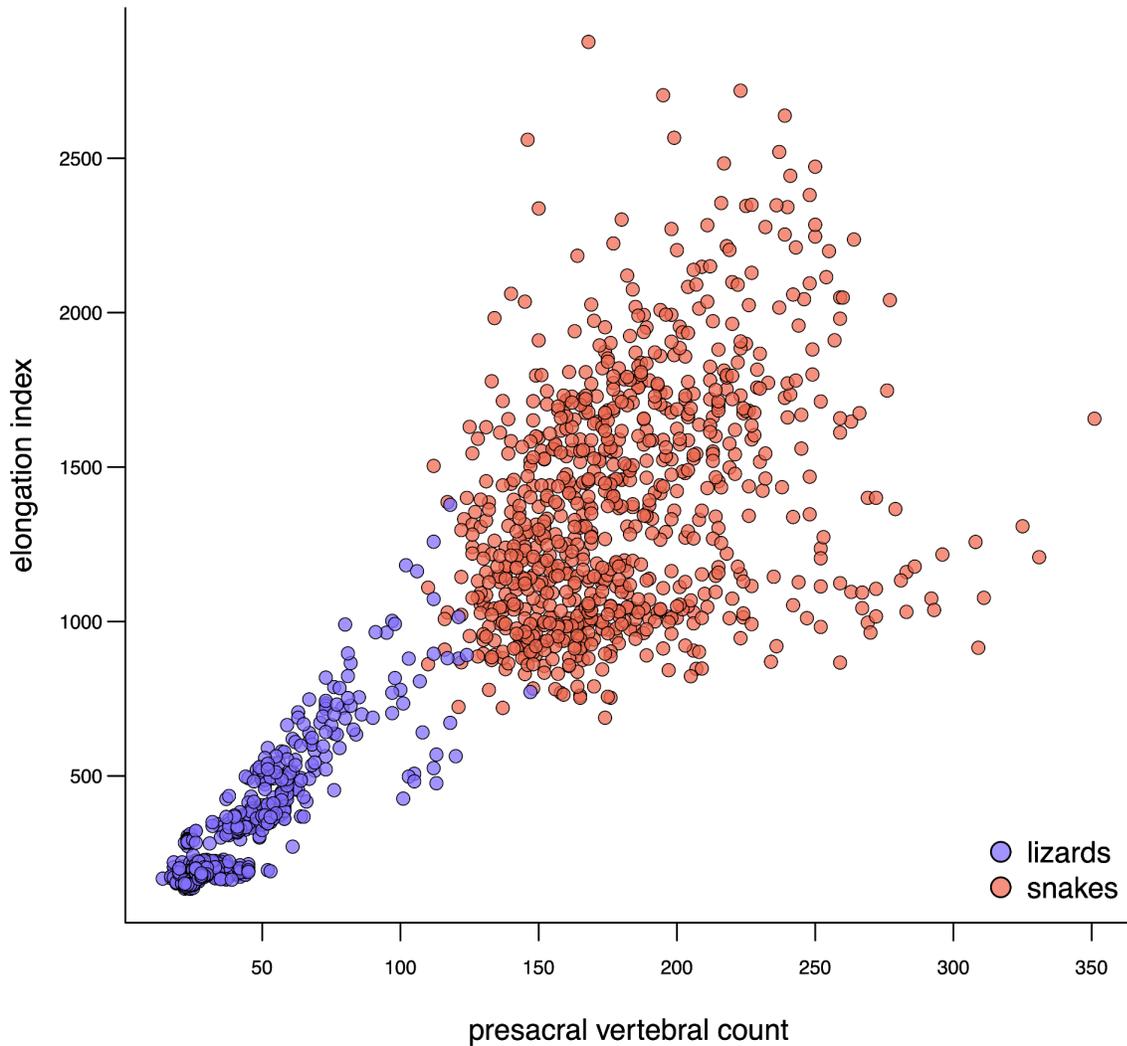
Figure S12: Relationship between the elongation index (as derived from SVL and mass) and the number of presacral vertebrae. Snakes exhibit greater elongation and greater vertebral counts, but also great variance in this relationship, relative to non-snake lizards. The increased variance in this relationship is consistent with our estimates of faster evolutionary rates for both of these traits (Fig. 1), and for a large jump in phenotype along the branch leading to extant snakes (Fig. 2, fig. S15).
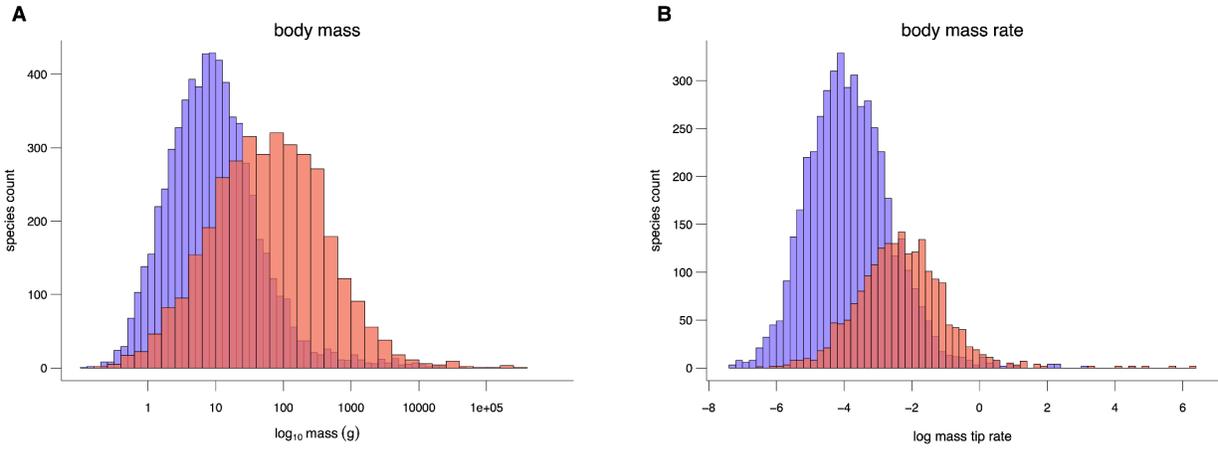
Figure S13: Distribution of non-snake lizards (blue) and snakes (red) for log10-transformed (**A**) body mass and (**B**) its associated tip rate. Squamates as a whole exhibit a large range in body mass, and lizards and snakes overlap in body mass considerably. Snakes exhibit a slightly faster rate of body size evolution as defined by body mass.
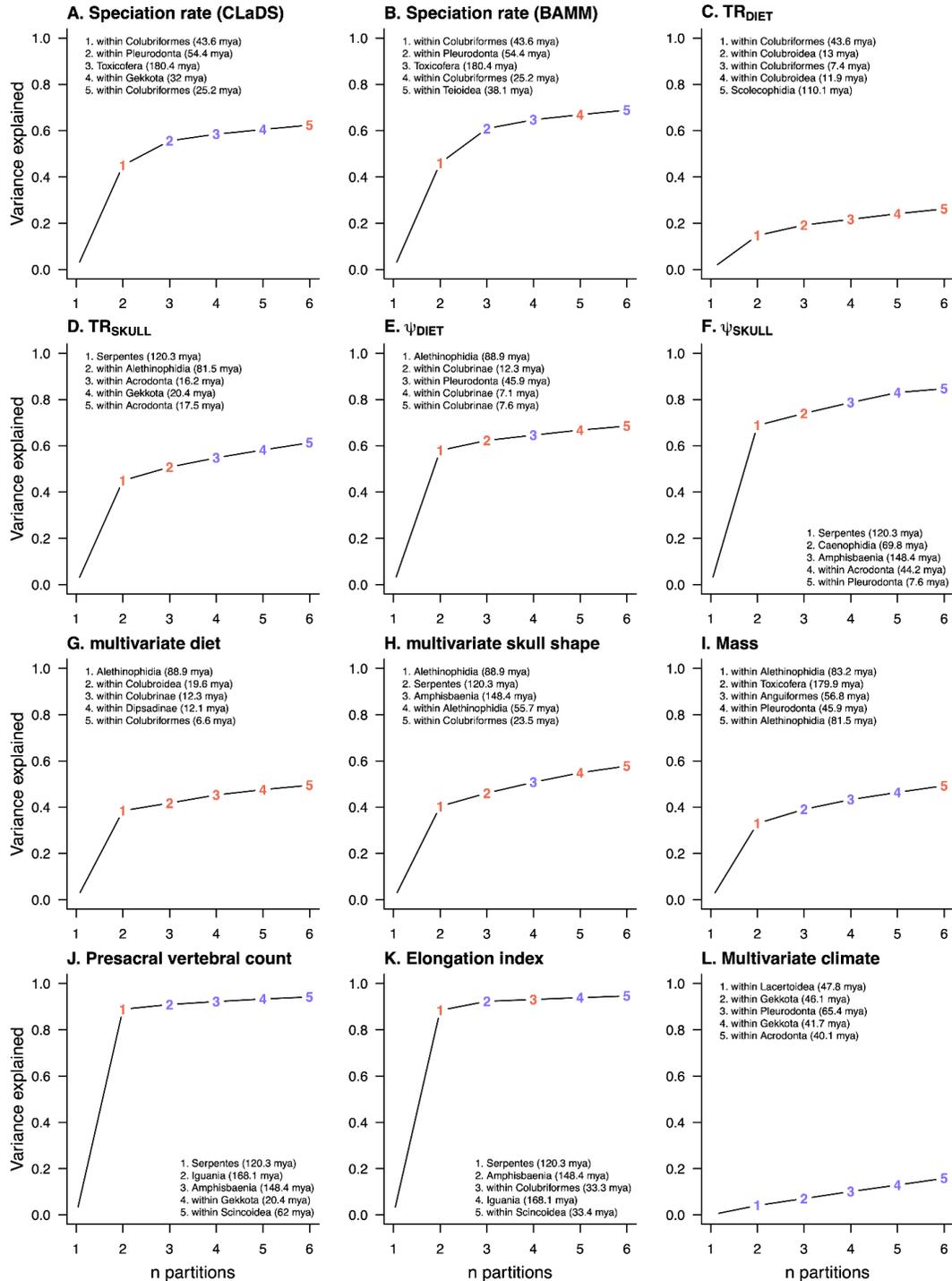
Figure S14: Variance partitioning for diversification rates and main ecomorphological traits evaluated in this study. For each trait, we identified (using an unsupervised approach) phylogenetic partitions (or clades) that explain a significant proportion of the variance in species phenotypes. Plots show how the percent of total variance increases with an increasing number of phylogenetic partitions. Partitions are colored blue for non-snake lizard nodes and red for snake nodes. For all traits but climatic niche, a deep node in snakes explains the most variance in traits.
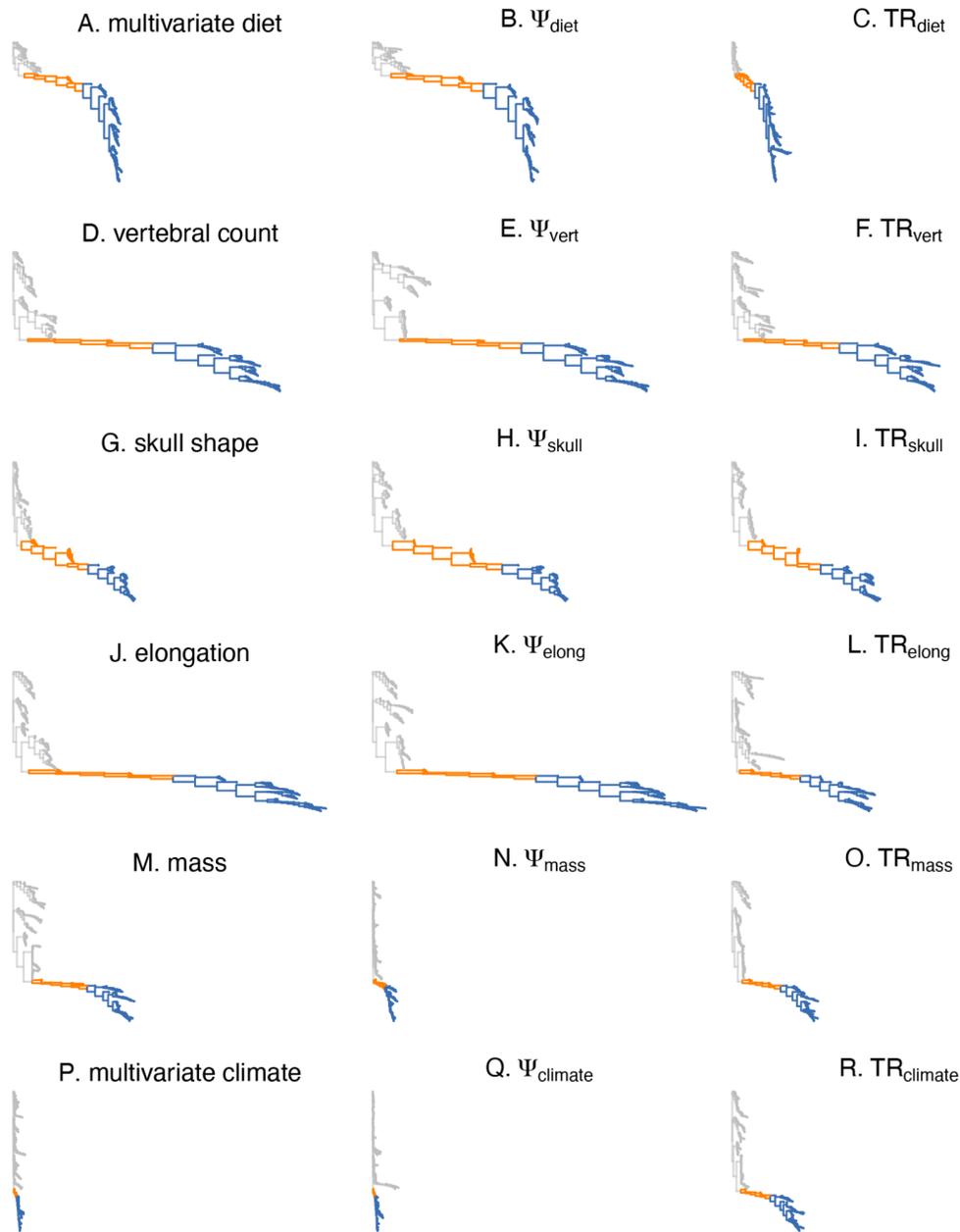
Figure S15: Variance partitioning across six primary traits, their innovation indices, and rate estimates (as shown in Figure 1). For each trait, and for each node, we calculated the R^2 explained by splitting the tree into two partitions at that node. Tree branch lengths reflect nodal R^2 values, and all trees are shown on the same scale. Gray branches show all non-snake lizards; blue (Colubriformes) and orange (non-Colubriformes) branches show snakes. For some traits like climate, trait values are so phylogenetically labile that any one clade explains only a negligible proportion of the total trait variation. However, for most other traits, creating just a single partition between snakes and all other squamates explains a significant amount of the variation in a trait (>80%).
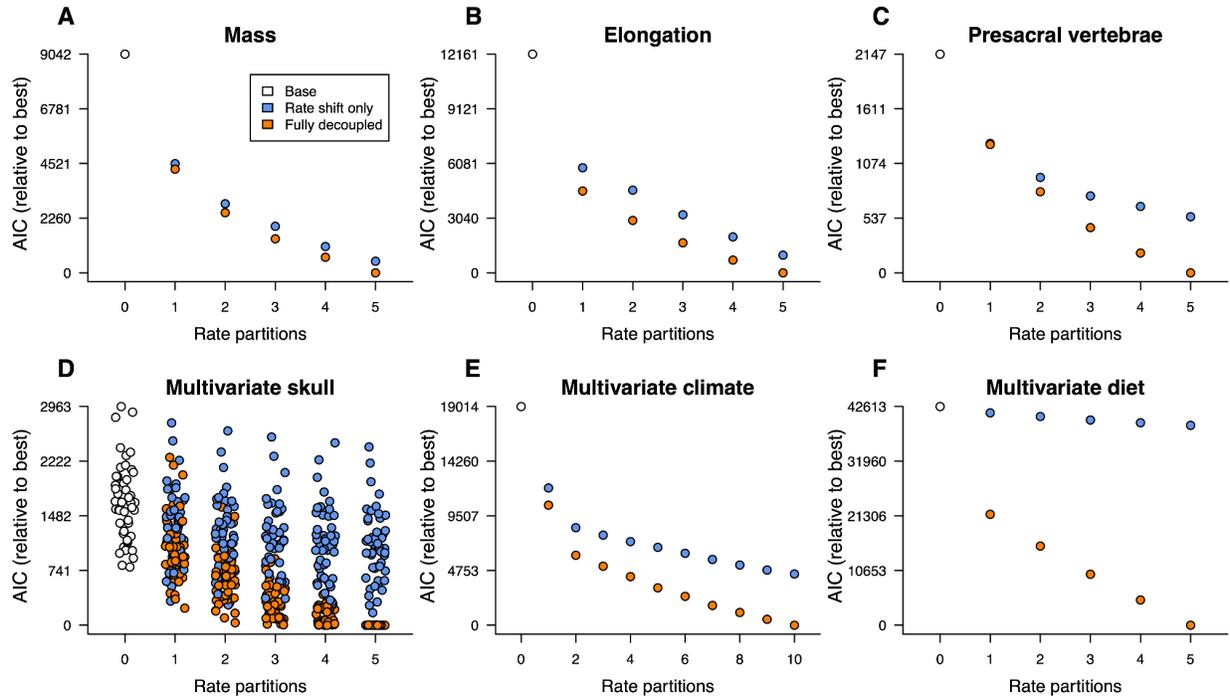
Figure S16: Comparison of different models of evolution and different numbers of phylogenetic rate partitions for the main ecomorphological traits evaluated in this study: (**A**) mass, (**B**) elongation index, (**C**) presacral vertebrae, (**D**) multivariate skull shape, (**E**) multivariate climate, and (**F**) multivariate diet composition. Models include a base single-partition tree-wide Brownian motion (BM) model, a *rate shift* BM model (covariances and variances scalar multiples of the base) with increasing numbers of partitions, and *a rate-state shift model* fully decoupled BM model with separate means and covariance terms. The skull shape dataset (**D**) consisted of 40 Procrustes-transformed variables, so we repeated the model fitting procedure 50 times with a random subset of 10 skull shape variables each time. Across these traits, the fully decoupled model is always a better fit than the rate-shift only model. Further, adding additional rate partitions typically improved the fit of the model as measured by Akaike Information Criterion (AIC), but the biggest improvement typically came from the first partition. For all traits but multivariate climate (**E**), this partition occurred at the root of snakes or within a deep node in snakes (see Figure 2 for location of partitions).
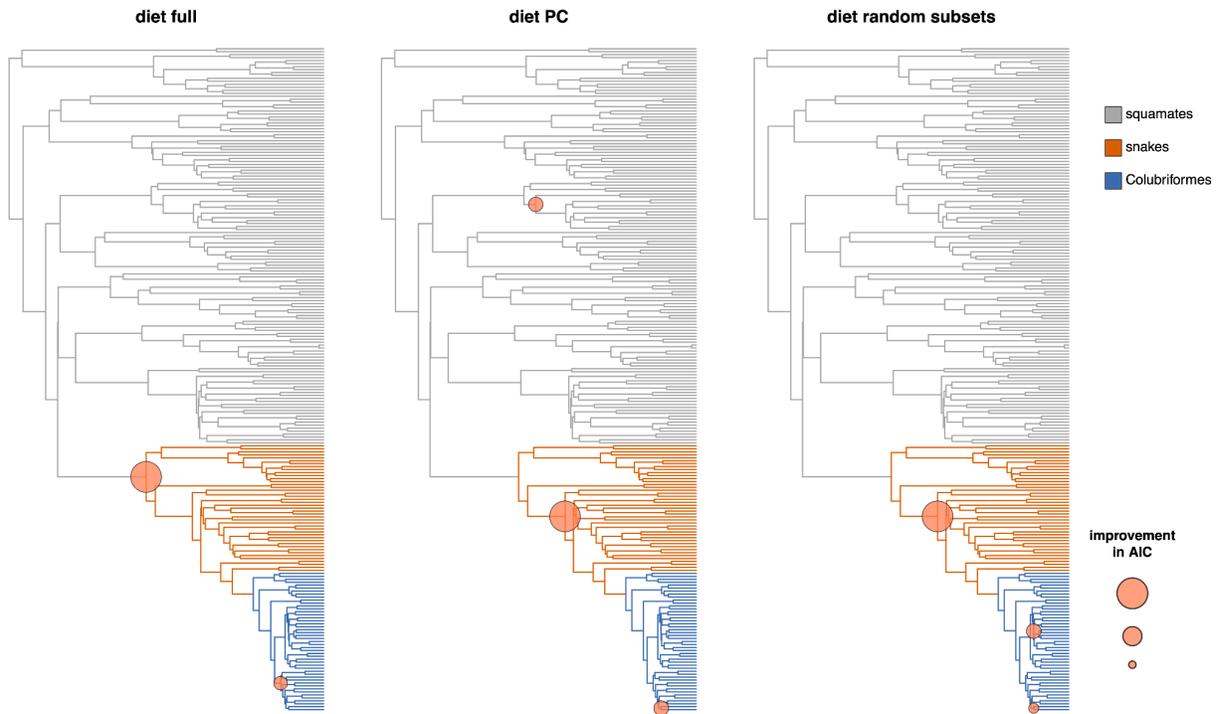
Figure S17: For multivariate diet, we fit a further round of censored models to diet states inferred using a non-phylogenetic Dirichlet process mixture model (see Section 2.2.6.3). Model fits and AIC improvement are shown for the full dataset (left), for the principal components accounting for 95% of variance (middle), and for 10 random subsets of 15 diet variables (right). In all cases, similar to what is seen for the phylogenetically informed approach, the node partition that most improved model fit occurred at the most recent common ancestor of alethinophidian snakes.

Relative cumulative proportions of prey type
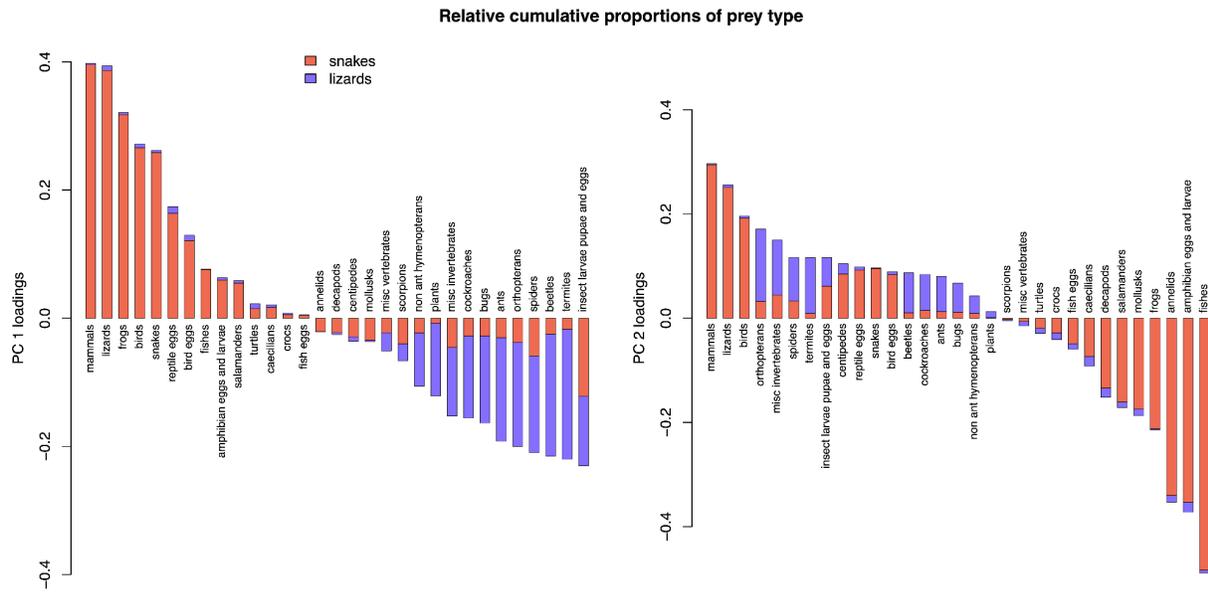
Figure S18: Squamate diet principal component analysis (PCA) predictor loadings. Loadings for PC axes 1 and 2 are shown, corresponding to Figure 3 in the main text. Bar colors show the relative use of these dietary categories by non-snake lizards and snakes, calculated as the summed proportions across species. Snakes have evolved to feed on a number of prey (e.g., mammals, other snakes, and birds) that are not found in the diets of lizards.
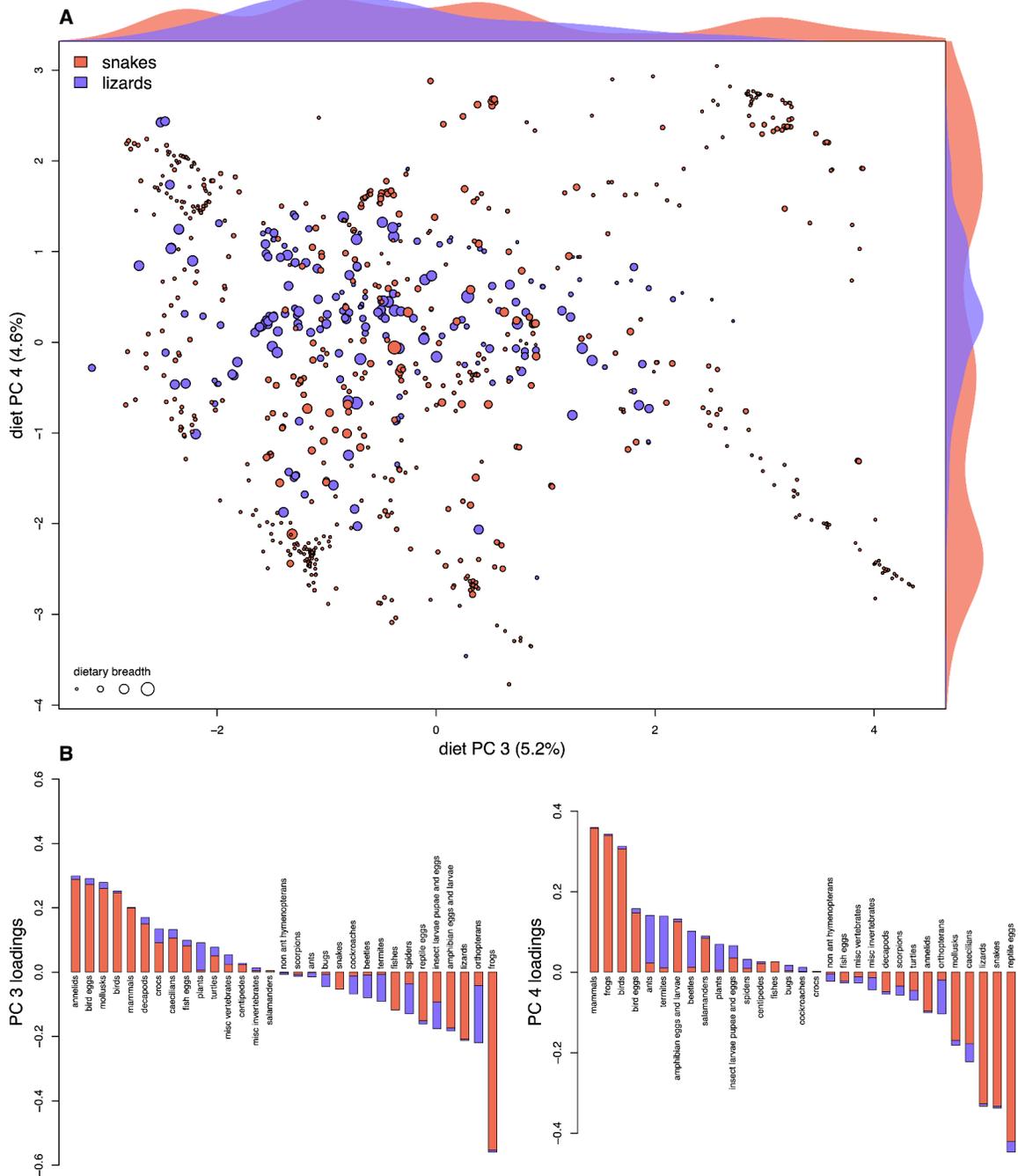
Figure S19: Squamate diet principal component analysis (PCA), focusing on PC axes 3 and 4. Points represent species and have been rescaled to reflect relative dietary breadth (A). PC loadings (B) have been colored to reflect the relative usage of each dietary category by non-snake lizards and snakes. Patterns across diet PC 1 and 2 (Fig. 3, fig. S18) are similar to those seen for PC axes 3 and 4: snakes (as a whole) occupy a broader dietary space than lizards but individual snake species tend to have narrower dietary breadth than that of individual lizard species.
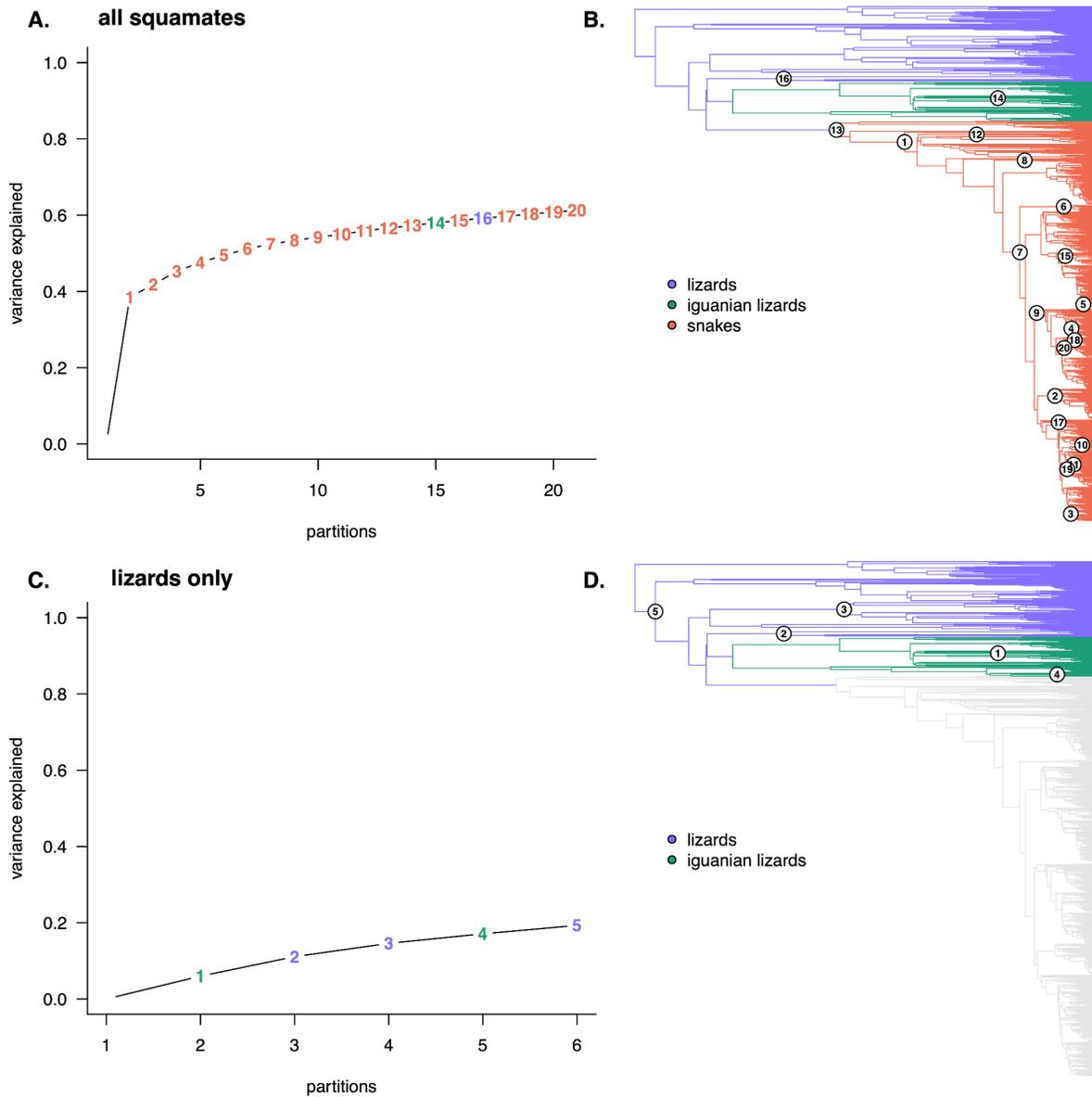
Figure S20: Variance partitioning of diet proportions across all squamates (A, B) and with lizards only (no snakes) (C, D). Present-day squamate diets are thought to reflect major trophic shifts that occurred deep in the evolutionary history of the group (the "Deep History" hypothesis in squamate diets; (*7*, *24*)). However, we find that the single most important node for explaining tip variance in diet proportions corresponds to advanced snakes, explaining almost 40% of the variance. This node explains far more of the variance than any nodes outside of snakes, thereby dwarfing the trophic shifts considered for the Deep History hypothesis. The most important node in explaining variance in lizard diets corresponds to Iguanidae (C, D), a group of primarily herbivorous species. The overall variance explained across diet proportions increases with the inclusion of additional nodes, which are colored in accordance with the region of the tree they belong to. Numbers in the variance plots correspond to node numbers on the phylogenies.
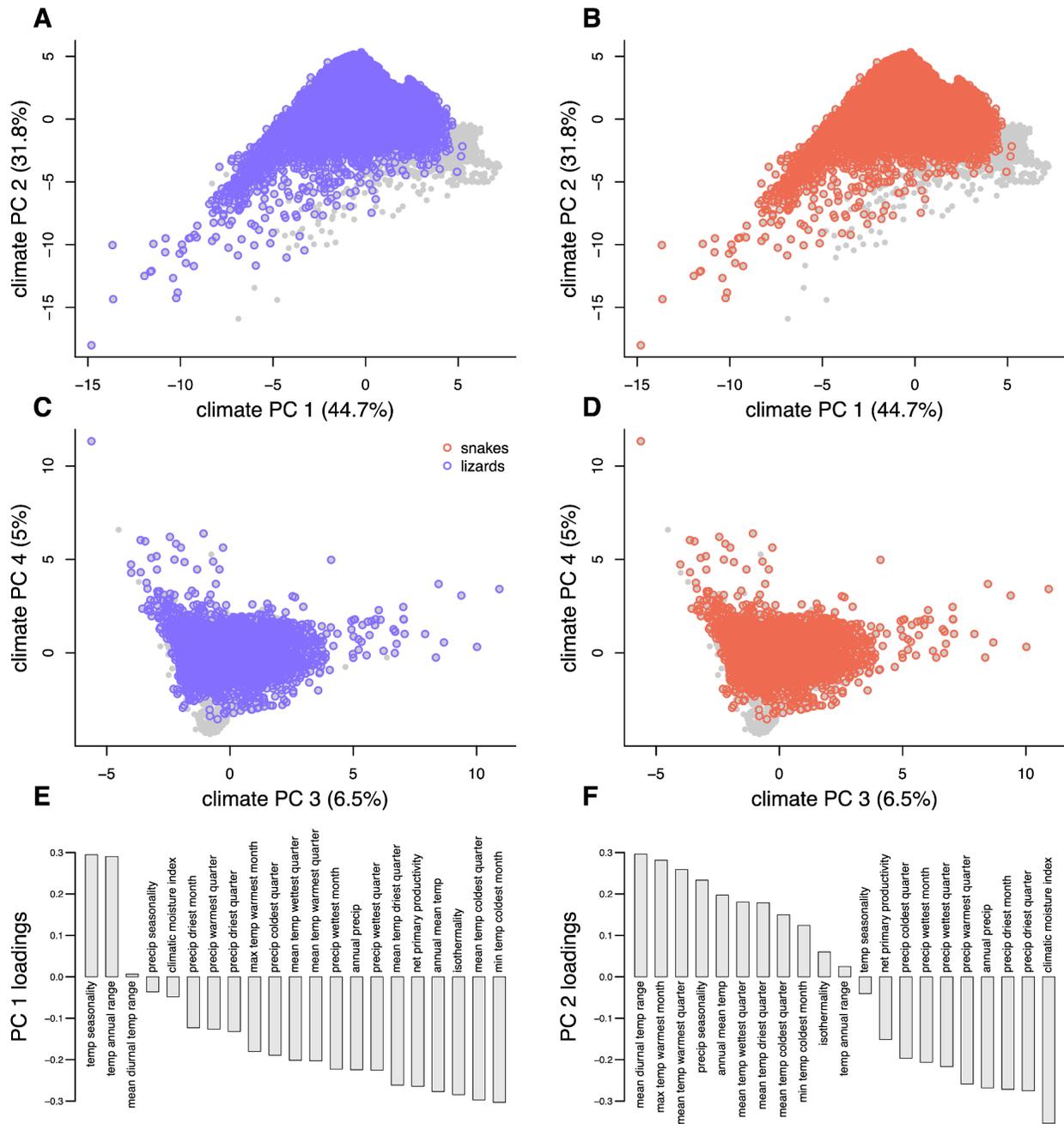
Figure S21: Climate space occupied by snakes and non-snake lizards. A principal component analysis (PCA) was conducted on climate data sampled at 10,000 locations across landmasses of the world; these background points are shown in gray. For climate data, we used 19 bioclimatic variables, climatic moisture index and net primary productivity (*168*, *170*). We then determined which of these coordinates intersected with the geographic ranges of lizards and snakes (*10*) and projected the climate occupied by these species onto this climate PCA space. Lizards and snakes both occupy nearly the same range of diverse climates, suggesting that neither group exhibits broad-scale climate conservatism.
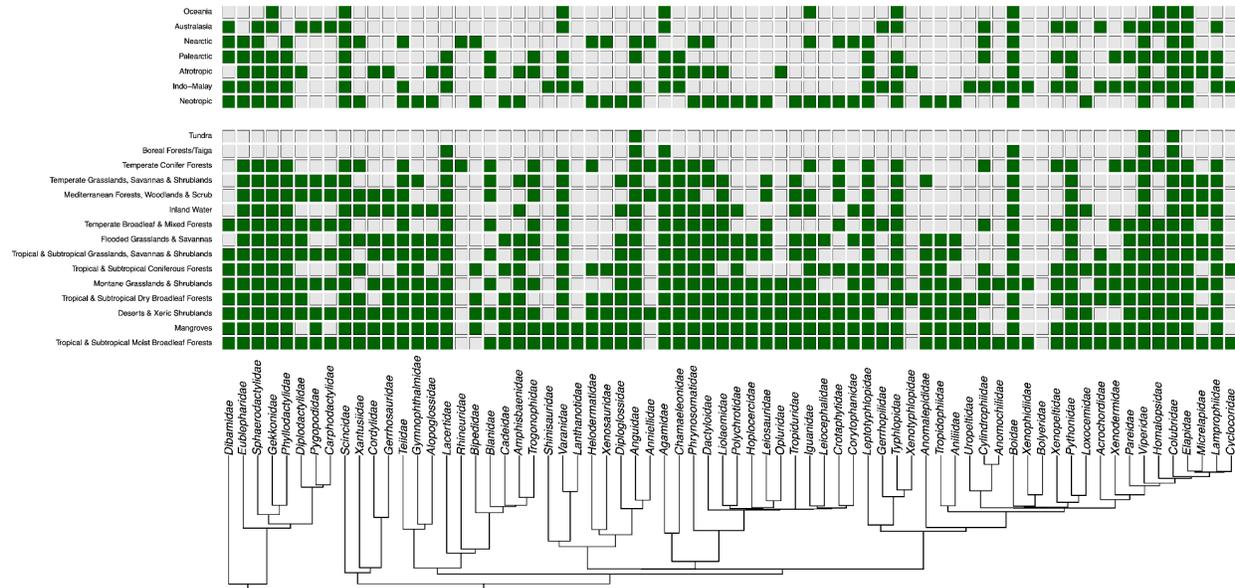
Figure S22: Family-level occupation of global biomes and geographic realms (*210*). Bolyeridae is not associated with any biome or realm because it consists of only a single species found on a single island (Mauritius). Most squamate families (which range in size from one to 1,967 species) are found across multiple biomes and multiple geographic realms, suggesting that even closely related squamate species can survive across quite different climatic conditions and that climate niche conservatism rarely persists across broad phylogenetic scales.
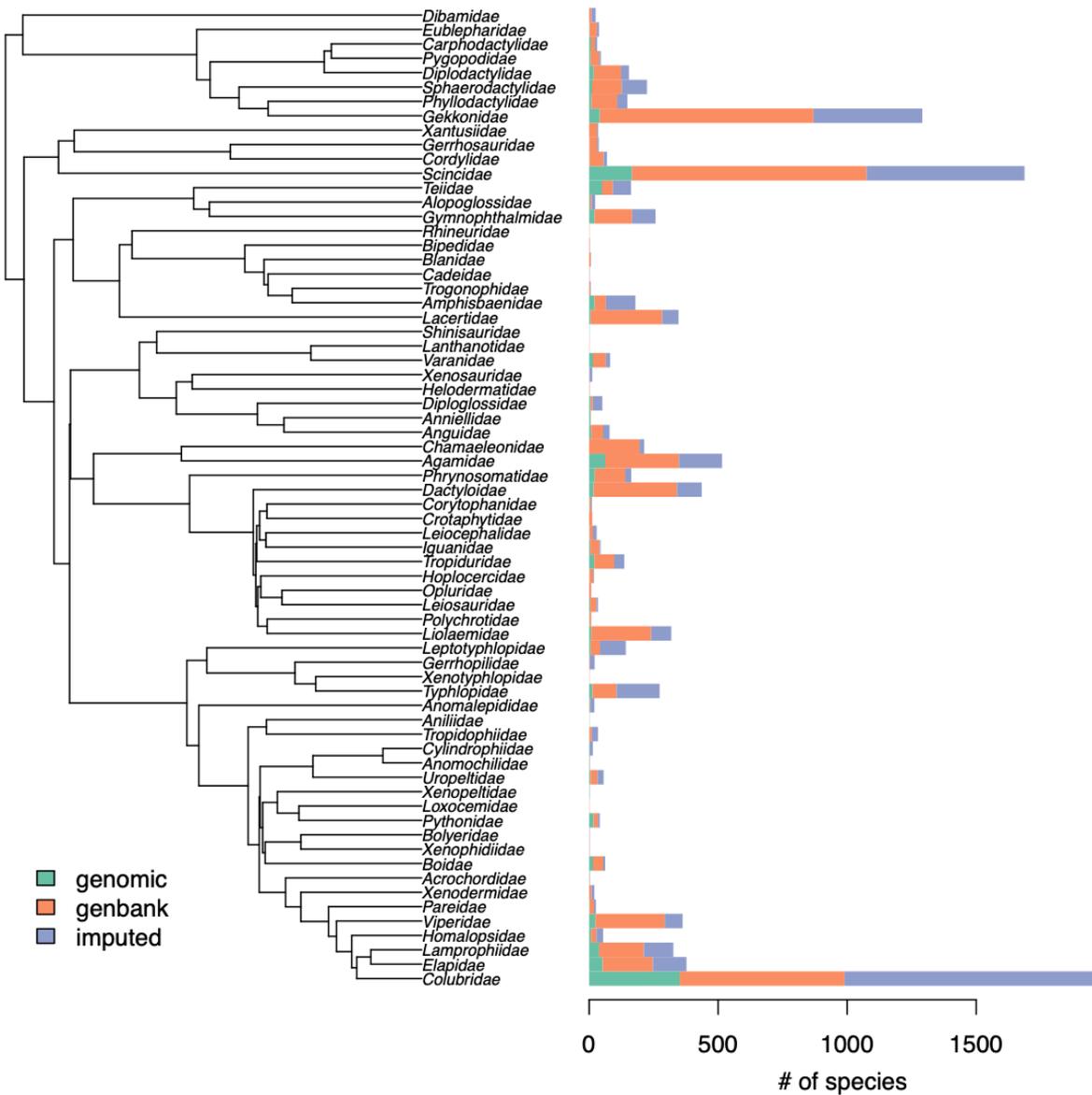
Figure S23: Proportion of species in each squamate family represented in our phylogeny by either phylogenomic data, GenBank-scraped data, or imputed. Shown is our primary phylogeny subsampled to show only one tip per family. Fifty-one of the 68 families were represented by at least one phylogenomic individual; sixty-four of the 68 families were represented by at least one GenBank individual. All families were sampled for either phylogenomic or GenBank data.
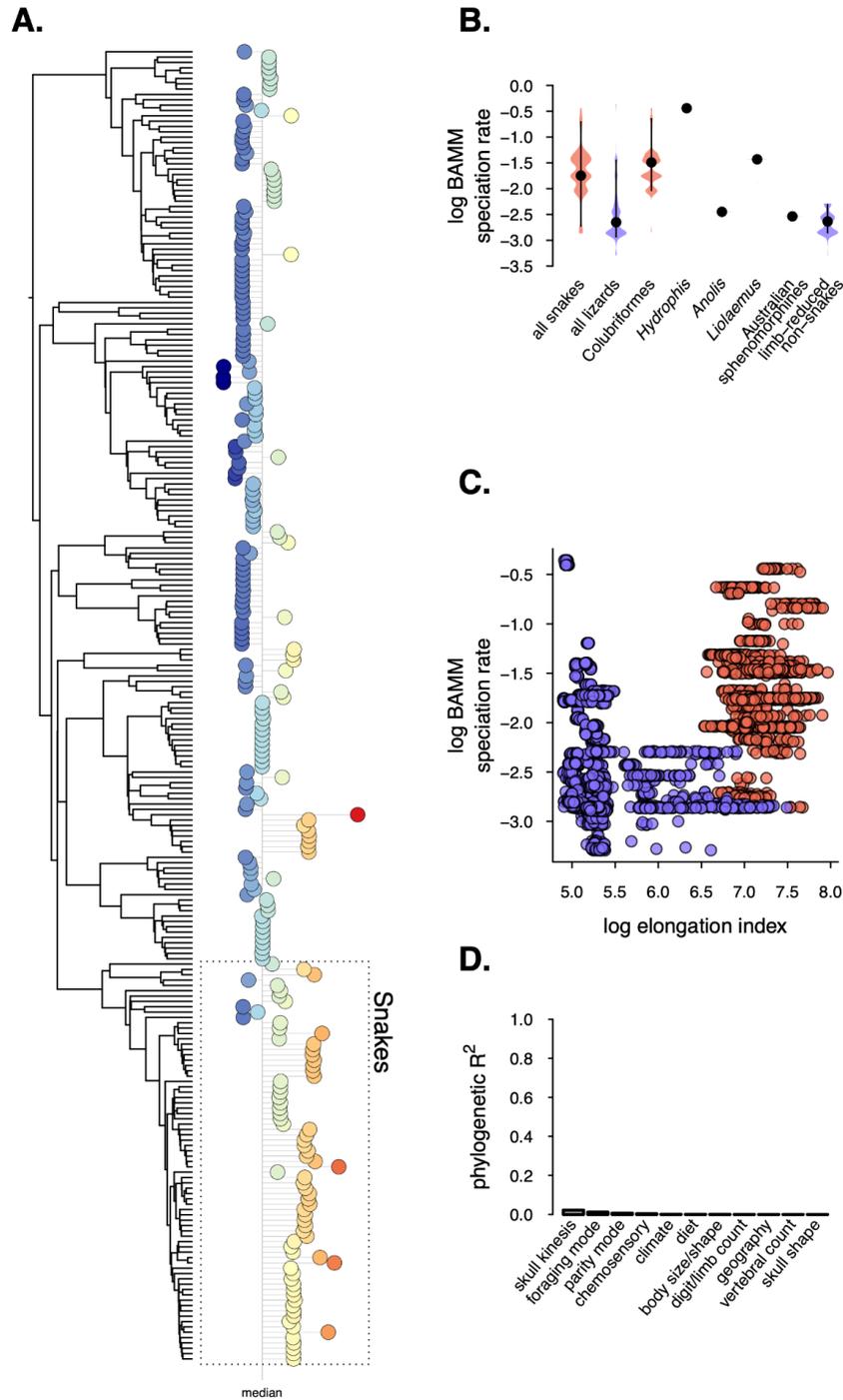
Figure S24: (a) Variation in BAMM speciation rates across the squamate tree. (b) Summary of BAMM speciation rates for clades of interest. (c) The relationship between BAMM speciation rates and species-specific elongation indices. (d) R^2 values for phylogenetic regression models with BAMM speciation rates as the response. Our primary results are robust to the approach used to estimate speciation rate (CLaDS versus BAMM; Fig. 4): snakes show elevated rates of speciation relative to non-snake lizards and no trait in our dataset appears to explain speciation rate variation after large clade effects (e.g., snakes) are accounted for.
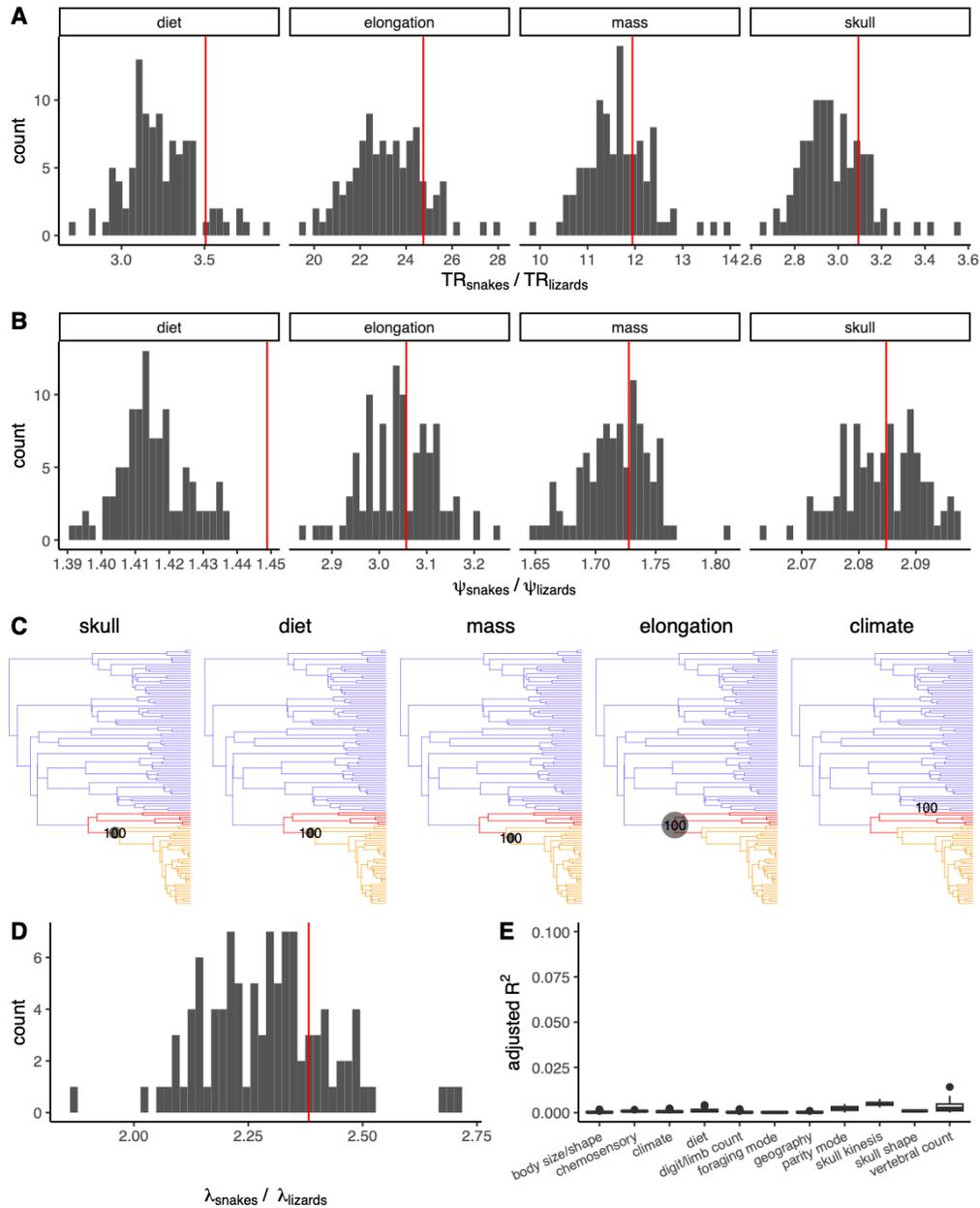
Figure S25: Results of main analyses repeated across the 100 trees in our pseudo-posterior set. (**A**) The ratio of trait rate evolution in snakes versus lizards across the tree distribution. Value from our primary tree shown by the red line. (**B**) The ratio of trait innovation in snakes versus lizards across the tree distribution. Value from our primary tree shown by the red line. For both (A) and (B), diet composition was estimated using Bayesian hierarchical clustering, a non-phylogenetic approach. Values here thus differ slightly from those reported in the main text. (**C**) Location of trait shifts in the lizard and snake phylogeny, as inferred using canonical phylogenetic ordination. Blue branches are lizards; red branches are Scolecophidia (blind snakes); orange branches are Alethinophidia (non-blind snakes). Circles at nodes are sized by the proportion of variance they explain, and numbers reflect the number of trees (out of 100) in which that node was inferred as the most explanatory node. (**D**) Ratio of snake to non-snake lizard tip speciation rates, computed across imputations of the pseudo-posterior set using CLaDS.

Value from our primary tree shown by the red line. (**E**) Phylogenetic adjusted R^2 estimated using phylogenetically corrected linear regression of predictor traits against speciation rates (see Table S3). Our results that (1) net innovation and rate of trait evolution were higher in snakes than lizards, (2) the primary shift in trait state and rate occurred at the base of snakes (or very near to it), (3) snakes had higher tip speciation rates than lizards, and (4) no model explains speciation rate variation seen across lizards and snakes are robust to the phylogenetic uncertainty captured by our pseudo-posterior set of trees.
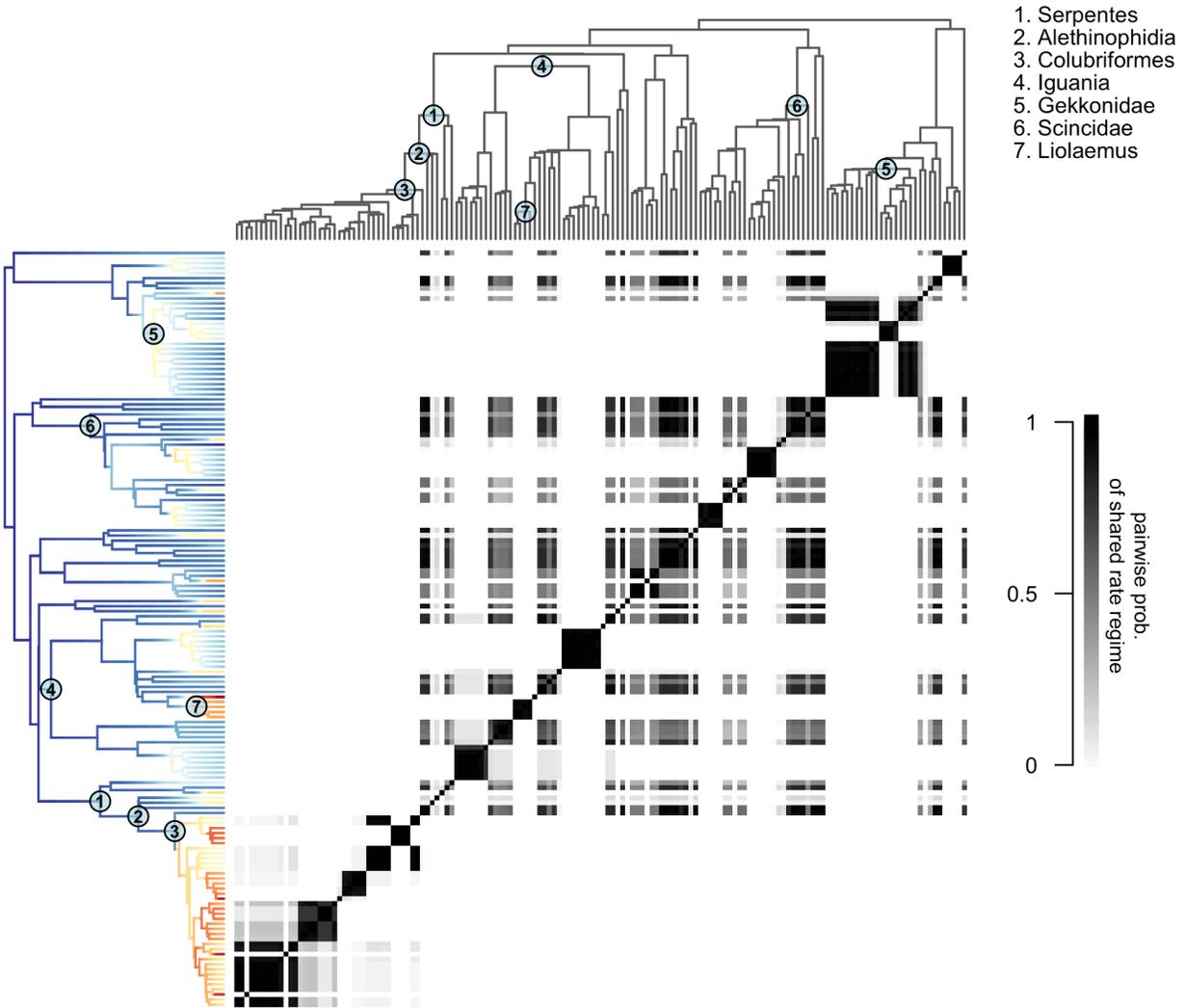
Figure S26: Cohort analysis of speciation rate variation (BAMM) across the squamate phylogeny, showing pairwise probabilities that any two clades share an identical rate regime by virtue of shared evolutionary history. The BAMM analysis was conducted on the primary tree of 6,885 species. For visual clarity, we proportionally subsampled the tree to 150 regularly sampled taxa. Notable clades of interest are indicated with numbered nodes. The so-called "advanced snakes" – Colubriformes (node 3) – exhibit speciation dynamics that are fully decoupled from all other squamate lineages, with rates that are over two-fold higher than those across other squamates (Fig. 4D).
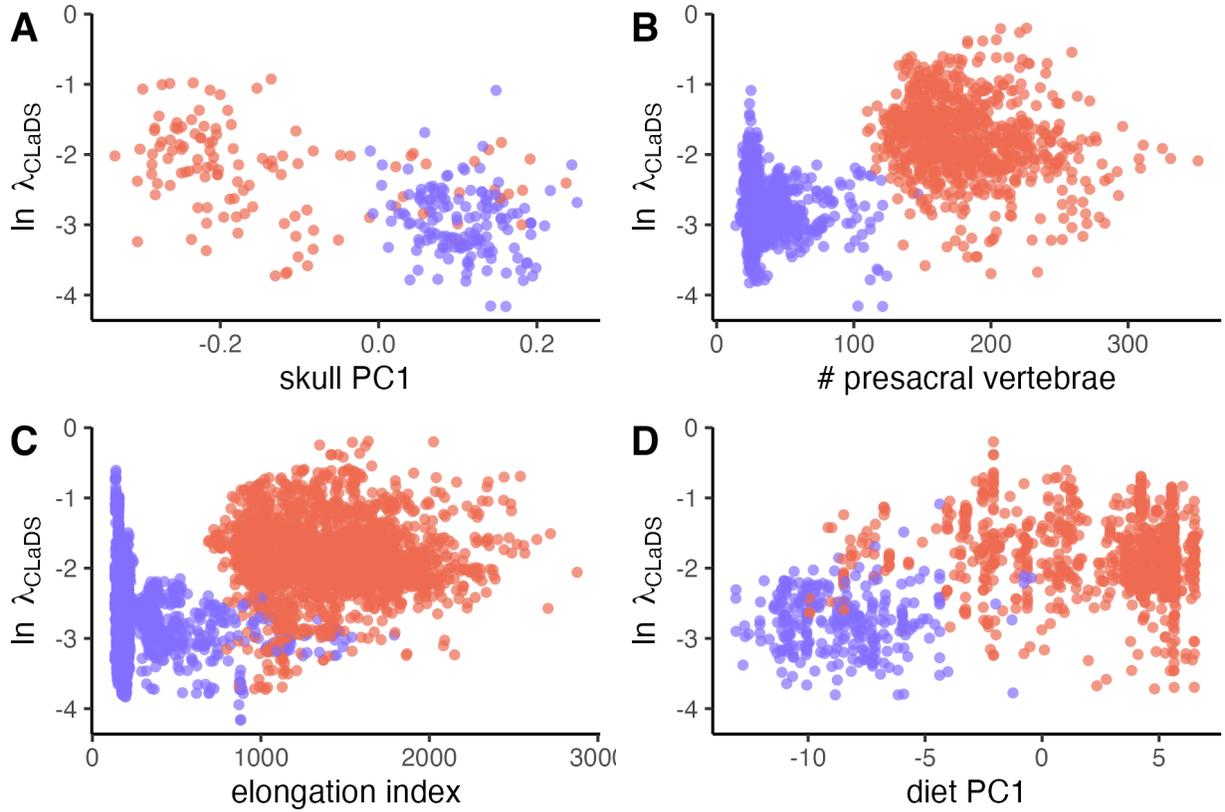
Figure S27: Correlations between log-transformed speciation rate as estimated with CLaDS (λ_{CLaDS}) and (**A**) skull shape (skull PC1), (**B**) number of presacral vertebrae, (**C**) elongation index, and (**D**) diet composition PC1. The visually apparent correlations between species traits and speciation are almost entirely driven by a single phylogenetic contrast: the split between non-snake lizards (in blue) and snakes (in red).
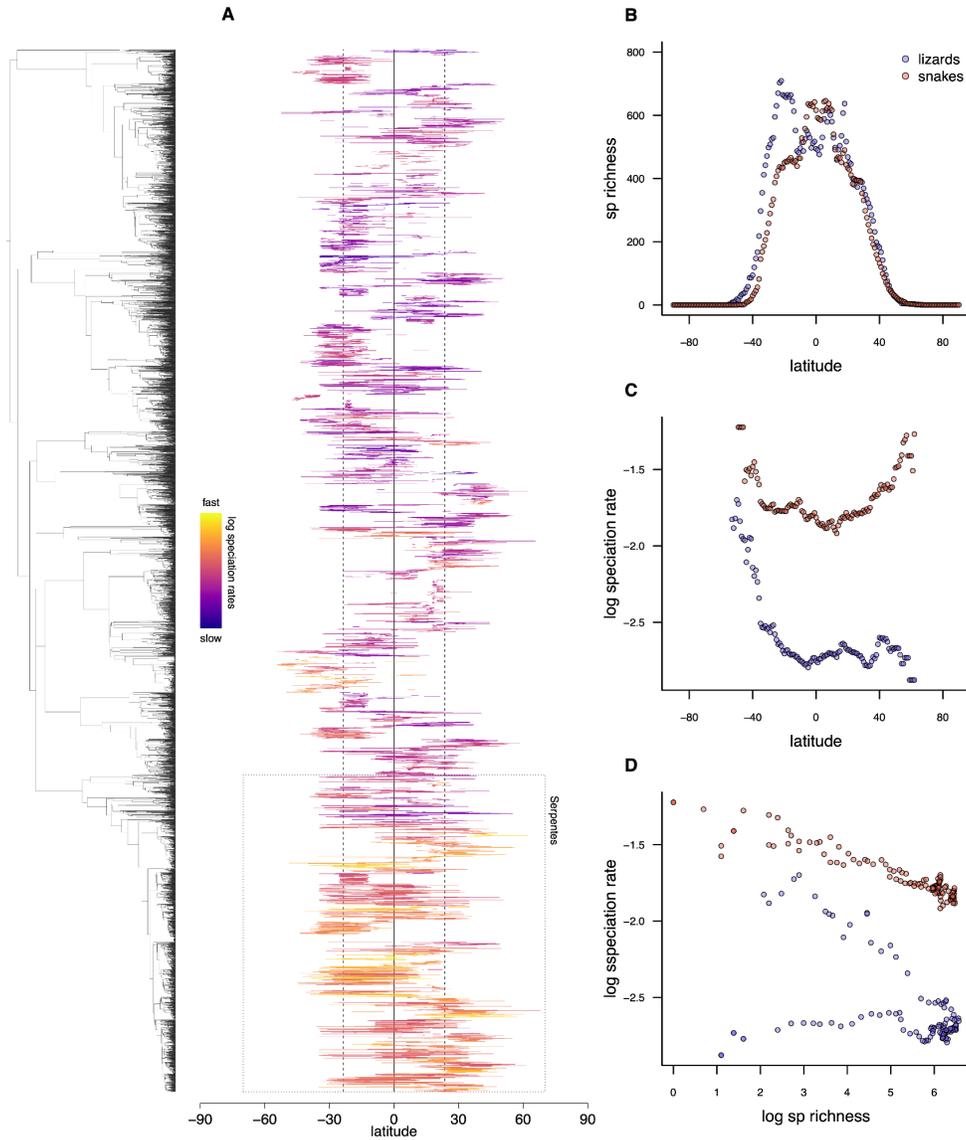
Figure S28: Relationship between species richness, speciation rates and latitudes. (**A**) Latitudinal ranges for all species represented in the phylogeny. Warmer colors denote species with greater speciation rates as estimated by CLaDS. (**B**) The latitudinal diversity gradient in species richness for lizards and snakes. (**C**) The latitudinal gradient in speciation rates for lizards and snakes. (**D**) The relationship between species richness and speciation rates across latitudinal bins. For B, C and D, species were assigned to latitudinal bins in 1-degree increments, according to their minimum and maximum latitudinal extent. For C & D, only latitudinal bins with five or more species are shown. Although we recapitulate previous support for a Latitudinal Diversity Gradient in species richness in squamates (*211*, *212*), we find no evidence that this pattern results from a latitudinal gradient in speciation rate. Much of the peak in lizard speciation rate in the southern hemisphere is driven by high speciation rates in the genus *Liolaemus* (Fig. 4D, fig. S24).
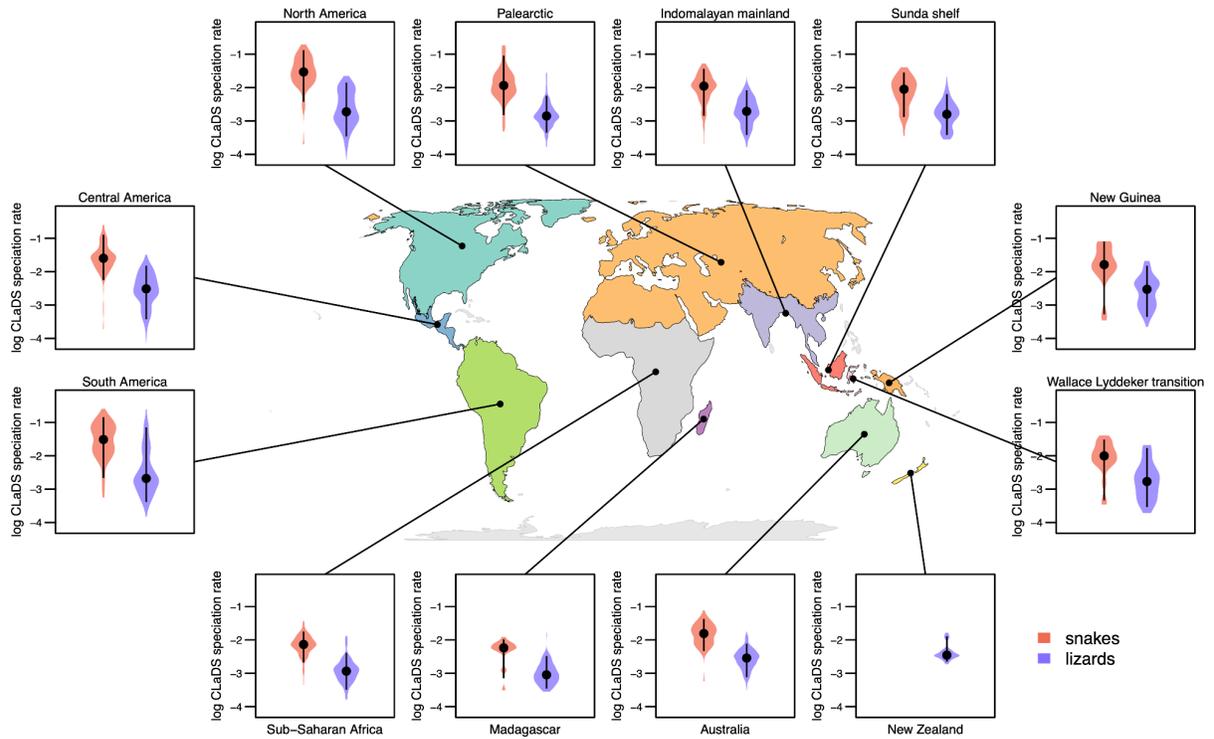
Figure S29: Comparison of snake vs non-snake lizard speciation rates for species found in a given biogeographic region (excluding sea snakes). If species geographic ranges spanned multiple biogeographic regions, they were included in each. Note that no snake species are found in New Zealand. Snakes exhibit higher speciation rates than lizards across all biogeographic regions, suggesting faster speciation rates in snakes is not a biome-specific phenomenon.
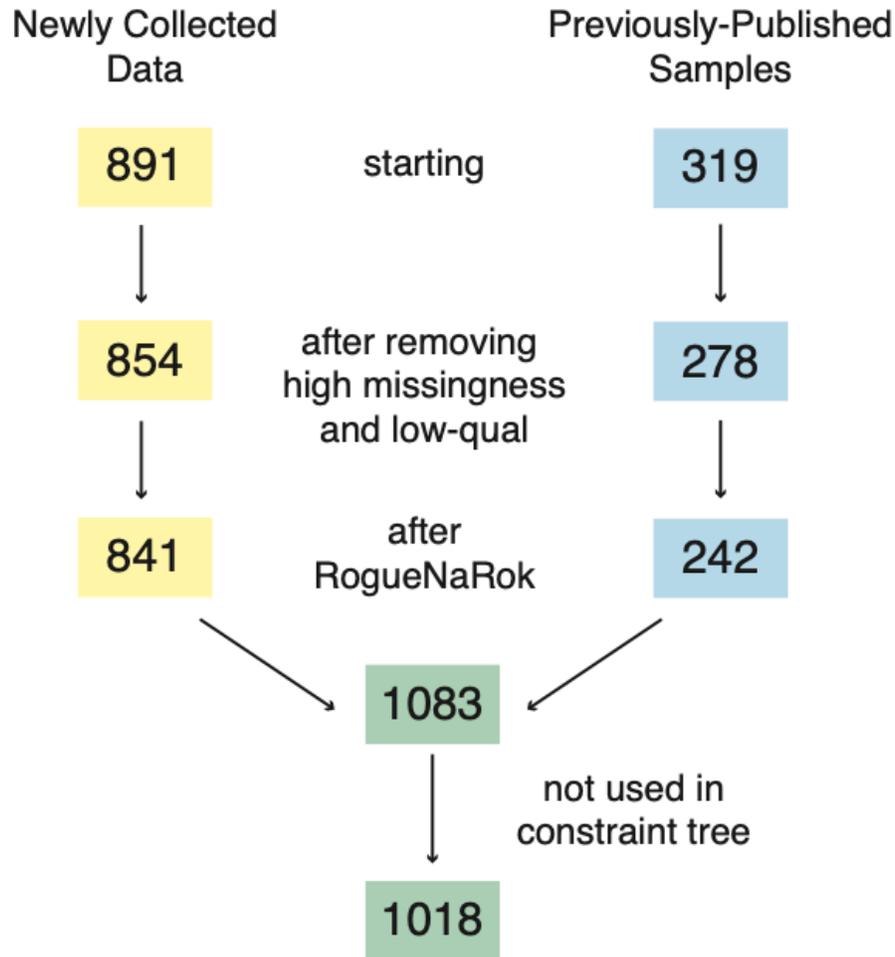
Figure S30: Number of phylogenomic taxa included in our phylogenomic pipeline newly-collected in this study and published previously in other studies (Data S1). Sampled individuals were removed either if their sequencing quality was low quality, if they had high missing data, or if they were identified as rogue taxa by RogueNaRok. In total, we sampled 1,083 ingroup taxa, of which 1,018 could be used in our constraint tree. Some taxa could not be included in our constraint tree because there were too few taxa in that family (nTaxa < 3) to generate a constraint topology.

Figure S31: Comparison of our phylogenomic topology inferred with different approaches. Our primary phylogenomic topology was inferred using concatenated data with IQTree. Shown here is how this topology (depicted on the left) compares to that generated (**A**) by a coalescent-based approach (ASTRAL) and (**B**) by another concatenated approach (ExaML). Trees were subsampled to subfamily level for ease of visualization. Red nodes are discordant between the visualized tree and the IQTree tree. While the two concatenated approaches are largely concordant, the coalescent-based topology is quite different from the concatenated topology. Many of the discordances are in disagreement with existing notions of squamate evolutionary relationships – gleaned from decades of analysis of both molecular and morphological data – suggesting that the coalescent-based approach might be exhibiting unexpected behavior.

Figure S32: Our phylogenomic tree and its bootstraps, as inferred using IQTree2. Only thirteen nodes (1.1% of total nodes) had less than 100 bootstrap support; these nodes are labeled with red circles. Overall, our phylogenomic tree had strong nodal support as measured by bootstraps, however, nodes with high genealogical discordance can still exhibit strong statistical support with phylogenomic datasets (*50*, *71*, *76*).
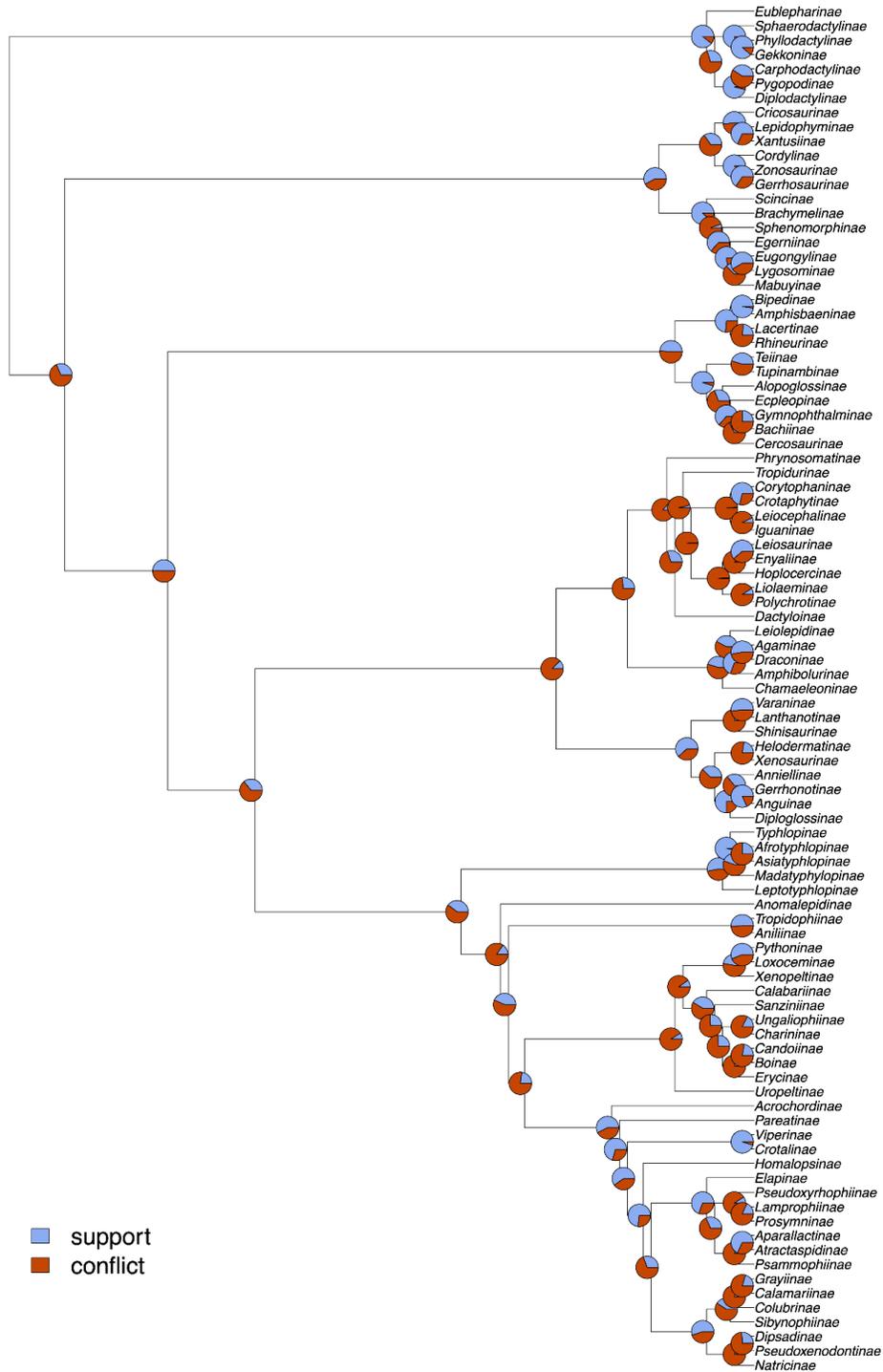
Figure S33: Levels of gene tree support and conflict across our phylogenomic tree, subsampled to the subfamily level. We measured gene tree support and conflict using PhyParts (*77*) on rooted gene trees, filtering out any gene tree nodes with <20% support as measured by Shimodaira-Hasegawa-like values. Many nodes exhibit high levels of gene tree discordance despite also having high bootstrap support. Discordance is particularly high in the rapid snake and iguanid radiations (*50*, *71*).
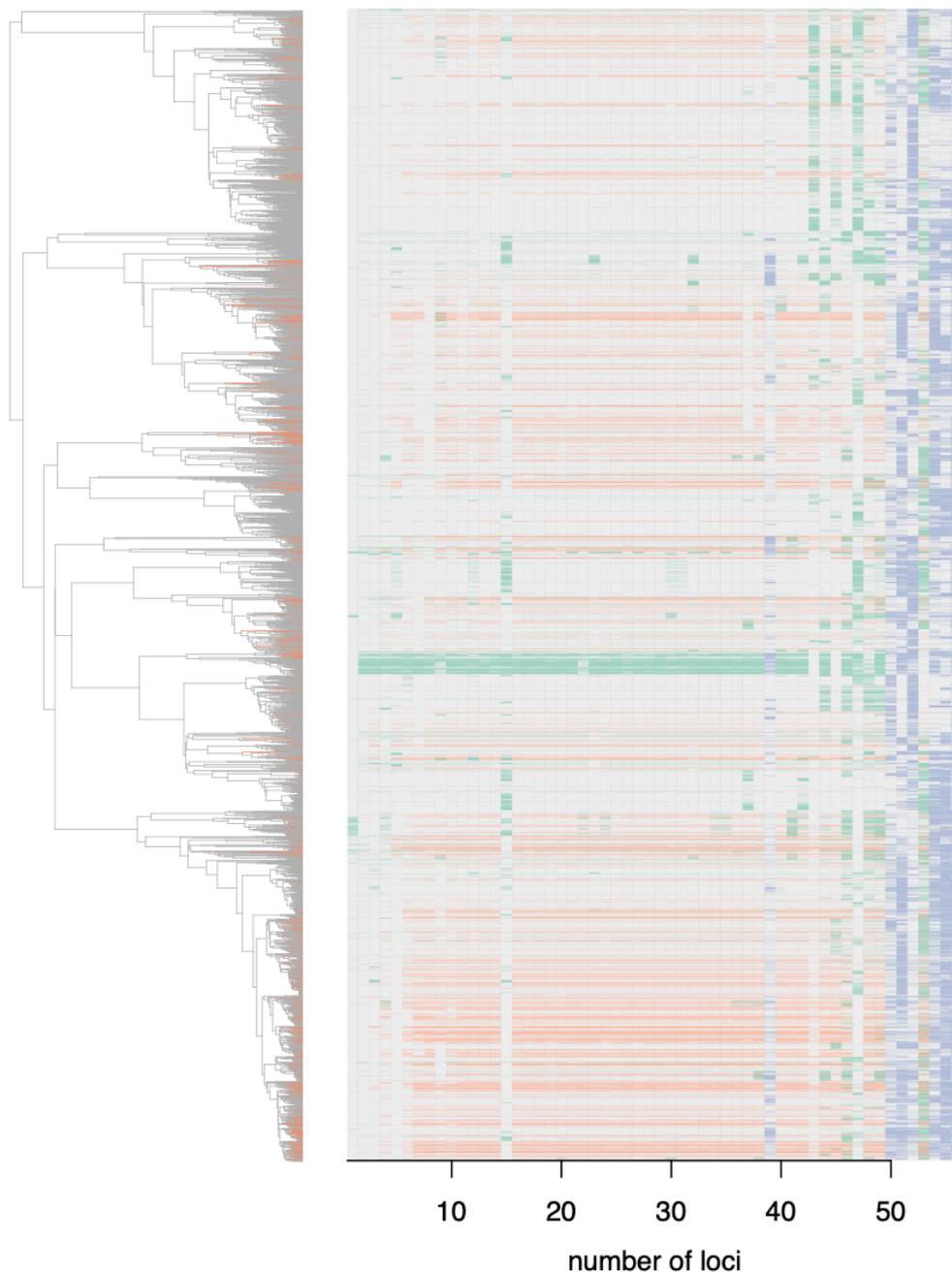
Figure S34: Supermatrix alignment used to construct our squamate phylogeny of 6,885 species. The left panel shows our primary phylogenetic tree, with tips in our phylogenomic constraint shown in orange. The right panel shows our supermatrix of 56 loci, with loci ranked in increasing order of completeness. Blue cells represent mitochondrial loci, and orange and green cells represent newly collected phylogenomic and GenBank-scraped loci, respectively. Like most supermatrices, our supermatrix is patchy but the inclusion of newly collected data substantially increases its completeness.
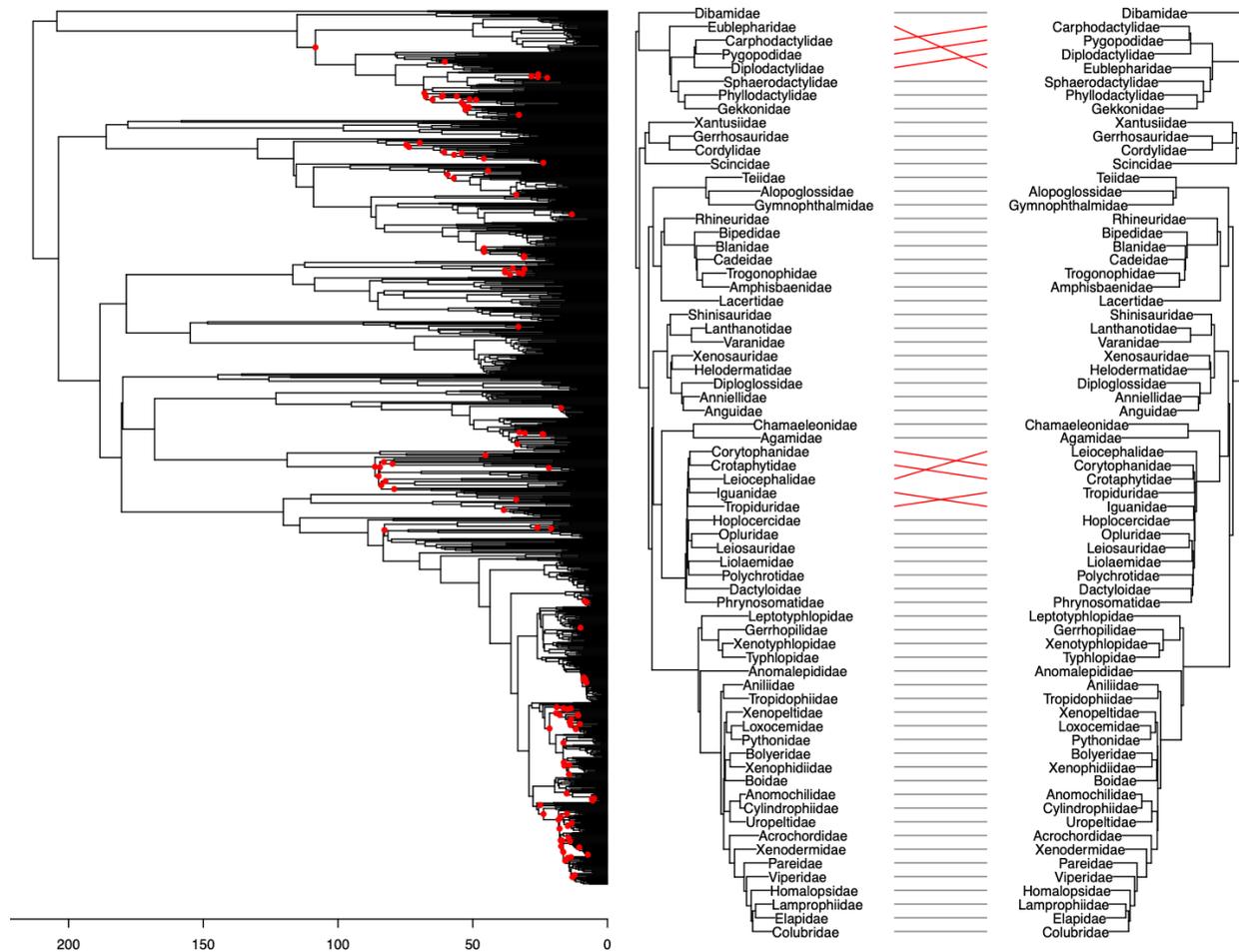
Figure S35: Topological differences between our constrained and unconstrained phylogenetic analyses. In our constrained analysis, the 6,885-taxon supermatrix was constrained by a phylogenomic backbone (fig. S3). In the unconstrained analysis, no constraint was placed. Left: the genus-level constrained and dated phylogeny; red nodes (12% of total nodes) are discordant between the constrained and unconstrained trees. Right: a family-level comparison of constrained and unconstrained trees. Overall, the two trees are highly concordant, outside of discrepancies in two known areas of high discordance in squamates: relationships within Iguania and among gecko families.
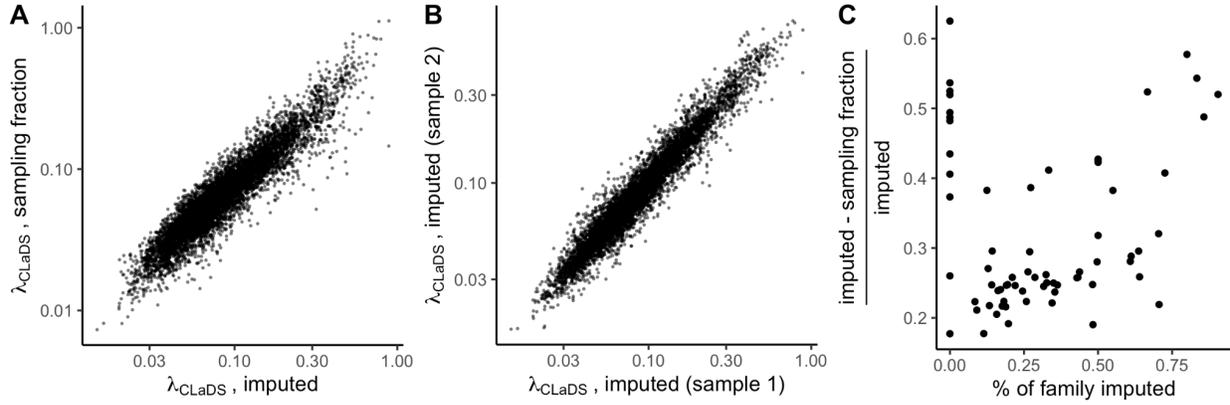
Figure S36: Differences in speciation rate (λ_{CLaDS}) as measured on a fully sampled, imputed tree versus a genetic-only tree with sampling fractions. For our primary tree, we generated 100 imputations to account for uncertainty in imputation. Additionally, we ran CLaDS on a genetic-only tree with family-level sampling fractions. (**A**) Average correlation between speciation rate across the two approaches was relatively high (mean correlation = 0.91 across 100 imputations) but (**B**) lower than the correlation across imputations (mean correlation = 0.96). Shown here is a randomly selected sample of two imputations. (**C**) Average difference between the two approaches (measured as $\frac{\lambda imputed - \lambda sampling\ fraction}{\lambda imputed}$) did not vary predictably with the percentage of the family that consisted of imputed tips. These results suggest that, although imputation introduces error, inferring speciation rate on an imputed tree results in more consistent rates than approaches accounting for missing data.
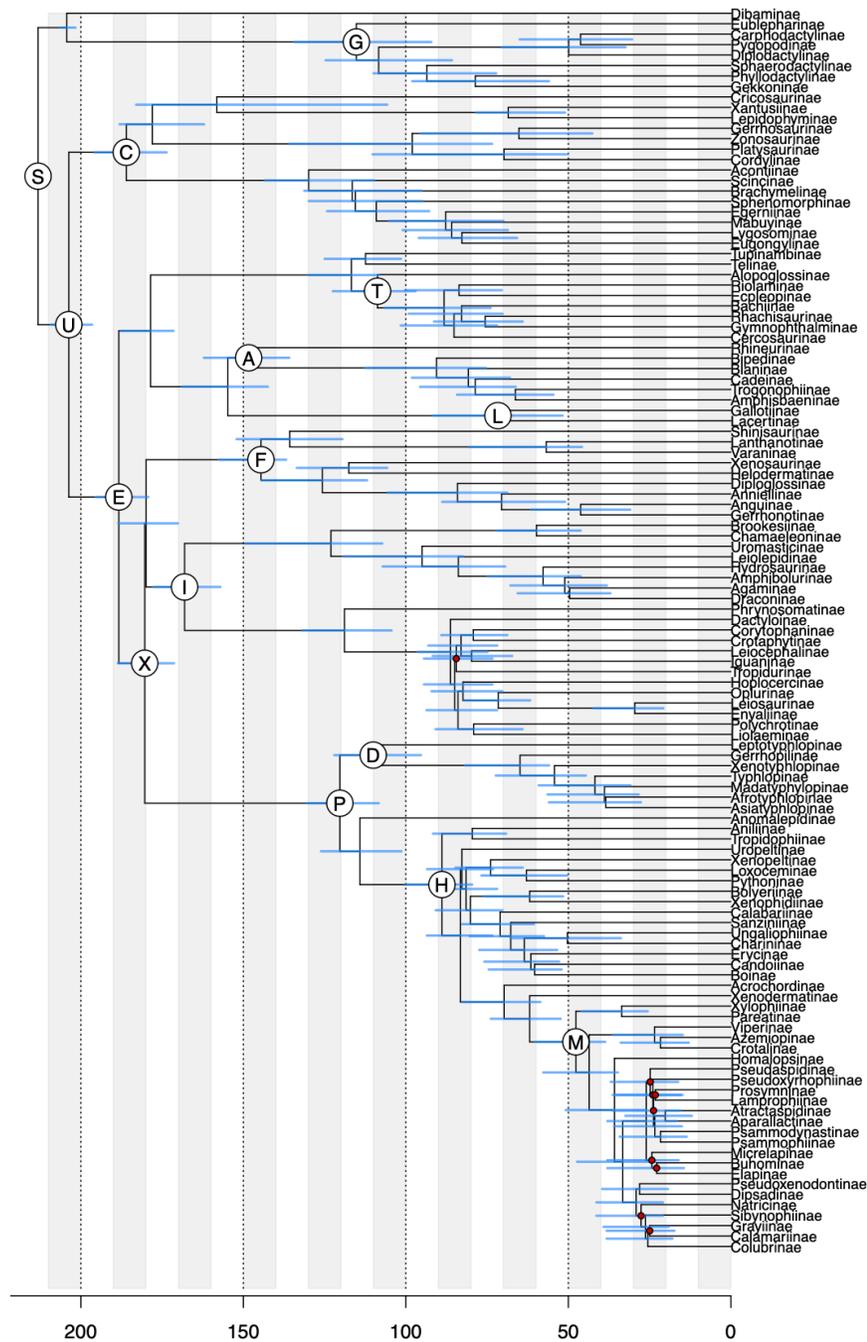
Figure S37: Topological and divergence time variation across our pseudo-posterior set of trees. We generated 100 trees to capture uncertainty in topology and divergence dating; these trees serve as our pseudo-posterior set of trees. Nodes representing major squamate clades are labeled with letters; see Table S5 for codings. Shown is our primary tree, subsampled to one random representative per subfamily, with error bars on divergence times. Nodes that appear in <95% of the pseudo-posterior set of trees are marked with a red circle.
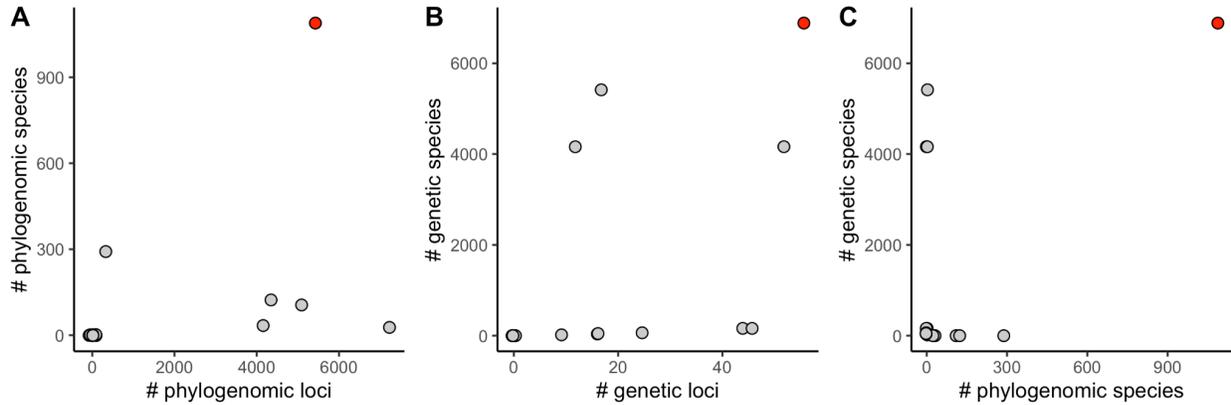
Figure S38: Data content of our phylogenetic tree (red) and fourteen other squamate phylogenies (gray) published in the last 20 years: (*20, 50, 54, 69, 71, 83, 93, 108, 118, 123–127*). (A) Number of species sampled for phylogenomic data and number of loci included in the phylogenomic alignment. (B) Number of species sampled for genetic data (e.g., non-phylogenomic datasets) and number of loci included in this alignment. (C) In a given phylogeny, the number of species sequenced for phylogenomic vs. genetic datasets. Relative to other trees, our phylogeny spans more species (whether for genetic and genomic data) and almost always more loci (whether for genetic or genomic data). While more data do not automatically imply greater accuracy, our phylogeny remains the most comprehensive squamate phylogeny published to date.
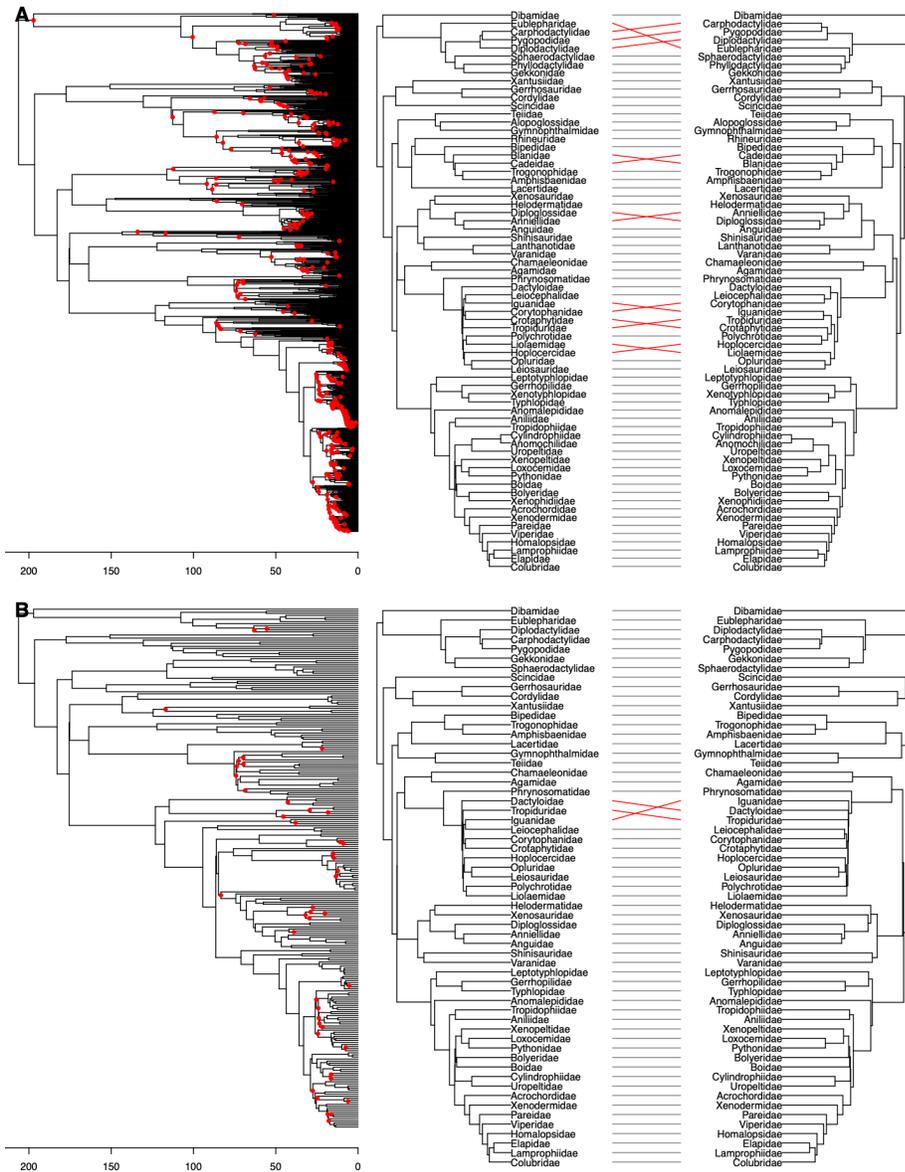
Figure S39: Topological differences between our primary phylogeny and previously published topologies: (**A**) the 5,415-tip tree published by (*83*) and (**B**) the 289-tip phylogenomic tree published by (*71*). (**A**) left: genus-level phylogeny inferred in our study; red nodes (38% of total nodes) are discordant between our and the (*83*) tree. Right: a family-level comparison between our and the (*83*) tree. (**B**) left: our phylogeny showing all tips also sampled by (*71*); red nodes (18% of total nodes) are discordant between the two trees. Right: a family-level comparison between our and the (*71*) tree. Family-level relationships are highly concordant across the three trees, outside of a few discrepancies within Iguania. Below-family relationships are highly concordant across the two phylogenomic phylogenies, outside of discrepancies in two known "anomaly zones" in squamates: Iguania and advanced snakes (*50*).
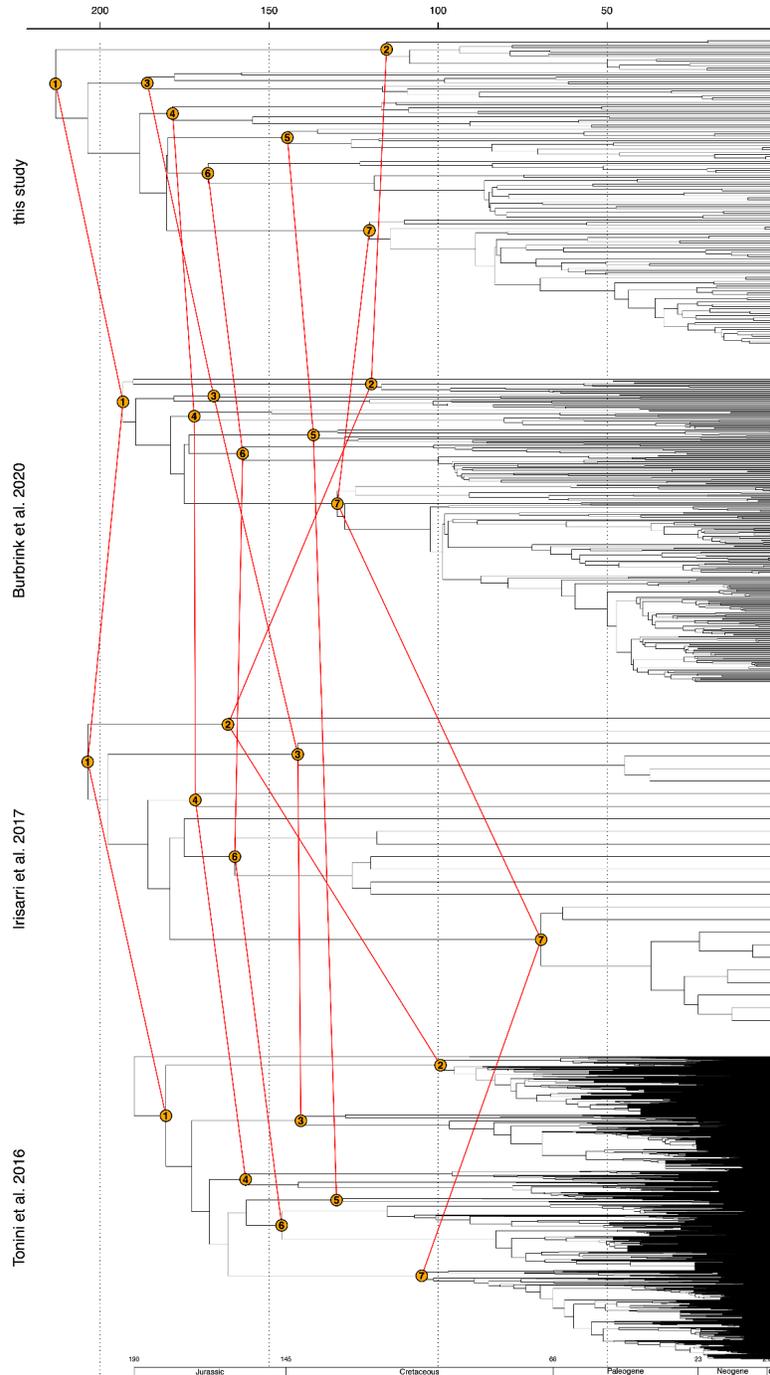
Figure S40: A comparison of major squamate clades between the time-calibrated genomic phylogeny from this study to three recently published phylogenies (*71*, *83*, *127*). All trees are plotted on the same chronological scale, and equivalent nodes are linked together. Node numbers correspond to the following crown clades: (1) Squamata, (2) Gekkota, (3) Scincoidea, (4) Lacertoidea, (5) Anguimorpha, (6) Iguania, (7) Serpentes. Note that Anguimorpha is not defined in (*127*). There is some variation in clade age across these trees, most notably for Gekkota and Serpentes in (*127*), compared to the other squamate phylogenies.
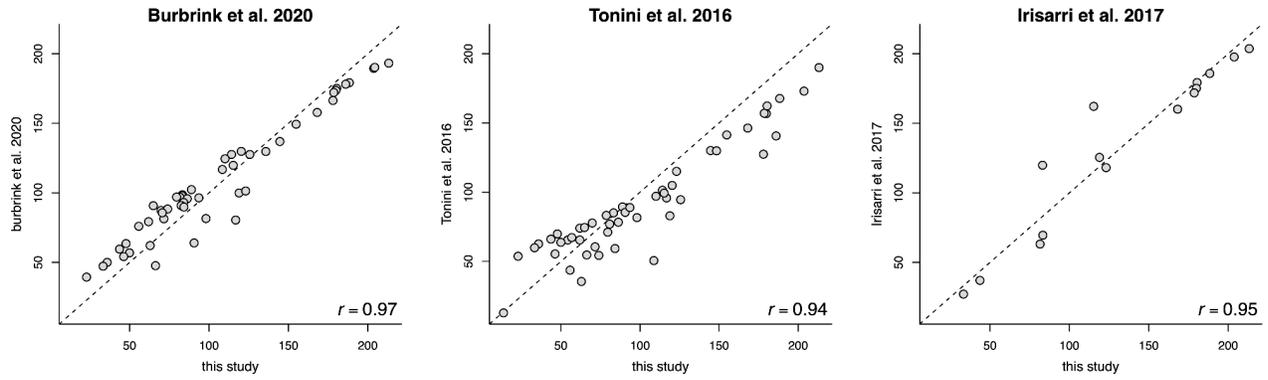
Figure S41: A comparison of family crown ages across the phylogenies also shown in figure S40 (*71, 83, 127*). Pearson correlation coefficients are reported in the lower right corner. We find that family crown ages are highly congruent, with the tree in this study being most aligned with Burbrink et al. (*71*).

**Proportional error in body
size ratio imputation**
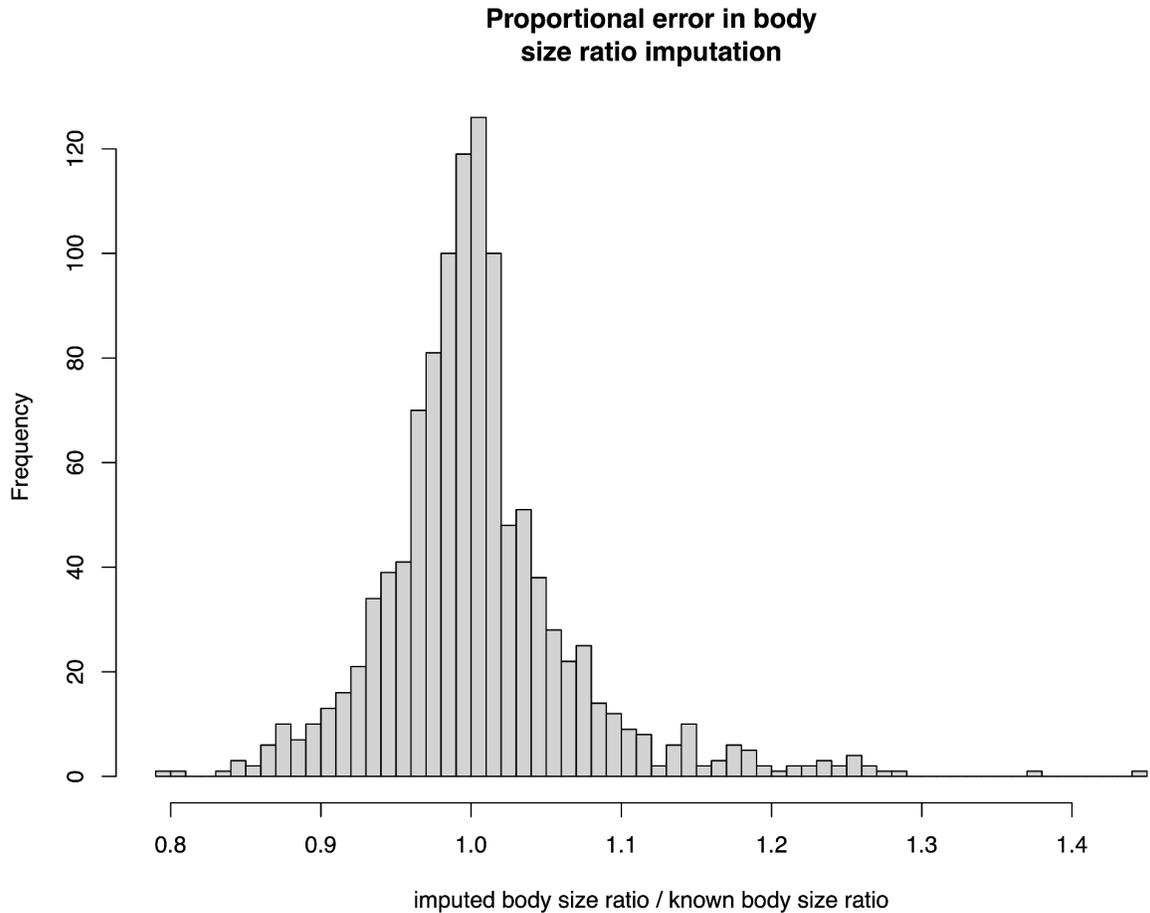
Figure S42: Cross-validation analysis of size ratio imputation for snakes. We estimated the proportional error in imputed size ratio when either SVL and total length, or actual size ratio, were known (1,112 snake species), using leave-one-out cross-validation. Proportional error, with mean = 1 and sd = 0.07, indicates that the imputation procedure is relatively accurate, as a value of 1 implies perfect accuracy. Note that we used phylogenetic imputation to estimate size ratios for 982 of 2,094 snake species where the size ratio was unknown (either SVL, total length, or both were missing for individual species; see section 2.2.2).
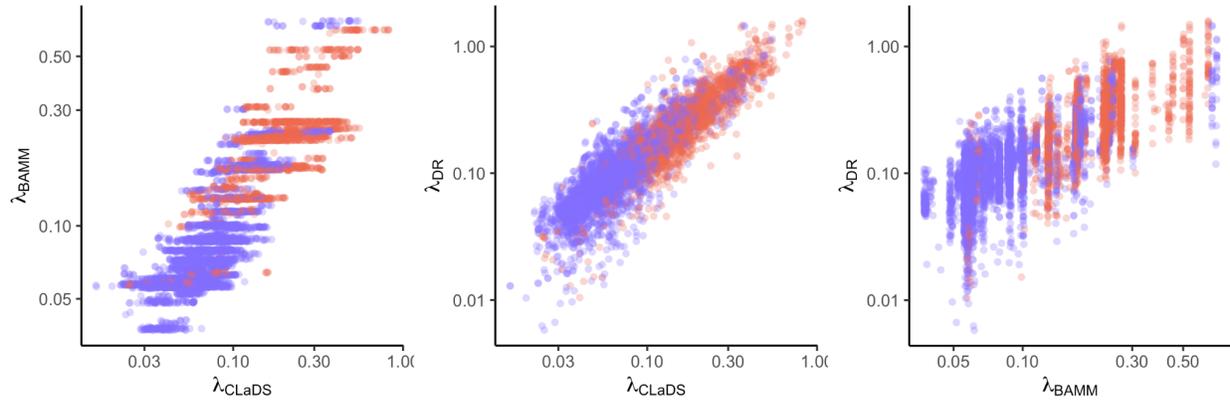
Figure S43: Speciation rates across the squamate tree measured using three methods: CLaDS, BAMM, and the DR statistic. Points are colored red for snakes and blue for non-snake lizards. Despite the differing assumptions of these methods, speciation rates are highly correlated across approaches, and we draw similar conclusions irrespective of which method is used (see fig. S24).
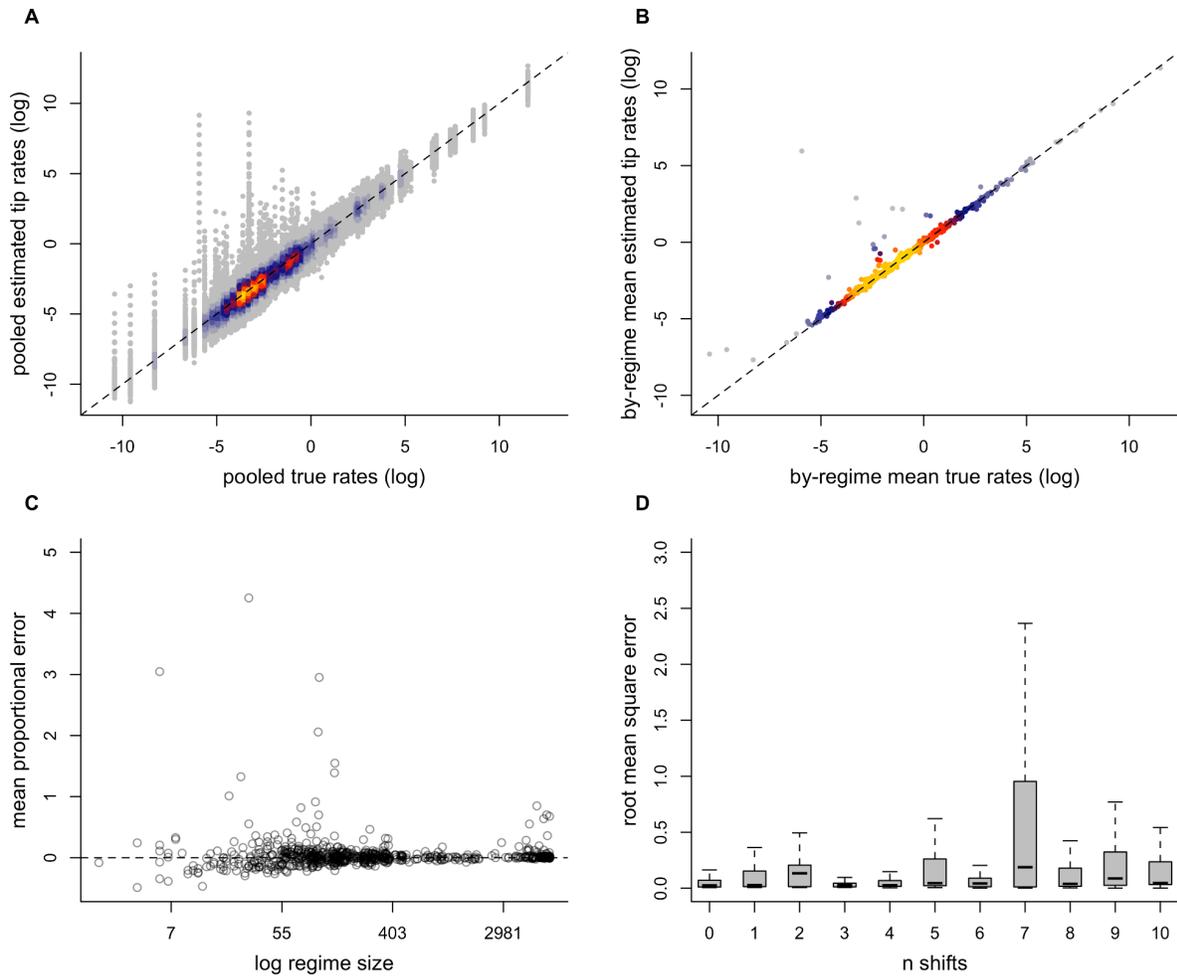
Figure S44: Simulation-based evaluation of the multivariate tip rate metric for trait evolution. Tip rates are computed from a set of multivariate, multirate discrete-shift simulations on the full squamate phylogeny. (**A**) A comparison of all simulated to estimated tip rates. The datasets involved between 0 and 10 phenotypic rate shifts, simulated on the empirical squamate phylogeny. Nodes needed to include at least five descendant tips to be considered for a rate shift, and all trait datasets had five dimensions. (**B**) A comparison of simulated to estimated tip rates, when rates are averaged by true rate regime. (**C**) Mean proportional error for estimated tip rates, organized by rate regime size. Mean proportional error is defined as: sum(((estimated - true) / true)) / regime size. 12 (out of 659) outlier values are not shown in the interest of visualizing the majority of the data. (**D**) Root mean square error for estimated tip rates, organized by number of simulated rate shifts. Colors in panels (A) and (B) reflect point density.

Table S1: List of fossils for node-based divergence time estimation. Ages are in millions of years, and node labels correspond to figure S4.

fossil	min age constraint	max age constraint	group	references	node label
Hylonomus lyelli	314	340	Amniota	(*213*)	C1
Protorosaurus speneri	255.9	295.9	Sauria	(*214*)	C2
Xilousuchus sapingensis	247.2	256	Archosauria	(*215*)	C3
Paramacellodidae	170		Scincoidea	(*216*)	C4
Dorsetisaurus purbeckensis	144		crown Anguimorpha	(*92, 217–220*)	C5
Primaderma nessovi	98.32		*Heloderma+ Anguis+Anniella+ Xenosaurus*	(*90–94*)	C6
Saichangurvel davidsoni	68		Pleurodonta	(*221*)	C7
Cretaceogekko burmae	97		crown Gekkota	(*222, 223*)	C8
Ptilotodon wilsoni	112		Teiidae	(*224*)	C9
Boipeba tayasuensis	66		Typhlopoid-leptotyphlopid divergence	(*225*)	C10
Afairiguana avius	49.1		*Anolis+ Gambelia*	(*95, 226*)	C11
Odaxosaurus roosevelti	74.5		Anguidae	(*98, 227*)	C12
Australophis anilioides	72.1		Amerophidia (Aniliidae+ Tropidophiidae)	(*228*)	C13
Procerophis sahnii	50.5	72.1	Colubroidea+ (Acrochordus+	(*229*)	C14

			Xenodermatidae)		
Messelopython freyi	47.57		stem Pythonidae	(*230*)	C15
Titanoboa cerrejonensis	58	64	stem Boinae	(*228*)	C16
Saniwa ensidens	51.4		*Varanus+ Lanthanotus*	(*231*)	C17
Corallus priscus	50.2	64	*Corallus+* (Chilobothrus+ Epicrates+ Eunectes)	(*228*)	C18
Calamagras weigeli	35.2		Ungaliophiinae+ Charininae	(*228*)	C19
Geiseltaliellus maarius	47		Corytophanes+ Basiliscus	(*232, 233*)	C20
Ophisaurus sp.	33		Anguinae	(*90*)	C21
unnamed	18.7		*Charina+Lichanura*	(*228*)	C22
Vipera aspis complex	20	23.8	Crotalinae+ Viperinae	(*229*)	C23
Egernia gillespieae	14.8		Egernia	(*234*)	C24
Natrix aff. *longivertebrata*	13.8		crown Natricidae	(*84, 235*)	C25
Paleheterodon tiheni	12.08		*Heterodon+ Farancia*	(*229*)	C26
Crotalinae gen. & sp. indet. A	11.2		stem Crotalinae	(*84, 236*)	C27
Morelia riversleighensis	13		*Morelia+Liasis*	(*228*)	C28
Bungarus sp.	10.215		genus *Bungarus*	(*229*)	C29
Incongruelaps iteratus	10		Laticauda+ Oxyuraninae	(*229*)	C30
Pantherophis sp.	11.93		*Pantherophis+ Pituophis*	(*229*)	C31

Table S2: Ecological, morphological, environmental, and biogeographic variables considered in this study. Sample size (n) reflects the number of species for which the trait was measured that are also represented in our genetic phylogeny of 6,885 species. Traits were grouped into four different categories: primary traits, secondary traits (type 1), secondary traits (type 2), and biogeographic traits. See Section 2.1 for more details on these categories. All traits listed below were considered as predictors of speciation rate variation in squamate evolution (see Table S3). We define ***primary traits*** as those that have a well-defined distance metric associated with character state differences (e.g., excludes categorical data) and where trait values for individual species are not simply averaged or generalized state assignments applied to entire clades. For example, foraging mode and cranial kinesis are classic traits in squamate biology but available summaries typically assign entire clades (e.g, snakes) to a single state ("highly kinetic") while masking extensive within-clade variation. These traits are considered secondary traits (type 2). ***Primary traits*** also excluded *numbers of digits* and *numbers of limbs*, because variation in these traits does not generally correlate with species-level environmental or ecological diversity; rather, variation in those traits typically reflects intermediate stages of an evolutionary sequence leading to body elongation and complete limb loss. These traits are considered secondary traits (type 1). Net innovation (ψ) and evolutionary rates (TR) were estimated for primary traits only (highlighted in yellow), due to concerns about data quality/completeness and non-metric properties of secondary traits.

Trait categories	Trait type	trait	n	description
Primary traits	morphological	mass	6,692	Estimated maximum body mass of adult individuals
		Snout-vent length	6,692	Length of adult individual from snout (or tip of rostrum) to vent (cloacal slit)
		Elongation index	6,692	Index of body elongation: ratio of length to width
		Number of presacral vertebrae	2,116	Number of vertebral elements anterior to sacrum
		multivariate skull shape	268	40 Procrustes transformed coordinates describing skull shape from 2D lateral images; used to infer skull PC1 & 2
	environmental	Multivariate climate space	6,387	Average values across the range for 19 bioclimatic variables, net primary productivity and climatic moisture index; used to infer climate PC1 - 6
	ecological	Chemosensory index	6,872	Sum of derived character states for nine morphological traits associated with chemoreception; higher values of index denote increased chemosensory ability
		multivariate diet	1,314	Model-inferred multivariate dietary niche; frequency distribution across 31 taxonomic resource categories (Section 2.2.6). These variables were also used to infer diet PC1 & 2

		Diet breadth	1,314	Degree of dietary specialization, calculated from inferred multivariate niche estimates
Secondary traits, type 1	morphological	Number of digits	6,884	Summed total of digits on hindlimbs and forelimbs on one side of individual (zero to ten)
		Number of limbs	6,884	Hindlimb plus forelimb total on one side (0, 1, 2)
Secondary traits, type 2	Morphological	Skull kinesis type	6,885	Akinetic, mesokinesis, metakinesis, hypokinesis, or hyperkinetic
		Prehension mechanism	6,885	How prey are captured – jaw, lingual, or both
	Ecological	parity	5,369	Oviparous (laying eggs), viviparous (birthing live young), mixed
		Foraging mode	6,699	Active (movement through habitat to find prey), ambush (individual waits for prey to approach), herbivore, mixed
Biogeographic traits		Latitude	6,393	Latitude of species range centroid
		elevation	6,393	Average elevation across a species range

Table S3: Explanatory power of 11 different sets of predictor traits on speciation rate variation across squamates. Traits were grouped together by type to create multivariate models. For each model, we ran a phylogenetically corrected linear regression of predictor traits against speciation rate, as estimated by CLaDS (λ_{CLaDS}) or BAMM (λ_{BAMM}). We additionally ran a phylogenetic regression that uses time-calibrated branch lengths in the model. Shown are the sample size – or, number of included species – and the explanatory power of each model, as measured by R^2. All species whose phylogenetic placement were imputed were dropped prior to regression. Although some predictor traits are statistically significant, they explain a very minimal amount of speciation rate variation. Our best model only explains ~2% of the variation in speciation rate.

model	n	Predictor traits	adj. R^2 (λ_{CLaDS})	adj. R^2 (λ_{BAMM})	adj. R^2 (λ_{CLaDS}) - br. len. model
skull kinesis	6,884	Kinesis type, prehension mechanism	0.009	0.022	0
parity mode	5,368	Parity type	0.004	0.007	0.005
chemosensory	6,871	chem (Chemosensory index)	0.002	0.004	0
climate	6,386	climate PC1 & climate PC2	0.001	0.001	0
foraging mode	6,698	Foraging mode	0	0.012	0
body size/shape	6,691	Log mass, log snout-vent length, log elongation index	0	0.001	0.001
digit/limb count	6,883	num. of digits, num. of limbs	0	0	0
geography	6,392	Latitude (range center), elevation	0	0	0
skull shape	267	Skull PC1 and skull PC2	-0.007	-0.002	-0.002
diet	1,313	Diet composition (PC1), Diet composition (PC2), log diet breadth	-0.001	0.001	0.005
vertebral count	1,957	num. of presacral vertebrae	0	0	0.001

Table S4: Nine of the anchored hybrid enrichment (AHE) loci are identical to genes commonly used in squamate phylogenetics (*54*). Our target phylogenomic loci included 38 other genes that have been commonly used in squamate phylogenetics – i.e., *RAG2*, *cmos*, and *R35 (51)*. For these 47 genes, we were able to combine previously sequenced data available on GenBank with our internal phylogenomic alignments.

AHE locus	Corresponding gene name
AHE-L50	*MSH6*
AHE-L60	*ZEB2*
AHE-L113	*GHSR*
AHE-L183	*DLL1*
AHE-L203	*VCPIP1*
AHE-L259	*RAG1*
AHE-L288	*CAND1*
AHE-L309	*SLC8A3*
AHE-L381	*ADNP*

Table S5: Divergence times for key crown groups in squamate evolutionary history. Shown are clade names, the node they map to in fig. S37, their median & 95% HPD as inferred for the phylogenomic tree (see Section 1.4.2), the median and range in the pseudo-posterior set of trees (fig. S37), and the geological epoch and stage associated with this node.

node	clade	median (95% HPD)	fossil con-straint	full tree (pseudo-posterior range)	stage	epoch
S	crown squamata	213.19 (203.57-223.11)		213.19 (200.36-221.84)	Norian	Upper Triassic
U	Unidentata	203.72 (194.65-212.06)		203.72 (191.89-214.1)	Rhaetian	Upper Triassic
E	Episquamata	188.34 (180.52-195.88)		188.34 (177.17-199.4)	Pleinsbachian	Lower Jurassic
C	Scincoidea	186.04 (177.2-195.36)	C5	186.04 (176.94-196.28)	Toarcian	Lower Jurassic
X	Toxicofera	180.36 (173.14-187.52)		180.36 (171.39-190.53)	Toarcian	Lower Jurassic
I	Iguania	168.1 (160.72-175.99)		168.1 (158.37-179.23)	Bathonian-Bajocian	Middle Jurassic
A	Amphisbaenia	(not in genomic time tree)		148.38 (136.9-159.85)	Tithonian	Upper Jurassic
F	Anguiformes	144.6 (140.97-149.03)	C8	144.6 (140.27-150.28)	Berriasian	Lower Cretaceous
P	Serpentes	120.31 (114.57-126.55)		120.31 (113.88-130.67)	Aptian	Lower Cretaceous
D	Scolecophidia	115.23 (98.65-125.58)		115.23 (98.98-132.47)	Albian	Lower Cretaceous
T	Teioidea	110.06 (102.34-117.65)		110.06 (100.79-118.62)	Albian	Lower Cretaceous
G	Gekkota	108.73 (101.96-114.97)	C21	108.73 (98.46-118.26)	Aptian	Lower Cretaceous
H	Alethinophidia	88.91 (84.47-93.36)	C1	88.91 (83.41-95.48)	Coniacian	Upper Cretaceous
L	Lacertoidea	(not in genomic time tree)		71.68 (53.34-89.16)	Maastrictian	Late Cretaceous
M	Colubriformes	47.71 (43.43-51.32)		47.71 (42.85-52.98)	Lutetian-Ypresian	Eocene

Data S1: Data for the 1,083 phylogenomic samples included in our study, of which 841 were newly collected and 242 were sourced from previous studies (*124, 237–249*). For data that were collected in previous studies, SRA accession is NA; please refer to the original study for data access. Reported is the taxonomic identity for each sample, the source of the data, the number of loci and their average link, and the SRA accession where raw data can be found. All newly collected data are available at Bioproject PRJNA918674 on NCBI. Institutional codes for voucher specimens with newly collected sequence data: ABTC, Australian Biological Tissue Collection; AMNH, American Museum of Natural History; AMS, Australian Museum, Sydney; ANWC, Australian National Wildlife Collection; BNHS, Bombay Natural History Society; BPBM, Bernice Pauahi Bishop Museum; CAS, California Academy of Sciences; CHUNB, Coleção Herpetológica da Universidade de Brasília; CUMV, Cornell University Museum of Vertebrates; FMNH, Field Museum of Natural History; KU, Biodiversity Institute - University of Kansas; MCZ, Museum of Comparative Zoology; MPEG, Museu Paraense "Emilio Goeldi", Belém; MUSM, Museo de Historia Natural, Universidad Nacional Mayor de San Marcos, Lima; MVZ, Museum of Vertebrate Zoology; NTM, Museums and Art Galleries of the Northern Territory; NVM, Museums Victoria, Melbourne; PEM, Port Elizabeth Museum; QM, Queensland Museum; SAM, South Australian Museum; TAU, Tel Aviv University Zoological Museum; UFMT, Universidade Federal de Mato Grosso; UMMZ, University of Michigan Museum of Zoology; UPRM, University of Puerto Rico, Mayagüez; USNM, Smithsonian Institution, National Museum of Natural History; UWBM, University of Washington, Burke Museum of Natural History and Culture; WAM, Western Australian Museum.

Data S2: Taxonomy and metadata associated with the genetic and genomic sequences used in our phylogenetic inference. We provide the original taxon names associated with the sequences (headers *ncbiTaxon*, *ncbiTaxon_ssp* and *ncbiTaxonID* provide the species, subspecies and NCBI ID's), as well as the taxon names of our standardized taxonomy that we employ in our phylogeny and across all trait datasets in this study (header *finalTipName*). We additionally provide accession numbers, locus names and the sequence lengths. The sources of the sequence data are listed in the *source* field, and we also indicate whether or not the species was part of the taxonomic constraint we applied to the inference of the full tree.

Data S3: List of constraints used in imputing taxa to create "fully sampled" phylogenies. Constraints were done at the generic level; 651 genera had missing species. For each genus, we show: constraint category (see Section 1.5 for details), spanning taxon for the constraint, number of species in the genus represented in our genetic phylogeny, number of missing species in the genus, and if the constraint defined an inclusion or exclusion for placement.

References and Notes

1. C. L. Camp, Classification of the Lizards. *Bull. Am. Mus. Nat. Hist.* **48**, 289–480 (1923).

2. T. Townsend, A. Larson, E. Louis, J. R. Macey, Molecular phylogenetics of squamata: The position of snakes, amphisbaenians, and dibamids, and the root of the squamate tree. *Syst. Biol.* **53**, 735–757 (2004).

3. H. W. Greene, *Snakes: The Evolution of Mystery in Nature* (Univ. of California Press, 1997).

4. J. J. Wiens, M. C. Brandley, T. W. Reeder, Why does a trait evolve multiple times within a clade? Repeated evolution of snakelike body form in squamate reptiles. *Evolution* **60**, 123–141 (2006).

5. K. Schwenk, The evolution of chemoreception in squamate reptiles: A phylogenetic approach. *Brain Behav. Evol.* **41**, 124–137 (1993).

6. K. Metzger, "Cranial kinesis in lepidosaurs: skulls in motion" in *Topics in Functional and Ecological Vertebrate Morphology*, P. Aerts, K. D'Aout, A. Herrel, R. Van Damme, Eds. (Shaker Publishing, Düren and Maastricht, 2002), pp. 15–46.

7. L. J. Vitt, E. R. Pianka, Deep history impacts present-day ecology and biodiversity. *Proc. Natl. Acad. Sci. U.S.A.* **102**, 7877–7881 (2005).

8. A. Watanabe, A.-C. Fabre, R. N. Felice, J. A. Maisano, J. Müller, A. Herrel, A. Goswami, Ecomorphological diversification in squamates from conserved pattern of cranial integration. *Proc. Natl. Acad. Sci. U.S.A.* **116**, 14688–14697 (2019).

9. F. O. Da Silva, A.-C. Fabre, Y. Savriama, J. Ollonen, K. Mahlow, A. Herrel, J. Müller, N. Di-Poï, The ecological origins of snakes as revealed by skull evolution. *Nat. Commun.* **9**, 376 (2018).

10. U. Roll, A. Feldman, M. Novosolov, A. Allison, A. M. Bauer, R. Bernard, M. Böhm, F. Castro-Herrera, L. Chirio, B. Collen, G. R. Colli, L. Dabool, I. Das, T. M. Doan, L. L. Grismer, M. Hoogmoed, Y. Itescu, F. Kraus, M. LeBreton, A. Lewin, M. Martins, E. Maza, D. Meirte, Z. T. Nagy, C. de C Nogueira, O. S. G. Pauwels, D. Pincheira-Donoso, G. D. Powney, R. Sindaco, O. J. S. Tallowin, O. Torres-Carvajal, J. F. Trape, E. Vidan, P. Uetz, P. Wagner, Y. Wang, C. D. L. Orme, R. Grenyer, S. Meiri, The global distribution of tetrapods reveals a need for targeted reptile conservation. *Nat. Ecol. Evol.* **1**, 1677–1682 (2017).

11. G. G. Simpson, *Tempo and Mode in Evolution* (Columbia Univ. Press, 1944).

12. M. J. Landis, J. G. Schraiber, Pulsed evolution shaped modern vertebrate body sizes. *Proc. Natl. Acad. Sci. U.S.A.* **114**, 13224–13229 (2017).

13. C. R. Cooney, J. A. Bright, E. J. R. Capp, A. M. Chira, E. C. Hughes, C. J. A. Moody, L. O. Nouri, Z. K. Varley, G. H. Thomas, Mega-evolutionary dynamics of the adaptive radiation of birds. *Nature* **542**, 344–347 (2017).

14. G. Navalón, A. Bjarnason, E. Griffiths, R. B. J. Benson, Environmental signal in the evolutionary diversification of bird skeletons. *Nature* **611**, 306–311 (2022).

15. A. Goswami, E. Noirault, E. J. Coombs, J. Clavel, A.-C. Fabre, T. J. D. Halliday, M. Churchill, A. Curtis, A. Watanabe, N. B. Simmons, B. L. Beatty, J. H. Geisler, D. L. Fox,

R. N. Felice, Attenuated evolution of mammals through the Cenozoic. *Science* **378**, 377–383 (2022).

16. J. W. Valentine, D. Jablonski, D. H. Erwin, Fossils, molecules and embryos: New perspectives on the Cambrian explosion. *Development* **126**, 851–859 (1999).

17. Materials and methods are available as supplementary materials.

18. W. Jetz, G. H. Thomas, J. B. Joy, K. Hartmann, A. O. Mooers, The global diversity of birds in space and time. *Nature* **491**, 444–448 (2012).

19. N. P. Giannini, Canonical phylogenetic ordination. *Syst. Biol.* **52**, 684–695 (2003).

20. T. R. Simões, O. Vernygora, M. W. Caldwell, S. E. Pierce, Megaevolutionary dynamics and the timing of evolutionary innovation in reptiles. *Nat. Commun.* **11**, 3322 (2020).

21. O. Seehausen, C. E. Wagner, Speciation in freshwater fishes. *Annu. Rev. Ecol. Evol. Syst.* **45**, 621–651 (2014).

22. D. Schluter, *The Ecology of Adaptive Radiation* (Oxford Univ. Press, 2000).

23. T. Price, *Speciation in Birds* (W. H. Freeman, 2008).

24. T. J. Colston, G. C. Costa, L. J. Vitt, Snake diets and the deep history hypothesis. *Biol. J. Linn. Soc. Lond.* **101**, 476–486 (2010).

25. M. C. Grundler, D. L. Rabosky, Rapid increase in snake dietary diversity and complexity following the end-Cretaceous mass extinction. *PLOS Biol.* **19**, e3001414 (2021).

26. D. L. Rabosky, J. Chang, P. O. Title, P. F. Cowman, L. Sallan, M. Friedman, K. Kaschner, C. Garilao, T. J. Near, M. Coll, M. E. Alfaro, An inverse latitudinal gradient in speciation rate for marine fishes. *Nature* **559**, 392–395 (2018).

27. L. F. Henao Diaz, L. J. Harmon, M. T. C. Sugawara, E. T. Miller, M. W. Pennell, Macroevolutionary diversification rates show time dependency. *Proc. Natl. Acad. Sci. U.S.A.* **116**, 7403–7408 (2019).

28. J. C. Uyeda, R. Zenil-Ferguson, M. W. Pennell, Rethinking phylogenetic comparative methods. *Syst. Biol.* **67**, 1091–1109 (2018).

29. B. G. Fry, H. Scheib, L. van der Weerd, B. Young, J. McNaughtan, S. F. R. Ramjan, N. Vidal, R. E. Poelmann, J. A. Norman, Evolution of an arsenal: Structural and functional diversification of the venom system in the advanced snakes (Caenophidia). *Mol. Cell. Proteomics* **7**, 215–246 (2008).

30. H. W. Greene, Dietary Correlates of the Origin and Radiation of Snakes1. *Integr. Comp. Biol.* **23**, 431–441 (2015).

31. G. I. M. Pasquesi, R. H. Adams, D. C. Card, D. R. Schield, A. B. Corbin, B. W. Perry, J. Reyes-Velasco, R. P. Ruggiero, M. W. Vandewege, J. A. Shortt, T. A. Castoe, Squamate reptiles challenge paradigms of genomic repeat element evolution set by birds and mammals. *Nat. Commun.* **9**, 2774 (2018).

32. T. A. Castoe, A. P. J. de Koning, K. T. Hall, D. C. Card, D. R. Schield, M. K. Fujita, R. P. Ruggiero, J. F. Degner, J. M. Daza, W. Gu, J. Reyes-Velasco, K. J. Shaney, J. M. Castoe, S. E. Fox, A. W. Poole, D. Polanco, J. Dobry, M. W. Vandewege, Q. Li, R. K. Schott, A. Kapusta, P. Minx, C. Feschotte, P. Uetz, D. A. Ray, F. G. Hoffmann, R. Bogden, E. N.

Smith, B. S. W. Chang, F. J. Vonk, N. R. Casewell, C. V. Henkel, M. K. Richardson, S. P. Mackessy, A. M. Bronikowski, M. Yandell, W. C. Warren, S. M. Secor, D. D. Pollock, The Burmese python genome reveals the molecular basis for extreme adaptation in snakes. *Proc. Natl. Acad. Sci. U.S.A.* **110**, 20645–20650 (2013).

33. F. C. Patchell, R. Shine, Feeding Mechanisms in Pygopodid Lizards: How Can Lialis Swallow Such Large Prey? *J. Herpetol.* **20**, 59–64 (1986).

34. T. H. Frazzetta, From Hopeful Monsters to Bolyerine Snakes? *Am. Nat.* **104**, 55–72 (1970).

35. C. E. Wagner, L. J. Harmon, O. Seehausen, Ecological opportunity and sexual selection together predict adaptive radiation. *Nature* **487**, 366–369 (2012).

36. A. de Queiroz, Contingent predictability in evolution: Key traits and diversification. *Syst. Biol.* **51**, 917–929 (2002).

37. C. Venditti, A. Meade, M. Pagel, Multiple routes to mammalian diversity. *Nature* **479**, 393–396 (2011).

38. D. L. Mahler, T. Ingram, L. J. Revell, J. B. Losos, Exceptional convergence on the macroevolutionary landscape in island lizard radiations. *Science* **341**, 292–295 (2013).

39. D. N. Reznick, R. E. Ricklefs, Darwin's bridge between microevolution and macroevolution. *Nature* **457**, 837–842 (2009).

40. D. Jablonski, Background and mass extinctions: The alternation of macroevolutionary regimes. *Science* **231**, 129–133 (1986).

41. G. C. Williams, *Natural Selection: Domains, Levels, and Challenges* (Oxford Univ. Press, 1992).

42. P. O. Title, S. Singhal, M. C. Grundler, G. C. Costa, R. A. Pyron, T. J. Colston, M. R. Grundler, I. Prates, N. Stepanova, M. E. H. Jones, L. B. Q. Cavalcanti, G. R. Colli, N. Di-Poï, S. C. Donnellan, C. Moritz, D. O. Mesquita, E. R. Pianka, S. A. Smith, L. J. Vitt, D. L. Rabosky, Data from: The macroevolutionary singularity of snakes, Dryad (2023); https://doi.org/10.5061/dryad.p5hqbzkvb.

43. P. O. Title, S. Singhal, M. C. Grundler, G. C. Costa, R. A. Pyron, T. J. Colston, M. R. Grundler, I. Prates, N. Stepanova, M. E. H. Jones, L. B. Q. Cavalcanti, G. R. Colli, N. Di-Poï, S. C. Donnellan, C. Moritz, D. O. Mesquita, E. R. Pianka, S. A. Smith, L. J. Vitt, D. L. Rabosky, Data from: The macroevolutionary singularity of snakes, Version v1, Zenodo (2023); https://doi.org/10.5281/zenodo.8250112.

44. V. A. Funk, R. Edwards, S. Keeley, The problem with(out) vouchers. *Taxon* **67**, 3–5 (2018).

45. J. C. Buckner, R. C. Sanders, B. C. Faircloth, P. Chakrabarty, The critical importance of vouchers in genomics. *eLife* **10**, e68264 (2021).

46. C. W. Thompson, K. L. Phelps, M. W. Allard, J. A. Cook, J. L. Dunnum, A. W. Ferguson, M. Gelang, F. A. A. Khan, D. L. Paul, D. M. Reeder, N. B. Simmons, M. P. M. Vanhove, P. W. Webala, M. Weksler, C. W. Kilpatrick, Preserve a Voucher Specimen! The Critical Need for Integrating Natural History Collections in Infectious Disease Studies. *mBio* **12**, e02698-20 (2021).

47. K. R. Johnson, I. F. P. Owens; Global Collection Group, A global approach for natural history museum collections. *Science* **379**, 1192–1194 (2023).

48. M. R. Grundler, S. Singhal, M. A. Cowan, D. L. Rabosky, Is genomic diversity a useful proxy for census population size? Evidence from a species-rich community of desert lizards. *Mol. Ecol.* **28**, 1664–1674 (2019).

49. S. Singhal, G. R. Colli, M. R. Grundler, G. C. Costa, I. Prates, D. L. Rabosky, No link between population isolation and speciation rate in squamate reptiles. *Proc. Natl. Acad. Sci. U.S.A.* **119**, e2113388119 (2022).

50. S. Singhal, T. J. Colston, M. R. Grundler, S. A. Smith, G. C. Costa, G. R. Colli, C. Moritz, R. A. Pyron, D. L. Rabosky, Congruence and conflict in the higher-level phylogenetics of squamate reptiles: An expanded phylogenomic perspective. *Syst. Biol.* **70**, 542–557 (2021).

51. S. Singhal, M. Grundler, G. Colli, D. L. Rabosky, Squamate Conserved Loci (SqCL): A unified set of conserved loci for phylogenomics and population genetics of squamate reptiles. *Mol. Ecol. Resour.* **17**, e12–e24 (2017).

52. A. R. Lemmon, S. A. Emme, E. M. Lemmon, Anchored hybrid enrichment for massively high-throughput phylogenomics. *Syst. Biol.* **61**, 727–744 (2012).

53. B. C. Faircloth, J. E. McCormack, N. G. Crawford, M. G. Harvey, R. T. Brumfield, T. C. Glenn, Ultraconserved elements anchor thousands of genetic markers spanning multiple evolutionary timescales. *Syst. Biol.* **61**, 717–726 (2012).

54. J. J. Wiens, C. R. Hutter, D. G. Mulcahy, B. P. Noonan, T. M. Townsend, J. W. Sites Jr., T. W. Reeder, Resolving the phylogeny of lizards and snakes (Squamata) with extensive sampling of genes and species. *Biol. Lett.* **8**, 1043–1046 (2012).

55. S. M. Aljanabi, I. Martinez, Universal and rapid salt-extraction of high quality genomic DNA for PCR-based techniques. *Nucleic Acids Res.* **25**, 4692–4693 (1997).

56. K. Bi, D. Vanderpool, S. Singhal, T. Linderoth, C. Moritz, J. M. Good, Transcriptome-based exon capture enables highly cost-effective comparative genomic data collection at moderate evolutionary scales. *BMC Genomics* **13**, 403 (2012).

57. D. M. Portik, L. L. Smith, K. Bi, An evaluation of transcriptome-based exon capture for frog phylogenomics across multiple scales of divergence (Class: Amphibia, Order: Anura). *Mol. Ecol. Resour.* **16**, 1069–1083 (2016).

58. W. J. Kent, BLAT—The BLAST-like alignment tool. *Genome Res.* **12**, 656–664 (2002).

59. H. Li, B. Handsaker, A. Wysoker, T. Fennell, J. Ruan, N. Homer, G. Marth, G. Abecasis, R. Durbin; 1000 Genome Project Data Processing Subgroup, The Sequence Alignment/Map format and SAMtools. *Bioinformatics* **25**, 2078–2079 (2009).

60. A. M. Bolger, M. Lohse, B. Usadel, Trimmomatic: A flexible trimmer for Illumina sequence data. *Bioinformatics* **30**, 2114–2120 (2014).

61. J. Zhang, K. Kobert, T. Flouri, A. Stamatakis, PEAR: A fast and accurate Illumina Paired-End reAd mergeR. *Bioinformatics* **30**, 614–620 (2014).

62. M. G. Grabherr, B. J. Haas, M. Yassour, J. Z. Levin, D. A. Thompson, I. Amit, X. Adiconis, L. Fan, R. Raychowdhury, Q. Zeng, Z. Chen, E. Mauceli, N. Hacohen, A. Gnirke, N. Rhind, F. di Palma, B. W. Birren, C. Nusbaum, K. Lindblad-Toh, N. Friedman, A.

Regev, Full-length transcriptome assembly from RNA-Seq data without a reference genome. *Nat. Biotechnol.* **29**, 644–652 (2011).

63. H. Li, Aligning sequence reads, clone sequences and assembly contigs with BWA-MEM. ArXiv:1303.3997 [q-bio.GN] (2013)..

64. K. Katoh, G. Asimenos, H. Toh, Multiple alignment of DNA sequences with MAFFT. *Methods Mol. Biol.* **537**, 39–64 (2009).

65. M. G. Harvey, G. A. Bravo, S. Claramunt, A. M. Cuervo, G. E. Derryberry, J. Battilana, G. F. Seeholzer, J. S. McKay, B. C. O'Meara, B. C. Faircloth, S. V. Edwards, J. Pérez-Emán, R. G. Moyle, F. H. Sheldon, A. Aleixo, B. T. Smith, R. T. Chesser, L. F. Silveira, J. Cracraft, R. T. Brumfield, E. P. Derryberry, The evolution of a tropical biodiversity hotspot. *Science* **370**, 1343–1348 (2020).

66. A. Stamatakis, RAxML version 8: A tool for phylogenetic analysis and post-analysis of large phylogenies. *Bioinformatics* **30**, 1312–1313 (2014).

67. S. Guindon, J.-F. Dufayard, V. Lefort, M. Anisimova, W. Hordijk, O. Gascuel, New algorithms and methods to estimate maximum-likelihood phylogenies: Assessing the performance of PhyML 3.0. *Syst. Biol.* **59**, 307–321 (2010).

68. C. Zhang, M. Rabiee, E. Sayyari, S. Mirarab, ASTRAL-III: Polynomial time species tree reconstruction from partially resolved gene trees. *BMC Bioinformatics* **19** (Suppl 6), 153 (2018).

69. D. M. Portik, J. J. Wiens, Do Alignment and Trimming Methods Matter for Phylogenomic (UCE) Analyses? *Syst. Biol.* **70**, 440–462 (2021).

70. J. H. Degnan, N. A. Rosenberg, Gene tree discordance, phylogenetic inference and the multispecies coalescent. *Trends Ecol. Evol.* **24**, 332–340 (2009).

71. F. T. Burbrink, F. G. Grazziotin, R. A. Pyron, D. Cundall, S. Donnellan, F. Irish, J. S. Keogh, F. Kraus, R. W. Murphy, B. Noonan, C. J. Raxworthy, S. Ruane, A. R. Lemmon, E. M. Lemmon, H. Zaher, Interrogating Genomic-Scale Data for Squamata (Lizards, Snakes, and Amphisbaenians) Shows no Support for Key Traditional Morphological Relationships. *Syst. Biol.* **69**, 502–520 (2020).

72. A. M. Kozlov, A. J. Aberer, A. Stamatakis, ExaML version 3: A tool for phylogenomic analyses on supercomputers. *Bioinformatics* **31**, 2577–2579 (2015).

73. X.-X. Shen, C. T. Hittinger, A. Rokas, Contentious relationships in phylogenomic studies can be driven by a handful of genes. *Nat. Ecol. Evol.* **1**, 0126 (2017).

74. K. Aberer, D. Krompaß, A. Stamatakis, "RogueNaRok: An efficient and exact algorithm for rogue taxon identification," Heidelberg Institute for Theoretical Studies (2011); https://cme.h-its.org/exelixis/pubs/Exelixis-RRDR-2011-10.pdf.

75. B. Q. Minh, H. A. Schmidt, O. Chernomor, D. Schrempf, M. D. Woodhams, A. von Haeseler, R. Lanfear, IQ-TREE 2: New Models and Efficient Methods for Phylogenetic Inference in the Genomic Era. *Mol. Biol. Evol.* **37**, 1530–1534 (2020).

76. O. Jeffroy, H. Brinkmann, F. Delsuc, H. Philippe, Phylogenomics: The beginning of incongruence? *Trends Genet.* **22**, 225–231 (2006).

77. S. A. Smith, M. J. Moore, J. W. Brown, Y. Yang, Analysis of phylogenomic datasets reveals conflict, concordance, and gene duplications with examples from animals and plants. *BMC Evol. Biol.* **15**, 150 (2015).

78. S. A. Smith, J. F. Walker, PyPHLAWD: A Python tool for phylogenetic dataset construction. *Methods Ecol. Evol.* **10**, 104–108 (2019).

79. G. S. C. Slater, E. Birney, Automated generation of heuristics for biological sequence comparison. *BMC Bioinformatics* **6**, 31 (2005).

80. T. Rognes, T. Flouri, B. Nichols, C. Quince, F. Mahé, VSEARCH: A versatile open source tool for metagenomics. *PeerJ* **4**, e2584 (2016).

81. C. Hahn, L. Bachmann, B. Chevreux, Reconstructing mitochondrial genomes directly from genomic next-generation sequencing reads—A baiting and iterative mapping approach. *Nucleic Acids Res.* **41**, e129–e129 (2013).

82. P. Uetz, P. Freed, R. Aguilar, J. Hošek, The Reptile Database (2021); http://www.reptile-database.org.

83. J. F. R. Tonini, K. H. Beard, R. B. Ferreira, W. Jetz, R. A. Pyron, Fully-sampled phylogenies of squamates reveal evolutionary patterns in threat status. *Biol. Conserv.* **204**, 23–31 (2016).

84. H. Zaher, R. W. Murphy, J. C. Arredondo, R. Graboski, P. R. Machado-Filho, K. Mahlow, G. G. Montingelli, A. B. Quadros, N. L. Orlov, M. Wilkinson, Y.-P. Zhang, F. G. Grazziotin, Large-scale molecular phylogeny, morphology, divergence-time estimation, and the fossil record of advanced caenophidian snakes (Squamata: Serpentes). *PLOS ONE* **14**, e0216148 (2019).

85. D. M. Portik, J. J. Wiens, SuperCRUNCH: A bioinformatics toolkit for creating and manipulating supermatrices and other large phylogenetic datasets. *Methods Ecol. Evol.* **11**, 763–772 (2020).

86. V. Ranwez, E. J. P. Douzery, C. Cambon, N. Chantret, F. Delsuc, MACSE v2: Toolkit for the Alignment of Coding Sequences Accounting for Frameshifts and Stop Codons. *Mol. Biol. Evol.* **35**, 2582–2584 (2018).

87. K. Katoh, D. M. Standley, MAFFT multiple sequence alignment software version 7: Improvements in performance and usability. *Mol. Biol. Evol.* **30**, 772–780 (2013). doi:10.1093/molbev/mst010 Medline

88. J. W. Brown, J. F. Walker, S. A. Smith, Phyx: Phylogenetic tools for unix. *Bioinformatics* **33**, 1886–1888 (2017).

89. J. B. Pease, J. W. Brown, J. F. Walker, C. E. Hinchliff, S. A. Smith, Quartet Sampling distinguishes lack of support from conflicting support in the green plant tree of life. *Am. J. Bot.* **105**, 385–403 (2018).

90. M. E. H. Jones, C. L. Anderson, C. A. Hipsley, J. Müller, S. E. Evans, R. R. Schoch, Integration of molecules and new fossils supports a Triassic origin for Lepidosauria (lizards, snakes, and tuatara). *BMC Evol. Biol.* **13**, 208 (2013).

91. R. L. Nydam, A new taxon of helodermatid-like lizard from the Albian–Cenomanian of Utah. *J. Vertebr. Paleontol.* **20**, 285–294 (2000).

92. J. L. Conrad, Phylogeny and systematics of Squamata (Reptilia) based on morphology. *Bull. Am. Mus. Nat. Hist.* **2008**, 1–182 (2008).

93. T. W. Reeder, T. M. Townsend, D. G. Mulcahy, B. P. Noonan, P. L. Wood Jr., J. W. Sites Jr., J. J. Wiens, Integrated analyses resolve conflicts over squamate reptile phylogeny and reveal unexpected placements for fossil taxa. *PLOS ONE* **10**, e0118199 (2015).

94. R. L. Cifelli, J. I. Kirkland, A. Weil, A. L. Deino, B. J. Kowallis, High-precision 40Ar/39Ar geochronology and the advent of North America's Late Cretaceous terrestrial fauna. *Proc. Natl. Acad. Sci. U.S.A.* **94**, 11163–11167 (1997).

95. J. L. Conrad, O. Rieppel, L. Grande, A Green River (Eocene) polychrotid (Squamata: Reptilia) and a re-examination of iguanian systematics. *J. Paleontol.* **81**, 1365–1373 (2007).

96. M. Elliot Smith, K. R. Chamberlain, B. S. Singer, A. R. Carroll, Eocene clocks agree: Coeval 40Ar/39Ar, U-Pb, and astronomical ages from the Green River Formation. *Geology* **38**, 527–530 (2010).

97. R. L. Nydam, A. L. Titus, M. A. Loewen, "Lizards and snakes from the Cenomanian through Campanian of southern Utah: Filling the gap in the fossil record of Squamata from the Late Cretaceous of the Western Interior of North America" in *At the Top of the Grand Staircase: the Late Cretaceous of Southern Utah*, A. L. Titus, M. A. Loewen, Eds. (Indiana Univ. Press, 2013), pp. 370–423.

98. E. M. Roberts, S. D. Sampson, A. L. Deino, S. A. Bowring, R. Buchwaldt, "The Kaiparowits Formation: A remarkable record of late Cretaceous terrestrial environments, ecosystems, and evolution in western North America" in *At the Top of the Grand Staircase: The Late Cretaceous of Southern Utah*, A. L. Titus, M. A. Loewen, Eds. (Indiana Univ. Press, 2013), p. 22.

99. M. W. Caldwell, R. L. Nydam, A. Palci, S. Apesteguía, The oldest known snakes from the Middle Jurassic-Lower Cretaceous provide insights on snake evolution. *Nat. Commun.* **6**, 5996 (2015).

100. A. R. H. LeBlanc, A. Palci, N. Anthwal, A. S. Tucker, R. Araújo, M. F. C. Pereira, M. W. Caldwell, A conserved tooth resorption mechanism in modern and fossil snakes. *Nat. Commun.* **14**, 742 (2023).

101. J. Head, R. Benson, S. E. Evans, Running with the devils: postcranial osteology of the enigmatic Jurassic parviraptorid squamates, and their implications for the evolution of the snake body form, *J. Vertebr. Paleontol., Program and Abstracts* (2023), p. 176.

102. S. E. Evans, "The origin and early diversification of squamates" in *The Origin and Early Evolutionary History of Snakes*, D. J. Gower, H. Zaher, Eds. (Cambridge Univ. Press, 2022), pp. 7–12.

103. V.-H. Reynoso, G. Callison, A new scincomorph lizard from the Early Cretaceous of Puebla, Mexico. *Zool. J. Linn. Soc.* **130**, 183–212 (2000).

104. A. Bolet, E. L. Stanley, J. D. Daza, J. S. Arias, A. Čerňanský, M. Vidal-García, A. M. Bauer, J. J. Bevitt, A. Peretti, S. E. Evans, Unusual morphology in the mid-Cretaceous lizard Oculudentavis. *Curr. Biol.* **31**, 3303–3314.e3 (2021).

105. C. D. Brownstein, D. L. Meyer, M. Fabbri, B. S. Bhullar, J. A. Gauthier, Evolutionary origins of the prolonged extant squamate radiation. *Nat. Commun.* **13**, 7087 (2022).

106. M. Tałanda, V. Fernandez, E. Panciroli, S. E. Evans, R. J. Benson, Synchrotron tomography of a stem lizard elucidates early squamate anatomy. *Nature* **611**, 99–104 (2022).

107. A. Čerňanský, E. L. Stanley, J. D. Daza, A. Bolet, J. S. Arias, A. M. Bauer, M. Vidal-García, J. J. Bevitt, A. M. Peretti, N. N. Aung, S. E. Evans, A new Early Cretaceous lizard in Myanmar amber with exceptionally preserved integument. *Sci. Rep.* **12**, 1660 (2022).

108. T. R. Simões, M. W. Caldwell, M. Tałanda, M. Bernardi, A. Palci, O. Vernygora, F. Bernardini, L. Mancini, R. L. Nydam, The origin of squamates revealed by a Middle Triassic lizard from the Italian Alps. *Nature* **557**, 706–709 (2018).

109. Z. Yang, PAML 4: Phylogenetic analysis by maximum likelihood. *Mol. Biol. Evol.* **24**, 1586–1591 (2007).

110. S. A. Smith, J. W. Brown, J. F. Walker, So many genes, so little time: A practical approach to divergence-time estimation in the genomic era. *PLOS ONE* **13**, e0197433 (2018).

111. Q. Tao, K. Tamura, F. U Battistuzzi, S. Kumar, A machine learning method for detecting autocorrelation of evolutionary rates in large phylogenies. *Mol. Biol. Evol.* **36**, 811–824 (2019).

112. Q. Tao, J. Barba-Montoya, S. Kumar, Data-driven speciation tree prior for better species divergence times in calibration-poor molecular phylogenies. *Bioinformatics* **37** (Suppl_1), i102–i110 (2021).

113. S. A. Smith, B. C. O'Meara, treePL: Divergence time estimation using penalized likelihood for large phylogenies. *Bioinformatics* **28**, 2689–2690 (2012).

114. D. L. Rabosky, No substitute for real data: A cautionary note on the use of phylogenies from birth-death polytomy resolvers for downstream comparative analyses. *Evolution* **69**, 3207–3216 (2015).

115. J. Chang, D. L. Rabosky, M. E. Alfaro, Estimating diversification rates on incompletely sampled phylogenies: Theoretical concerns and practical solutions. *Syst. Biol.* **69**, 602–611 (2020).

116. S. Nee, R. M. May, P. H. Harvey, The reconstructed evolutionary process. *Philos. Trans. R. Soc. Lond. Ser* **344**, 305–311 (1994).

117. N. Cusimano, T. Stadler, S. S. Renner, A new method for handling missing species in diversification analysis applicable to randomly or nonrandomly sampled phylogenies. *Syst. Biol.* **61**, 785–792 (2012).

118. R. A. Pyron, F. T. Burbrink, J. J. Wiens, A phylogeny and revised classification of Squamata, including 4161 species of lizards and snakes. *BMC Evol. Biol.* **13**, 93 (2013).

119. D. L. Rabosky, S. C. Donnellan, M. Grundler, I. J. Lovette, Analysis and visualization of complex macroevolutionary dynamics: An example from Australian scincid lizards. *Syst. Biol.* **63**, 610–627 (2014).

120. A. Skinner, A. F. Hugall, M. N. Hutchinson, Lygosomine phylogeny and the origins of Australian scincid lizards. *J. Biogeogr.* **38**, 1044–1058 (2011).

121. T. W. Reeder, A phylogeny of the Australian *Sphenomorphus* group (Scincidae: Squamata) and the phylogenetic placement of the crocodile skinks (*Tribolonotus*): Bayesian approaches to assessing congruence and obtaining confidence in maximum likelihood inferred relationships. *Mol. Phylogenet. Evol.* **27**, 384–397 (2003).

122. T. Stadler, Simulating trees with a fixed number of extant species. *Syst. Biol.* **60**, 676–684 (2011).

123. Y. Zheng, J. J. Wiens, Combining phylogenomic and supermatrix approaches, and a time-calibrated phylogeny for squamate reptiles (lizards and snakes) based on 52 genes and 4162 species. *Mol. Phylogenet. Evol.* **94** (Pt B), 537–547 (2016).

124. J. W. Streicher, J. J. Wiens, Phylogenomic analyses of more than 4000 nuclear loci resolve the origin of snakes among lizard families. *Biol. Lett.* **13**, 20170393 (2017).

125. N. Vidal, S. B. Hedges, The phylogeny of squamate reptiles (lizards, snakes, and amphisbaenians) inferred from nine nuclear protein-coding genes. *C. R. Biol.* **328**, 1000–1008 (2005).

126. D. G. Mulcahy, B. P. Noonan, T. Moss, T. M. Townsend, T. W. Reeder, J. W. Sites Jr., J. J. Wiens, Estimating divergence dates and evaluating dating methods using phylogenomic and mitochondrial data in squamate reptiles. *Mol. Phylogenet. Evol.* **65**, 974–991 (2012).

127. I. Irisarri, D. Baurain, H. Brinkmann, F. Delsuc, J.-Y. Sire, A. Kupfer, J. Petersen, M. Jarek, A. Meyer, M. Vences, H. Philippe, Phylotranscriptomic consolidation of the jawed vertebrate timetree. *Nat. Ecol. Evol.* **1**, 1370–1378 (2017).

128. R. A. Pyron, A likelihood method for assessing molecular divergence time estimates and the placement of fossil calibrations. *Syst. Biol.* **59**, 185–194 (2010).

129. X.-X. Shen, D. Liang, J.-Z. Wen, P. Zhang, Multiple genome alignments facilitate development of NPCL markers: A case study of tetrapod phylogeny focusing on the position of turtles. *Mol. Biol. Evol.* **28**, 3237–3252 (2011).

130. T. R. Simões, R. A. Pyron, The squamate tree of life. *Bull. Mus. Comp. Zool.* **163**, 47–95 (2021).

131. D. I. Whiteside, S. A. V. Chambi-Trowell, M. J. Benton, A Triassic crown squamate. *Sci. Adv.* **8**, eabq8274 (2022).

132. R. Vullo, S. Bailon, Y. Dauphin, H. Monchot, R. Allain, A reappraisal of Jeddaherdan aleadonta (Squamata: Acrodonta), the purported oldest iguanian lizard from Africa. *Cretac. Res.* **143**, 105412 (2023).

133. S. E. Evans, J. Barbadillo, Early Cretaceous lizards from Las Hoyas, Spain. *Zool. J. Linn. Soc.* **119**, 23–49 (2008).

134. S. E. Evans, M. E. H. Jones, R. Matsumoto, A new lizard skull from the Purbeck Limestone Group (Lower Cretaceous) of England. *Bull. Soc. Geol. Fr.* **183**, 517–524 (2012).

135. S. A. Magallón, Dating Lineages: Molecular and Paleontological Approaches to the Temporal Framework of Clades. *Int. J. Plant Sci.* **165** (S4), S7–S21 (2004).

136. G. P. Wagner, L. Altenberg, Perspective: Complex adaptations and the evolution of evolvability. *Evolution* **50**, 967–976 (1996).

137. A. Feldman, N. Sabath, R. A. Pyron, I. Mayrose, S. Meiri, Body sizes and diversification rates of lizards, snakes, amphisbaenians and the tuatara. *Glob. Ecol. Biogeogr.* **25**, 187–197 (2016).

138. S. Meiri, Traits of lizards of the world: Variation around a successful evolutionary design. *Glob. Ecol. Biogeogr.* **27**, 1168–1172 (2018).

139. C. M. Sheehy III, J. S. Albert, H. B. Lillywhite, The evolution of tail length in snakes associated with different gravitational environments. *Funct. Ecol.* **30**, 244–254 (2016).

140. R. B. King, Sexual dimorphism in snake tail length: Sexual selection, natural selection, or morphological constraint? *Biol. J. Linn. Soc. Lond.* **38**, 133–154 (1989).

141. A. M. Lawing, J. J. Head, P. D. Polly, "The ecology of morphology: The ecometrics of locomotion and macroenvironment in North American snakes" in *Paleontology in Ecology and Conservation*, J. Louys, Ed. (Springer, 2012), pp. 117–146.

142. A. Feldman, S. Meiri, Length–mass allometry in snakes. *Biol. J. Linn. Soc. Lond.* **108**, 161–172 (2012).

143. E. W. Goolsby, J. Bruggeman, C. Ané, Rphylopars: Fast multivariate phylogenetic comparative methods for missing data and within-species variation. *Methods Ecol. Evol.* **8**, 22–27 (2017).

144. E. N. Arnold, Relationships of the Palaeartic lizards assigned to the genera *Lacerta, Algyroides* and *Psammodromus* (Reptilia: Lacertidae). *Bulletin of the British Museum (Natural History). Zoology (Jena)* **25**, 291–366 (1973).

145. A. M. Bauer, A. P. Russell, G. L. Powell, The evolution of locomotor morphology in *Rhoptropus* (Squamata: Gekkonidae): Functional and phylogenetic considerations. *Afr. J. Herpetol.* **45**, 8–30 (1996).

146. P. D. Polly, J. J. Head, M. J. Cohn, "Testing modularity and dissociation: the evolution of regional proportions in snakes" in *Beyond Heterochrony: The Evolution of Development*, M. L. Zelditch, Ed. (Wiley-Liss, 2001), pp. 307–335.

147. R. Van Damme, B. Vanhooydonck, Speed versus manoeuvrability: Association between vertebral number and habitat structure in lacertid lizards. *J. Zool.* **258**, 327–334 (2002).

148. A. M. Bauer, Descriptions of seven new *Cyrtodactylus* (Squamata: Gekkonidae) with a key to the species of Myanmar (Burma). *Proc. Calif. Acad. Sci.* **54**, 463–498 (2003).

149. I. Das, N. Yaakob, A new species of *Dibamus* (Squamata: Dibamidae) from Peninsular Malaysia. *Raffles Bull. Zool.* **51**, 143–148 (2003).

150. A. Miralles, G. Rivas, W. E. Schargel, A new species of *Mabuya* (Squamata, Scincidae) from the Venezuelan Andes. *Zootaxa* **895**, 1–11 (2005).

151. R. A. Sadlier, A. M. Bauer, S. A. Smith, A new species of *Nannoscincus* Gunther (Squamata: Scincidae) from high elevation forest in southern New Caledonia. *Rec. Aust. Mus.* **58**, 29–36 (2006).

152. R. A. Sadlier, S. A. Smith, A. M. Bauer, A. H. Whitaker, Three new species of skink in the genus *Marmorosphax* Sadlier (Squamata: Scincidae) from New Caledonia. *Zoologia Neocaledonica* **7**, 373–390 (2009).

153. K. Ljubisavljević, O. Arribas, G. Džukić, S. Carranza, Genetic and morphological differentiation of Mosor rock lizards, *Dinarolacerta mosorensis* (Kolombatović, 1886), with the description of a new species from the Prokletije Mountain Massif (Montenegro) (Squamata: Lacertidae). *Zootaxa* **1613**, 1–22 (2007).

154. M. Carretero, G. Llorente, A. Kaliontzopoulou, Interspecific and intersexual variation in presacral vertebrae number in *Podarcis bocagei* and *P. carbonelli*. *Amphib.-Reptil.* **29**, 288–292 (2008).

155. P. M. Hampton, Ventral and sub-caudal scale counts are associated with macrohabitat use and tail specialization in viperid snakes. *Evol. Ecol.* **25**, 531–546 (2011).

156. P. J. Bergmann, D. J. Irschick, Vertebral evolution and the diversification of squamate reptiles. *Evolution* **66**, 1044–1058 (2012).

157. A. Miralles, M. Anjeriniaina, C. A. Hipsley, J. Müller, F. Glaw, M. Vences, Variations on a bauplan: Description of a new Malagasy "mermaid skink" with flipper-like forelimbs only (Scincidae, *Sirenoscincus* Sakata & Hikida, 2003). *Zoosystema* **34**, 701–719 (2012).

158. T. Tsuihiji, M. Kearney, O. Rieppel, Finding the neck-trunk boundary in snakes: Anteroposterior dissociation of myological characteristics in snakes and its implications for their neck and trunk body regionalization. *J. Morphol.* **273**, 992–1009 (2012).

159. M. Camaiti, A. R. Evans, C. A. Hipsley, M. N. Hutchinson, S. Meiri, R. O. Anderson, A. Slavenko, D. G. Chapple, A database of the morphology, ecology and literature of the world's limb-reduced skinks. *J. Biogeogr.* **49**, 1397–1406 (2022).

160. M. Camaiti, A. Villa, L. C. M. Wencker, A. M. Bauer, E. L. Stanley, M. Delfino, Descriptive osteology and patterns of limb loss of the European limbless skink *Ophiomorus punctatissimus* (Squamata, Scincidae). *J. Anat.* **235**, 313–345 (2019).

161. P. J. Bergmann, G. Morinaga, The convergent evolution of snake-like forms by divergent evolutionary pathways in squamate reptiles. *Evolution* **73**, 481–496 (2019).

162. L. Kratochvíl, L. Kubička, M. Vohralík, Z. Starostová, Variability in vertebral numbers does not contribute to sexual size dimorphism, interspecific variability, or phenotypic plasticity in body size in geckos (Squamata: Gekkota: *Paroedura*). *J. Exp. Zool. A Ecol. Integr. Physiol.* **329**, 185–190 (2018).

163. A. A. Alexander, C. Gans, The pattern of dermal-vertebral correlation in snakes and amphisbaenians. *Zool. Meded.* **41**, 171–190 (1966).

164. L. E. Lindell, The evolution of vertebral number and body size in snakes. *Funct. Ecol.* **8**, 708 (1994).

165. M. C. Grundler, SquamataBase: A natural history database and R package for comparative biology of snake feeding habits. *Biodivers. Data J.* **8**, e49943 (2020).

166. M. Grundler, D. L. Rabosky, Complex ecological phenotypes on phylogenetic trees: A Markov Process model for comparative analysis of multivariate count data. *Syst. Biol.* **69**, 1200–1211 (2020).

167. K. A. Heller, Z. Ghahramani, "Bayesian hierarchical clustering" in *Proceedings of the 22nd International Conference on Machine Learning* (ICML '05), Bonn, Germany, 7 to 11 August 2005 (Association for Computing Machinery, 2005), pp. 297–304.

168. D. N. Karger, O. Conrad, J. Böhner, T. Kawohl, H. Kreft, R. W. Soria-Auza, N. E. Zimmermann, H. P. Linder, M. Kessler, Climatologies at high resolution for the earth's land surface areas. *Sci. Data* **4**, 170122 (2017).

169. P. Brun, N. E. Zimmermann, C. Hari, L. Pellissier, D. N. Karger, Global climate-related predictors at kilometer resolution for the past and future. *Earth Syst. Sci. Data* **14**, 5573–5603 (2022).

170. P. O. Title, J. B. Bemmels, ENVIREM: An expanded set of bioclimatic and topographic variables increases flexibility and improves performance of ecological niche modeling. *Ecography* **41**, 291–307 (2018).

171. E. H. Taylor, Ceylonese lizards of the family Scincidae. *Univ. Kans. Sci. Bull.* **33**, 481–518 (1950).

172. G. Nilson, C. Andrén, A New Species of *Ophiomorus* (Sauria: Scincidae) from Kavir Desert, Iran. *Copeia* **1978**, 559 (1978).

173. T. Kohlsdorf, G. P. Wagner, Evidence for the reversibility of digit loss: a phylogenetic study of limb evolution in *Bachia* (Gymnophthalmidae: Squamata). *Evolution* **60**, 1896–1912 (2006).

174. M. C. Brandley, J. P. Huelsenbeck, J. J. Wiens, Rates and patterns in the evolution of snake-like body form in squamate reptiles: Evidence for repeated re-evolution of lost digits and long-term persistence of intermediate body forms. *Evolution* **62**, 2042–2064 (2008).

175. S. Carranza, E. N. Arnold, P. Geniez, J. Roca, J. A. Mateo, Radiation, multiple dispersal and parallelism in the skinks, *Chalcides* and *Sphenops* (Squamata: Scincidae), with comments on *Scincus* and *Scincopus* and the age of the Sahara Desert. *Mol. Phylogenet. Evol.* **46**, 1071–1094 (2008).

176. A. Skinner, M. S. Y. Lee, M. N. Hutchinson, Rapid and repeated limb loss in a clade of scincid lizards. *BMC Evol. Biol.* **8**, 310 (2008).

177. J. G. Roscito, K. Sameith, B. M. Kirilenko, N. Hecker, S. Winkler, A. Dahl, M. T. Rodrigues, M. Hiller, Convergent and lineage-specific genomic differences in limb regulatory elements in limbless reptile lineages. *Cell Rep.* **38**, 110280 (2022).

178. C. Gans, The Feeding Mechanism of Snakes and Its Possible Evolution. *Am. Zool.* **1**, 217–227 (1961).

179. V. Deolindo, C. Koch, M. Joshi, A. Martins, To move or not to move? Skull and lower jaw morphology of the blindsnake Afrotyphlops punctatus (Leach, 1819) (Serpentes, Typhlopoidea, Typhlopidae) with comments on its previously advocated cranial kinesis. *Anat. Rec. (Hoboken)* **304**, 2279–2291 (2021).

180. S. J. Beaupre, C. E. Montgomery, "The meaning and consequences of foraging mode in snakes" in *Lizard Ecology: The Evolutionary Consequences of Foraging Mode*, S. M. Reilly, L. D. McBrayer, D. B. Miles, Eds. (Cambridge Univ. Press, 2007), pp. 364–368.

181. R. Shine, Ecology of the Australian death adder *Acanthophis antarcticus* (Elapidae): Evidence for convergence with the Viperidae. *Herpetologica* **36**, 281–289 (1980).

182. E. R. Pianka, L. J. Vitt, *Lizards: Windows to the Evolution of Diversity* (Univ. of California Press, 2003).

183. J. H. Carothers, Correlates of foraging modes in lizards: A review. *Arch. Biol. Med. Exp.* **18**, R90–R91 (1985).

184. W. E. Cooper, L. J. Vitt, J. P. Caldwell, S. F. Fox, Foraging modes of some American lizards: Relationships among measurement variables and discreteness of modes. *Herpetologica* **57**, 65–76 (2001).

185. W. E. Cooper, M. J. Whiting, J. H. Van Wyk, Foraging modes of cordyliform lizards. *Afr. Zool.* **32**, 9–13 (1997).

186. W. E. Cooper, M. J. Whiting, Foraging modes in lacertid lizards from southern Africa. *Amphib.-Reptil.* **20**, 299–311 (1999).

187. W. E. Cooper Jr., Foraging mode, prey chemical discrimination, and phylogeny in lizards. *Anim. Behav.* **50**, 973–985 (1995).

188. A. du Toit, P. F. N. Mouton, H. Geertsema, A. F. Flemming, Foraging mode of serpentiform, grass-living cordylid lizards: A case study of *Cordylus anguina*. *Afr. Zool.* **37**, 141–149 (2002).

189. J. M. Greeff, M. J. Whiting, Foraging-Mode Plasticity in the Lizard *Platysaurus broadleyi*. *Herpetologica* **56**, 402–407 (2000).

190. D. O. Mesquita, G. C. Costa, G. R. Colli, T. B. Costa, D. B. Shepard, L. J. Vitt, E. R. Pianka, Life-History patterns of lizards of the world. *Am. Nat.* **187**, 689–705 (2016).

191. D. O. Mesquita, G. R. Colli, G. C. Costa, T. B. Costa, D. B. Shepard, L. J. Vitt, E. R. Pianka, Life history data of lizards of the world. *Ecology* **96**, 594 (2015).

192. G. Perry, The evolution of search modes: Ecological versus phylogenetic perspectives. *Am. Nat.* **153**, 98–109 (1999).

193. R. A. Pyron, F. T. Burbrink, Early origin of viviparity and multiple reversions to oviparity in squamate reptiles. *Ecol. Lett.* **17**, 13–21 (2014).

194. P. O. Title, D. L. Rabosky, Tip rates, phylogenies and diversification: What are we estimating, and how good are the estimates? *Methods Ecol. Evol.* **10**, 821–834 (2019).

195. D. L. Rabosky, Extinction rates should not be estimated from molecular phylogenies. *Evolution* **64**, 1816–1824 (2010).

196. S. Louca, M. W. Pennell, Extant timetrees are consistent with a myriad of diversification histories. *Nature* **580**, 502–505 (2020).

197. O. Maliet, F. Hartig, H. Morlon, A model with many small shifts for estimating species-specific diversification rates. *Nat. Ecol. Evol.* **3**, 1086–1092 (2019).

198. O. Maliet, H. Morlon, Fast and accurate estimation of species-specific diversification rates using data augmentation. *Syst. Biol.* **71**, 353–366 (2022).

199. D. L. Rabosky, Automatic detection of key innovations, rate shifts, and diversity-dependence on phylogenetic trees. *PLOS ONE* **9**, e89543 (2014).

200. T. Vasconcelos, B. C. O'Meara, J. M. Beaulieu, A flexible method for estimating tip diversification rates across a range of speciation and extinction scenarios. *Evolution* **76**, 1420–1433 (2022).

201. D. W. Redding, A. Ø. Mooers, Incorporating evolutionary measures into conservation prioritization. *Conserv. Biol.* **20**, 1670–1678 (2006).

202. A. Gelman, J. B. Carlin, H. S. Stern, D. B. Dunson, A. Vehtari, D. B. Rubin, *Bayesian Data Analysis* (CRC Press, 2014).

203. D. L. Rabosky, M. Grundler, C. Anderson, P. Title, J. J. Shi, J. W. Brown, H. Huang, J. G. Larson, BAMM tools: An R package for the analysis of evolutionary dynamics on phylogenetic trees. *Methods Ecol. Evol.* **5**, 701–707 (2014).

204. J. Felsenstein, Maximum-likelihood estimation of evolutionary trees from continuous characters. *Am. J. Hum. Genet.* **25**, 471–492 (1973).

205. E. A. Stone, Why the phylogenetic regression appears robust to tree misspecification. *Syst. Biol.* **60**, 245–260 (2011).

206. L. J. Harmon, J. B. Losos, T. Jonathan Davies, R. G. Gillespie, J. L. Gittleman, W. Bryan Jennings, K. H. Kozak, M. A. McPeek, F. Moreno-Roark, T. J. Near, A. Purvis, R. E. Ricklefs, D. Schluter, J. A. Schulte II, O. Seehausen, B. L. Sidlauskas, O. Torres-Carvajal, J. T. Weir, A. Ø. Mooers, Early bursts of body size and shape evolution are rare in comparative data. *Evolution* **64**, 2385–2396 (2010).

207. C. Venditti, A. Meade, M. Pagel, Phylogenies reveal new interpretation of speciation and the Red Queen. *Nature* **463**, 349–352 (2010).

208. B. C. O'Meara, C. Ané, M. J. Sanderson, P. C. Wainwright, Testing for different rates of continuous trait evolution using likelihood. *Evolution* **60**, 922–933 (2006).

209. J. M. Eastman, M. E. Alfaro, P. Joyce, A. L. Hipp, L. J. Harmon, A novel comparative method for identifying shifts in the rate of character evolution on trees. *Evolution* **65**, 3578–3589 (2011).

210. D. M. Olson, E. Dinerstein, E. D. Wikramanayake, N. D. Burgess, G. V. N. Powell, E. C. Underwood, J. A. D'amico, I. Itoua, H. E. Strand, J. C. Morrison, C. J. Loucks, T. F. Allnutt, T. H. Ricketts, Y. Kura, J. F. Lamoreux, W. W. Wettengel, P. Hedao, K. R. Kassem, Terrestrial Ecoregions of the World: A New Map of Life on Earth: A new global map of terrestrial ecoregions provides an innovative tool for conserving biodiversity. *Bioscience* **51**, 933–938 (2001).

211. S. J. Arnold, Species Densities of Predators and Their Prey. *Am. Nat.* **106**, 220–236 (1972).

212. A. G. Fischer, Latitudinal Variations in Organic Diversity. *Evolution* **14**, 64–81 (1960).

213. D. P. Ford, R. B. J. Benson, The phylogeny of early amniotes and the affinities of Parareptilia and Varanopidae. *Nat. Ecol. Evol.* **4**, 57–65 (2020).

214. M. D. Ezcurra, T. M. Scheyer, R. J. Butler, The origin and early evolution of Sauria: Reassessing the permian Saurian fossil record and the timing of the crocodile-lizard divergence. *PLOS ONE* **9**, e89165 (2014).

215. J. F. Parham, P. C. J. Donoghue, C. J. Bell, T. D. Calway, J. J. Head, P. A. Holroyd, J. G. Inoue, R. B. Irmis, W. G. Joyce, D. T. Ksepka, J. S. L. Patané, N. D. Smith, J. E. Tarver, M. van Tuinen, Z. Yang, K. D. Angielczyk, J. M. Greenwood, C. A. Hipsley, L. Jacobs, P. J. Makovicky, J. Müller, K. T. Smith, J. M. Theodor, R. C. M. Warnock, M. J. Benton, Best practices for justifying fossil calibrations. *Syst. Biol.* **61**, 346–359 (2012).

216. S. E. Evans, D. C. Chure, Paramacellodid lizard skulls from the Jurassic Morrison Formation at Dinosaur National Monument, Utah. *J. Vertebr. Paleontol.* **18**, 99–114 (1998).

217. R. Hoffstetter, Les serpents du Néogène du Pakistan (couches des Siwaliks). *Bull. Soc. Geol. Fr.* **7**, 467–474 (1964).

218. R. Estes, "Sauria terrestria, Amphisbaenia" in *Encyclopedia of Paleoherpetology*, vol. 10a, H.-D. Sues, O. Kuhn, P. Wellnhofer, R. M. Appleby, Eds. (1983).

219. S. E. Evans, D. J. Chure, "Upper Jurassic lizards from the Morrison Formation of Dinosaur National Monument, Utah" in *Vertebrate Paleontology in Utah*, Miscellaneous Publication 99-1, (Utah Geological Survey, 1999), pp. 151–160.

220. J. L. Conrad, J. C. Ast, S. Montanari, M. A. Norell, A combined evidence phylogenetic analysis of Anguimorpha (Reptilia: Squamata). *Cladistics* **27**, 230–277 (2011).

221. J. L. Conrad, M. A. Norell, A complete Late Cretaceous iguanian (Squamata, Reptilia) from the Gobi and identification of a new iguanian clade. *Am. Mus. Novit.* **2007**, 1–47 (2007).

222. J. D. Daza, E. L. Stanley, P. Wagner, A. M. Bauer, D. A. Grimaldi, Mid-Cretaceous amber fossils illuminate the past diversity of tropical lizards. *Sci. Adv.* **2**, e1501080 (2016).

223. E. N. Arnold, G. Poinar, A 100 million year old gecko with sophisticated adhesive toe pads, preserved in amber from Myanmar. *Zootaxa* **1847**, 62 (2008).

224. R. L. Nydam, R. L. Cifelli, Lizards from the Lower Cretaceous (Aptian–Albian) Antlers and Cloverly Formations. *J. Vertebr. Paleontol.* **22**, 286–298 (2002).

225. T. S. Fachini, S. Onary, A. Palci, M. S. Y. Lee, M. Bronzati, A. S. Hsiou, Cretaceous blind snake from Brazil fills major gap in snake evolution. *iScience* **24**, 102180 (2021).

226. M. Elliot Smith, A. R. Carroll, B. S. Singer, Synoptic reconstruction of a major ancient lake system: Eocene Green River Formation, western United States. *Geol. Soc. Am. Bull.* **120**, 54–84 (2008).

227. R. L. Nydam, T. B. Rowe, R. L. Cifelli, Lizards and snakes of the Terlingua Local Fauna (late Campanian), Aguja Formation, Texas, with comments on the distribution of paracontemporaneous squamates throughout the Western Interior of North America. *J. Vertebr. Paleontol.* **33**, 1081–1099 (2013).

228. J. J. Head, Fossil calibration dates for molecular phylogenetic analysis of snakes 1: Serpentes, Alethinophidia, Boidae, Pythonidae. *Palaeontol. Electronica* **18**, 1–17 (2015).

229. J. J. Head, K. Mahlow, J. Müller, Fossil calibration dates for molecular phylogenetic analysis of snakes 2: Caenophidia, Colubroidea, Elapoidea, Colubridae. *Palaeontol. Electronica* **19**, (2016).

230. H. Zaher, K. T. Smith, Pythons in the Eocene of Europe reveal a much older divergence of the group in sympatry with boas. *Biol. Lett.* **16**, 20200735 (2020).

231. K. T. Smith, B. S. Bhullar, G. Köhler, J. Habersetzer, The only known jawed vertebrate with four eyes and the bauplan of the pineal complex. *Curr. Biol.* **28**, 1101–1107.e2 (2018).

232. K. T. Smith, Eocene Lizards of the Clade *Geiseltaliellus* from Messel and Geiseltal, Germany, and the Early Radiation of Iguanidae (Reptilia: Squamata). *Bull. Peabody Mus. Nat. Hist.* **50**, 219–306 (2009).

233. K. T. Smith, The squamation of the Eocene stem-basilisk *Geiseltaliellus maarius* (Squamata: Iguanidae: Corytophaninae) from Messel, Germany. *Salamandra (Frankf.)* **53**, 519–530 (2017).

234. K. M. Thorn, M. N. Hutchinson, M. Archer, M. S. Y. Lee, A new scincid lizard from the Miocene of northern Australia, and the evolutionary history of social skinks (Scincidae: Egerniinae). *J. Vertebr. Paleontol.* **39**, e1577873 (2019).

235. J. C. Rage, Z. Szyndlar, *Natrix longivertebrata* from the European Neogene, a snake with one of the longest known stratigraphic ranges. *Neues Jahrb. Geol. Paläontol., Monatsh.* **1986**, 56–64 (1986).

236. M. Ivanov, The first European pit viper from the Miocene of Ukraine. *Acta Palaeontol. Pol.* **44**, 327–334 (1999).

237. J. W. Streicher, J. J. Wiens, Phylogenomic analyses reveal novel relationships among snake families. *Mol. Phylogenet. Evol.* **100**, 160–169 (2016).

238. J. W. Streicher, J. A. Schulte 2nd, J. J. Wiens, How should genes and taxa be sampled for phylogenomic analyses with missing data? an empirical study in Iguanian lizards. *Syst. Biol.* **65**, 128–145 (2016).

239. J. L. Grismer, J. A. Schulte 2nd, A. Alexander, P. Wagner, S. L. Travers, M. D. Buehler, L. J. Welton, R. M. Brown, The Eurasian invasion: Phylogenomic data reveal multiple Southeast Asian origins for Indian Dragon Lizards. *BMC Evol. Biol.* **16**, 43 (2016).

240. A. D. Leaché, C. W. Linkem, Phylogenomics of Horned Lizards (Genus: *Phrynosoma*) using targeted sequence capture data. *Copeia* **103**, 586–594 (2015).

241. A. D. Leaché, A. S. Chavez, L. N. Jones, J. A. Grummer, A. D. Gottscho, C. W. Linkem, Phylogenomics of phrynosomatid lizards: Conflicting signals from sequence capture versus restriction site associated DNA sequencing. *Genome Biol. Evol.* **7**, 706–719 (2015).

242. R. A. Pyron, C. R. Hendry, V. M. Chou, E. M. Lemmon, A. R. Lemmon, F. T. Burbrink, Effectiveness of phylogenomic data and coalescent species-tree methods for resolving difficult nodes in the phylogeny of advanced snakes (Serpentes: Caenophidia). *Mol. Phylogenet. Evol.* **81**, 221–231 (2014).

243. X. Chen, A. R. Lemmon, E. M. Lemmon, R. A. Pyron, F. T. Burbrink, Using phylogenomics to understand the link between biogeographic origins and regional diversification in ratsnakes. *Mol. Phylogenet. Evol.* **111**, 206–218 (2017).

244. D. B. Tucker, G. R. Colli, L. G. Giugliano, S. B. Hedges, C. R. Hendry, E. M. Lemmon, A. R. Lemmon, J. W. Sites Jr., R. A. Pyron, Methodological congruence in phylogenomic analyses with morphological support for teiid lizards (Sauria: Teiidae). *Mol. Phylogenet. Evol.* **103**, 75–84 (2016).

245. R. W. Bryson Jr., C. W. Linkem, C. J. Pavón-Vázquez, A. Nieto-Montes de Oca, J. Klicka, J. E. McCormack, A phylogenomic perspective on the biogeography of skinks in the

Plestiodon brevirostris group inferred from target enrichment of ultraconserved elements. *J. Biogeogr.* **44**, 2033–2044 (2017).

246. N. G. Crawford, B. C. Faircloth, J. E. McCormack, R. T. Brumfield, K. Winker, T. C. Glenn, More than 1000 ultraconserved elements provide evidence that turtles are the sister group of archosaurs. *Biol. Lett.* **8**, 783–786 (2012).

247. S. Ruane, C. J. Raxworthy, A. R. Lemmon, E. M. Lemmon, F. T. Burbrink, Comparing species tree estimation with large anchored phylogenomic and small Sanger-sequenced molecular datasets: An empirical study on Malagasy pseudoxyrhophiine snakes. *BMC Evol. Biol.* **15**, 221 (2015).

248. C. W. Linkem, V. N. Minin, A. D. Leaché, Detecting the Anomaly Zone in Species Trees and Evidence for a Misleading Signal in Higher-Level Skink Phylogeny (Squamata: Scincidae). *Syst. Biol.* **65**, 465–477 (2016).

249. R. A. Pyron, F. W. Hsieh, A. R. Lemmon, E. M. Lemmon, C. R. Hendry, Integrating phylogenomic and morphological data to assess candidate species-delimitation models in brown and red-bellied snakes (*Storeria*). *Zool. J. Linn. Soc.* **177**, 937–949 (2016).